Astrofisica Nucleare e Subnucleare

Gravitational Waves

Astrofisica Nucleare e Subnucleare

Gravitational Waves Science

Scientific achievements: properties of binary systems

"GWTC-1: A Gravitational-Wave Transient Catalog of Compact Binary Mergers Observed by LIGO and Virgo during the First and Second Observing Runs", LIGO Virgo Collaboration, [arXiv:1811.12907](https://arxiv.org/abs/1811.12907)

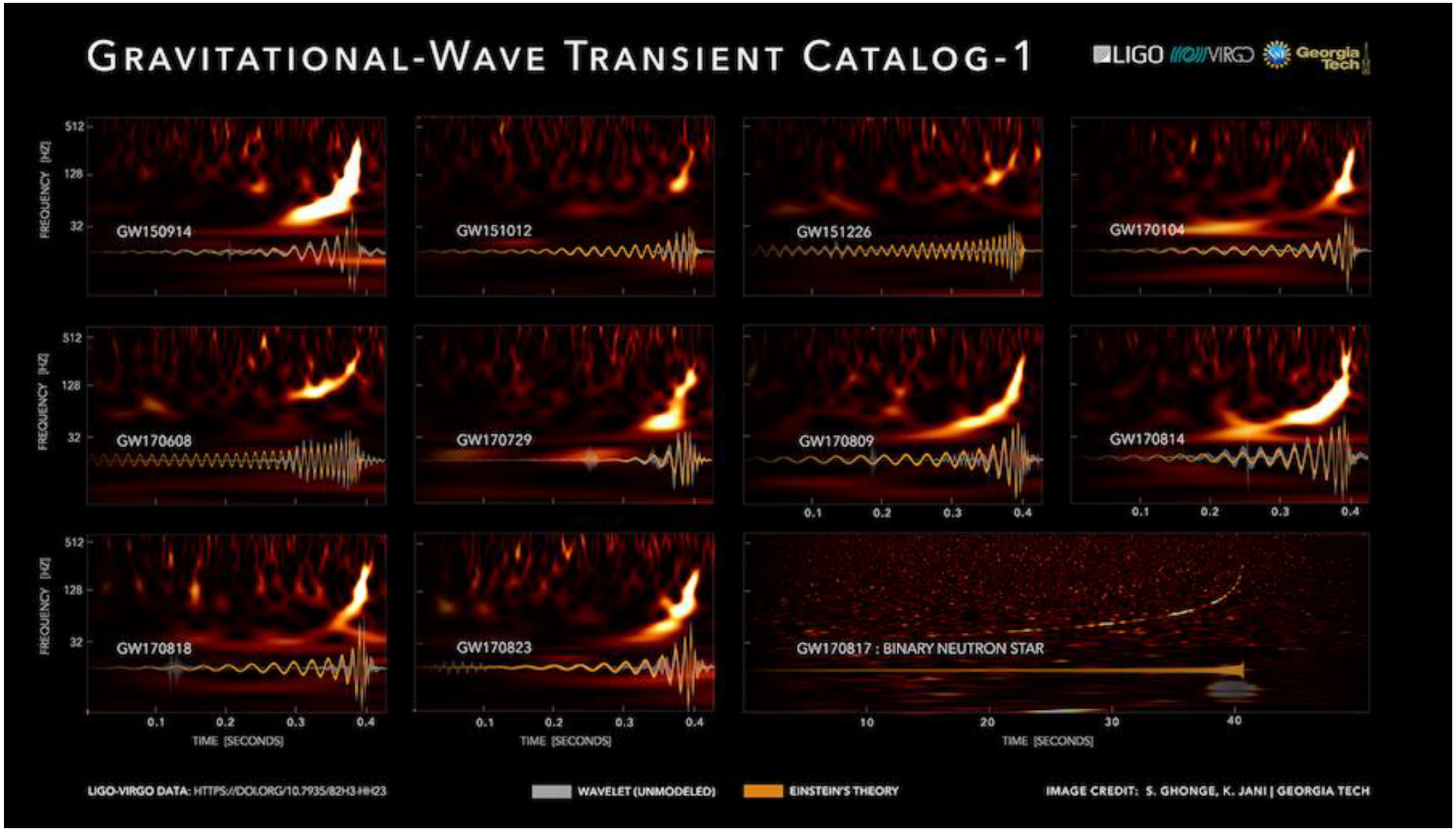

https://gracedb.ligo.org/latest/

Already 33 (= 41 - 8) public alerts in the 3rd science run: more candidates than O1 and O2 combined

Latest — as of 10 October 2019 17:29:34 UTC

Test and MDC events and superevents are not included in the search results by default; see the query help for information on how to search for events and superevents in those categories.

Query:

Search for: Superevent

Search

UTC

UID	Labels	t_start	t_0	t_end	FAR (Hz)	Created
S190930t	ADVOK EM_Selected SKYMAP_READY EMBRIGHT_READY PASTRO_READY DQOK GCN_PRELIM_SENT	1253889264.685342	1253889265.685342	1253889266.685342	1.543e-08	2019-09-30 14:34:30 UTC
S190930s	PE_READY ADVOK EM_Selected SKYMAP_READY EMBRIGHT_READY PASTRO_READY DQOK GCN_PRELIM_SENT	1253885758.235347	1253885759.246810	1253885760.253734	3.008e-09	2019-09-30 13:36:04 UTC
S190928c	ADVNO EM_Selected SKYMAP_READY DQOK GCN_PRELIM_SENT	1253671923.328316	1253671923.364500	1253671923.400684	6.729e-09	2019-09-28 02:14:18 UTC
S190924h	PE_READY ADVOK EM_Selected SKYMAP_READY EMBRIGHT_READY PASTRO_READY DQOK GCN_PRELIM_SENT	1253326743.785645	1253326744.846654	1253326745.876674	8.928e-19	2019-09-24 02:19:25 UTC
S190923y	ADVOK EM_Selected SKYMAP_READY EMBRIGHT_READY PASTRO_READY DQOK GCN_PRELIM_SENT	1253278576.645077	1253278577.645508	1253278578.654868	4.783e-08	2019-09-23 12:56:22 UTC
S190915ak	PE_READY ADVOK SKYMAP_READY EMBRIGHT_READY PASTRO_READY DQOK GCN_PRELIM_SENT	1252627039.685111	1252627040.690891	1252627041.730049	9.735e-10	2019-09-15 23:57:25 UTC
S190910h	PE_READY ADVOK SKYMAP_READY EMBRIGHT_READY PASTRO_READY DQOK GCN_PRELIM_SENT	1252139415.544299	1252139416.544448	1252139417.544448	3.584e-08	2019-09-10 08:30:21 UTC
S190910d	PE_READY ADVOK SKYMAP_READY EMBRIGHT_READY PASTRO_READY DQOK GCN_PRELIM_SENT	1252113996.241211	1252113997.242676	1252113998.264918	3.717e-09	2019-09-10 01:26:35 UTC
S190901ap	PE_READY ADVOK SKYMAP_READY EMBRIGHT_READY PASTRO_READY DQOK GCN_PRELIM_SENT	1251415878.837767	1251415879.837767	1251415880.838844	7.027e-09	2019-09-01 23:31:24 UTC
S190829u	PE_READY ADVNO SKYMAP_READY EMBRIGHT_READY PASTRO_READY DQOK GCN_PRELIM_SENT	1251147973.281494	1251147974.283940	1251147975.283940	5.151e-09	2019-08-29 21:06:19 UTC
S190828l	PE_READY ADVOK SKYMAP_READY EMBRIGHT_READY PASTRO_READY DQOK GCN_PRELIM_SENT	1251010526.884921	1251010527.886557	1251010528.913573	4.629e-11	2019-08-28 06:55:26 UTC
S190828j	PE_READY ADVOK SKYMAP_READY EMBRIGHT_READY PASTRO_READY DQOK GCN_PRELIM_SENT	1251009262.739486	1251009263.756472	1251009264.796332	8.474e-22	2019-08-28 06:34:21 UTC
S190822c	ADVNO SKYMAP_READY EMBRIGHT_READY PASTRO_READY DQOK GCN_PRELIM_SENT	1250472616.589125	1250472617.589203	1250472618.589203	6.145e-18	2019-08-22 01:30:23 UTC
S190816i	PE_READY ADVNO SKYMAP_READY EMBRIGHT_READY PASTRO_READY DQOK GCN_PRELIM_SENT	1249995888.757789	1249995889.757789	1249995890.757789	1.436e-08	2019-08-16 13:05:12 UTC
S190814bv	PE_READY ADVOK SKYMAP_READY EMBRIGHT_READY PASTRO_READY DQOK GCN_PRELIM_SENT	1249852255.996787	1249852257.012957	1249852258.021731	2.033e-33	2019-08-14 21:11:18 UTC
S190808ae	ADVNO SKYMAP_READY EMBRIGHT_READY PASTRO_READY DQOK GCN_PRELIM_SENT	1249338098.496141	1249338099.496141	1249338100.496141	3.366e-08	2019-08-08 22:21:45 UTC
S190728q	PE_READY ADVOK SKYMAP_READY EMBRIGHT_READY PASTRO_READY DQOK GCN_PRELIM_SENT	1248331527.497344	1248331528.546797	1248331529.706055	2.527e-23	2019-07-28 06:45:27 UTC
S190727h	PE_READY ADVOK SKYMAP_READY EMBRIGHT_READY PASTRO_READY DQOK GCN_PRELIM_SENT	1248242630.976288	1248242631.985887	1248242633.180176	1.378e-10	2019-07-27 06:03:51 UTC
S190720a	PE_READY ADVOK SKYMAP_READY EMBRIGHT_READY PASTRO_READY DQOK GCN_PRELIM_SENT	1247616533.703127	1247616534.704102	1247616535.860840	3.801e-09	2019-07-20 00:08:53 UTC
S190718y	ADVOK SKYMAP_READY EMBRIGHT_READY PASTRO_READY DQOK GCN_PRELIM_SENT	1247495729.067865	1247495730.067865	1247495731.067865	3.648e-08	2019-07-18 14:35:34 UTC
S190707q	PE_READY ADVOK SKYMAP_READY EMBRIGHT_READY PASTRO_READY DQOK GCN_PRELIM_SENT	1246527223.118398	1246527224.181226	1246527225.284180	5.265e-12	2019-07-07 09:33:44 UTC
S190706ai	PE_READY ADVOK SKYMAP_READY EMBRIGHT_READY PASTRO_READY DQOK GCN_PRELIM_SENT	1246487218.321541	1246487219.344727	1246487220.585938	1.901e-09	2019-07-06 22:26:57 UTC
S190701ah	PE_READY ADVOK SKYMAP_READY EMBRIGHT_READY PASTRO_READY DQOK GCN_PRELIM_SENT	1246048403.576563	1246048404.577637	1246048405.814941	1.916e-08	2019-07-01 20:33:24 UTC
S190630ag	PE_READY ADVOK SKYMAP_READY EMBRIGHT_READY PASTRO_READY DQOK GCN_PRELIM_SENT	1245955942.175325	1245955943.179550	1245955944.183184	1.435e-13	2019-06-30 18:52:28 UTC
S190602aq	PE_READY ADVOK SKYMAP_READY EMBRIGHT_READY PASTRO_READY DQOK GCN_PRELIM_SENT	1243533584.081266	1243533585.089355	1243533586.346191	1.901e-09	2019-06-02 17:59:51 UTC
S190524q	ADVNO SKYMAP_READY EMBRIGHT_READY PASTRO_READY DQOK GCN_PRELIM_SENT	1242708743.678669	1242708744.678669	1242708746.133301	6.971e-09	2019-05-24 04:52:30 UTC
S190521r	PE_READY ADVOK SKYMAP_READY EMBRIGHT_READY PASTRO_READY DQOK GCN_PRELIM_SENT	1242459856.453418	1242459857.460739	1242459858.642090	3.168e-10	2019-05-21 07:44:22 UTC
S190521g	PE_READY ADVOK SKYMAP_READY EMBRIGHT_READY PASTRO_READY DQOK GCN_PRELIM_SENT	1242442966.447266	1242442967.606934	1242442968.888184	3.801e-09	2019-05-21 03:02:49 UTC
S190519bj	PE_READY ADVOK SKYMAP_READY EMBRIGHT_READY PASTRO_READY DQOK GCN_PRELIM_SENT	1242315361.378873	1242315362.655762	1242315363.676270	5.702e-09	2019-05-19 15:36:04 UTC
S190518bb	ADVNO SKYMAP_READY EMBRIGHT_READY PASTRO_READY DQOK GCN_PRELIM_SENT	1242242376.474609	1242242377.474609	1242242380.922655	1.004e-08	2019-05-18 19:19:39 UTC
S190517h	PE_READY ADVOK SKYMAP_READY EMBRIGHT_READY PASTRO_READY DQOK GCN_PRELIM_SENT	1242107478.819517	1242107479.994141	1242107480.994141	2.373e-09	2019-05-17 05:51:23 UTC
S190513bm	PE_READY ADVOK SKYMAP_READY EMBRIGHT_READY PASTRO_READY DQOK GCN_PRELIM_SENT	1241816085.736106	1241816086.869141	1241816087.869141	3.734e-13	2019-05-13 20:54:48 UTC
S190512at	PE_READY ADVOK SKYMAP_READY EMBRIGHT_READY PASTRO_READY DQOK GCN_PRELIM_SENT	1241719651.411441	1241719652.416286	1241719653.518066	1.901e-09	2019-05-12 18:07:42 UTC
S190510g	ADVOK SKYMAP_READY EMBRIGHT_READY PASTRO_READY DQOK GCN_PRELIM_SENT	1241492396.291636	1241492397.291636	1241492398.293185	8.834e-09	2019-05-10 03:00:03 UTC
S190503bf	PE_READY ADVOK SKYMAP_READY EMBRIGHT_READY PASTRO_READY DQOK GCN_PRELIM_SENT	1240944861.288574	1240944862.412598	1240944863.422852	1.636e-09	2019-05-03 18:54:26 UTC
S190426c	PE_READY ADVOK SKYMAP_READY EMBRIGHT_READY PASTRO_READY DQOK GCN_PRELIM_SENT	1240327332.331668	1240327333.348145	1240327334.353516	1.947e-08	2019-04-26 15:22:15 UTC
S190425z	ADVOK SKYMAP_READY EMBRIGHT_READY PASTRO_READY DQOK	1240215502.011549	1240215503.011549	1240215504.018242	4.538e-13	2019-04-25 08:18:26 UTC
S190421ar	PE_READY ADVOK SKYMAP_READY EMBRIGHT_READY PASTRO_READY DQOK GCN_PRELIM_SENT	1239917953.250977	1239917954.409180	1239917955.409180	1.489e-08	2019-04-21 21:39:16 UTC
S190412m	PE_READY ADVOK SKYMAP_READY EMBRIGHT_READY PASTRO_READY DQOK GCN_PRELIM_SENT	1239082261.146717	1239082262.222168	1239082263.229492	1.683e-27	2019-04-12 05:31:03 UTC
S190408an	PE_READY ADVOK SKYMAP_READY EMBRIGHT_READY PASTRO_READY DQOK GCN_PRELIM_SENT	1238782699.268296	1238782700.287958	1238782701.359863	2.811e-18	2019-04-08 18:18:27 UTC
S190405ar	ADVNO SKYMAP_READY EMBRIGHT_READY PASTRO_READY DQOK	1238515307.863646	1238515308.863646	1238515309.863646	2.141e-04	2019-04-05 16:01:56 UTC

https://gracedb.ligo.org/superevents/public/O3/

Already 41 public alerts in the 3rd science run: more candidate events than O1 and O2 combined

Event ID	Possible Source (Probability)	UTC	GCN	Location	FAR	Comments
S190822c	BNS (>99%)	Aug. 22, 2019 01:29:59 UTC	GCN Circulars Notices | VOE		1 per 5.1566e+09 years	RETRACTED
S190816i	NSBH (83%), Terrestrial (17%)	Aug. 16, 2019 13:04:31 UTC	GCN Circulars Notices | VOE		1 per 2.2067 years	RETRACTED
S190814bv	NSBH (>99%)	Aug. 14, 2019 21:10:39 UTC	GCN Circulars Notices | VOE		1 per 1.559e+25 years	
S190808ae	Terrestrial (57%), BNS (43%)	Aug. 8, 2019 22:21:21 UTC	GCN Circulars Notices | VOE		1.0622 per year	RETRACTED
S190728q	BBH (95%), MassGap (5%)	July 28, 2019 06:45:10 UTC	GCN Circulars Notices | VOE		1 per 1.2541e+15 years	
S190727h	BBH (92%), Terrestrial (5%), MassGap (3%)	July 27, 2019 06:03:33 UTC	GCN Circulars Notices | VOE		1 per 229.92 years	
S190720a	BBH (99%), Terrestrial (1%)	July 20, 2019 00:08:36 UTC	GCN Circulars Notices | VOE		1 per 8.3367 years	
S190718y	Terrestrial (98%), BNS (2%)	July 18, 2019 14:35:12 UTC	GCN Circulars Notices | VOE		1.1514 per year	
S190707q	BBH (>99%)	July 7, 2019 09:33:26 UTC	GCN Circulars Notices | VOE		1 per 6018.9 years	
S190706ai	BBH (99%), Terrestrial (1%)	July 6, 2019 22:26:41 UTC	GCN Circulars Notices | VOE		1 per 16.673 years	
S190701ah	BBH (93%), Terrestrial (7%)	July 1, 2019 20:33:06 UTC	GCN Circulars Notices | VOE		1 per 1.6543 years	
S190630ag	BBH (94%), MassGap (5%)	June 30, 2019 18:52:05 UTC	GCN Circulars Notices | VOE		1 per 2.2077e+05 years	
S190602aq	BBH (99%)	June 2, 2019 17:59:27 UTC	GCN Circulars Notices | VOE		1 per 16.673 years	
S190524q	Terrestrial (71%), BNS (29%)	May 24, 2019 04:52:06 UTC	GCN Circulars Notices | VOE		1 per 4.5458 years	RETRACTED
S190521r	BBH (>99%)	May 21, 2019 07:43:59 UTC	GCN Circulars Notices | VOE		1 per 100.04 years	
S190521g	BBH (97%), Terrestrial (3%)	May 21, 2019 03:02:29 UTC	GCN Circulars Notices | VOE		1 per 8.3367 years	
S190519bj	BBH (96%), Terrestrial (4%)	May 19, 2019 15:35:44 UTC	GCN Circulars Notices | VOE		1 per 5.5578 years	
S190518bb	BNS (75%), Terrestrial (25%)	May 18, 2019 19:19:19 UTC	GCN Circulars Notices | VOE		1 per 3.1557 years	RETRACTED
S190517h	BBH (98%), MassGap (2%)	May 17, 2019 05:51:01 UTC	GCN Circulars Notices | VOE		1 per 13.354 years	
S190513bm	BBH (94%), MassGap (5%)	May 13, 2019 20:54:28 UTC	GCN Circulars Notices | VOE		1 per 84864 years	
S190512at	BBH (99%), Terrestrial (1%)	May 12, 2019 18:07:14 UTC	GCN Circulars Notices | VOE		1 per 16.673 years	
S190510g	Terrestrial (58%), BNS (42%)	May 10, 2019 02:59:39 UTC	GCN Circulars Notices | VOE		1 per 3.5872 years	
S190503bf	BBH (96%), MassGap (3%)	May 3, 2019 18:54:04 UTC	GCN Circulars Notices | VOE		1 per 19.368 years	
S190426c	BNS (49%), MassGap (24%), Terrestrial (14%), NSBH (13%)	April 26, 2019 15:21:55 UTC	GCN Circulars Notices | VOE		1 per 1.6276 years	
S190425z	BNS (>99%)	April 25, 2019 08:18:05 UTC	GCN Circulars Notices | VOE		1 per 69834 years	
S190421ar	BBH (97%), Terrestrial (3%)	April 21, 2019 21:38:56 UTC	GCN Circulars Notices | VOE		1 per 2.1285 years	
S190412m	BBH (>99%)	April 12, 2019 05:30:44 UTC	GCN Circulars Notices | VOE		1 per 1.883e+19 years	
S190408an	BBH (>99%)	April 8, 2019 18:18:02 UTC	GCN Circulars Notices | VOE		1 per 1.1273e+10 years	
S190405ar	Terrestrial (>99%)	April 5, 2019 16:01:30 UTC	GCN Circulars Notices | VOE		6756.4 per year	IMPORTANT: this trigger (S190405ar) is not considered to be astrophysical in o issued but the event ID was truncated to S190405a due to a bug. RETRACTED

https://gracedb.ligo.org/superevents/public/O3/

Black holes are now seen at distances up to 3.9 - 6.7 Gpc (redshift 0.9 - 1.6)

Event ID	Possible Source (Probability)	UTC	GCN	Location	FAR	Comments

RETRACTED
Terrestial noise

NSBH (99%)

RETRACTED

Event ID	Possible Source (Probability)	UTC	GCN	Location	FAR	Comments
S190728q	BBH (95%), MassGap (5%)	July 28, 2019 06:45:10 UTC	GCN Circulars Notices | VOE		1 per 1.2541e+15 years	
S190727h	BBH (92%), Terrestrial (5%), MassGap (3%)	July 27, 2019 06:03:33 UTC	GCN Circulars Notices | VOE		1 per 229.92 years	
S190720a	BBH (99%), Terrestrial (1%)	July 20, 2019 00:08:36 UTC	GCN Circulars Notices | VOE		1 per 8.3367 years	
S190718y	Terrestrial (98%), BNS (2%)	July 18, 2019 14:35:12 UTC	GCN Circulars Notices | VOE		1.1514 per year	
S190707q	BBH (>99%)	July 7, 2019 09:33:26 UTC	GCN Circulars Notices | VOE		1 per 6018.9 years	

BBH (99%) at 0.9 < z < 1.6

Event ID	Possible Source (Probability)	UTC	GCN	Location	FAR	Comments
S190701ah	BBH (93%), Terrestrial (7%)	July 1, 2019 20:33:06 UTC	GCN Circulars Notices | VOE		1 per 1.6543 years	
S190630ag	BBH (94%), MassGap (5%)	June 30, 2019 18:52:05 UTC	GCN Circulars Notices | VOE		1 per 2.2077e+05 years	
S190602aq	BBH (99%)	June 2, 2019 17:59:27 UTC	GCN Circulars Notices | VOE		1 per 16.673 years	

RETRACTED

Event ID	Possible Source (Probability)	UTC	GCN	Location	FAR	Comments
S190521r	BBH (>99%)	May 21, 2019 07:43:59 UTC	GCN Circulars Notices | VOE		1 per 100.04 years	
S190521g	BBH (97%), Terrestrial (3%)	May 21, 2019 03:02:29 UTC	GCN Circulars Notices | VOE		1 per 8.3367 years	
S190519bj	BBH (96%), Terrestrial (4%)	May 19, 2019 15:35:44 UTC	GCN Circulars Notices | VOE		1 per 5.5578 years	

RETRACTED

Event ID	Possible Source (Probability)	UTC	GCN	Location	FAR	Comments
S190517h	BBH (98%), MassGap (2%)	May 17, 2019 05:51:01 UTC	GCN Circulars Notices | VOE		1 per 13.354 years	
S190513bm	BBH (94%), MassGap (5%)	May 13, 2019 20:54:28 UTC	GCN Circulars Notices | VOE		1 per 84864 years	
S190512at	BBH (99%), Terrestrial (1%)	May 12, 2019 18:07:14 UTC	GCN Circulars Notices | VOE		1 per 16.673 years	

BNS (42%) TERRESTIAL (58%)

Event ID	Possible Source (Probability)	UTC	GCN	Location	FAR	Comments
S190503bf	BBH (96%), MassGap (3%)	May 3, 2019 18:54:04 UTC	GCN Circulars Notices | VOE		1 per 19.368 years	

BNS (49%) NSBH (13%) M GAP (24%)

BNS (99%)

Event ID	Possible Source (Probability)	UTC	GCN	Location	FAR	Comments
S190421ar	BBH (97%), Terrestrial (3%)	April 21, 2019 21:38:56 UTC	GCN Circulars Notices | VOE		1 per 2.1285 years	
S190412m	BBH (>99%)	April 12, 2019 05:30:44 UTC	GCN Circulars Notices | VOE		1 per 1.883e+19 years	
S190408an	BBH (>99%)	April 8, 2019 18:18:02 UTC	GCN Circulars Notices | VOE		1 per 1.1273e+10 years	

RETRACTED

(S190405ar) is not considered to be astrophysical in o
as truncated to S190405a due to a bug. RETRACTED

GraceDB **Public Alerts** Latest Search Documentation Login

Please log in to view full database contents.

LIGO/Virgo O3 Public Alerts

Detection candidates: 56

https://gracedb.ligo.org/superevents/public/O3/

SORT: EVENT ID (A-Z) ▼

Event ID	Possible Source (Probability)	UTC	GCN	Location	FAR	Comments
S200316bj	MassGap (>99%)	March 16, 2020 21:57:56 UTC	GCN Circulars Notices | VOE	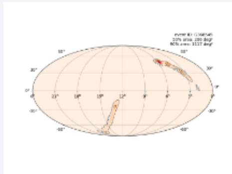	1 per 446.44 years	
S200311bg	BBH (>99%)	March 11, 2020 11:58:53 UTC	GCN Circulars Notices | VOE	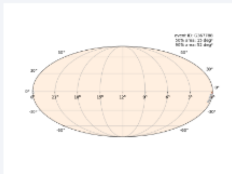	1 per 3.5448e+17 years	
S200308e	NSBH (83%), Terrestrial (17%)	March 8, 2020 01:19:27 UTC	GCN Circulars Notices | VOE	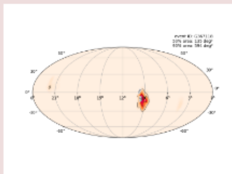	1 per 8.757 years	RETRACTED

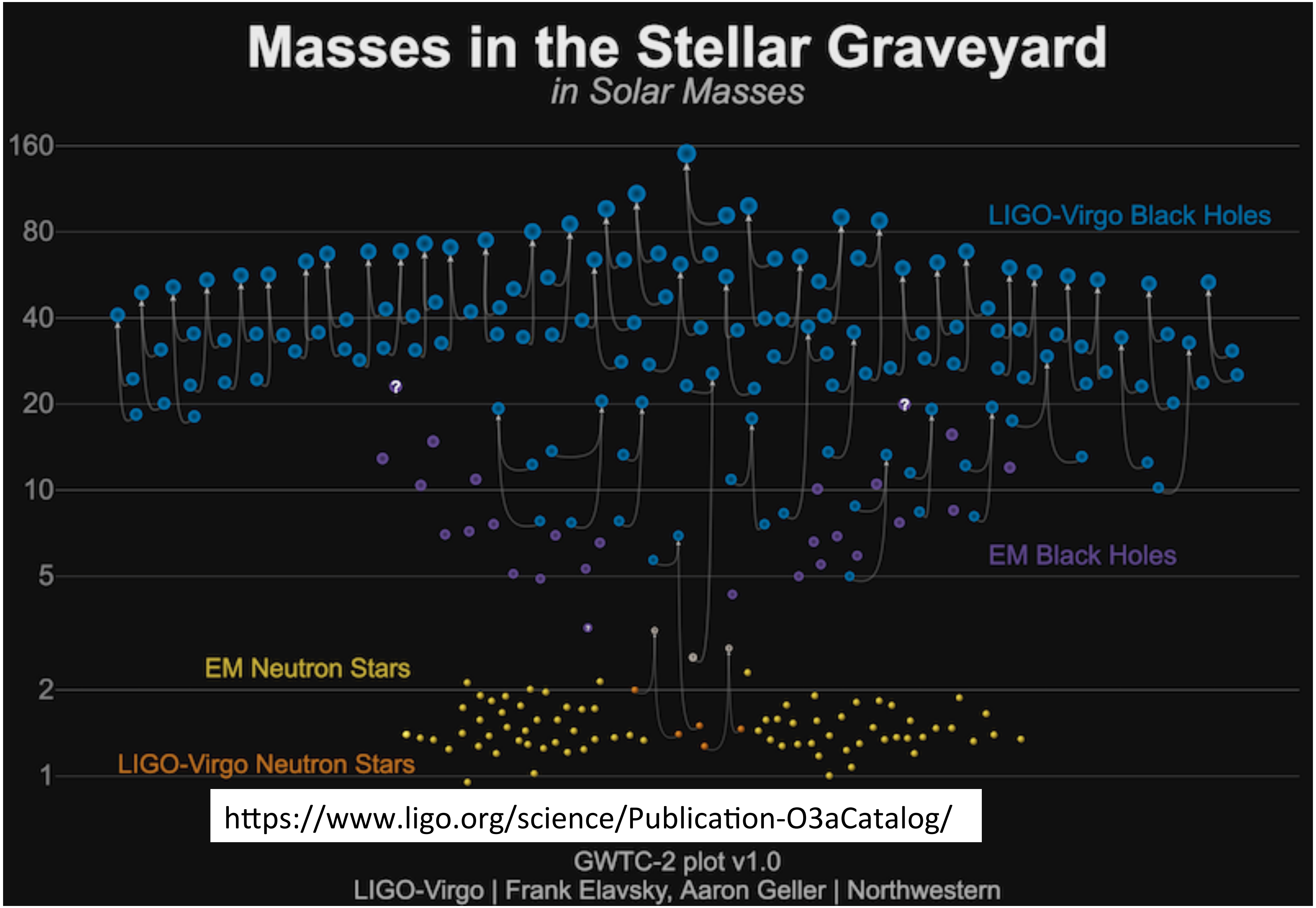
Masses in the Stellar Graveyard
in Solar Masses
160
80
40
20
10
5
2
1
LIGO-Virgo Black Holes
EM Black Holes
EM Neutron Stars
LIGO-Virgo Neutron Stars
https://www.ligo.org/science/Publication-O3aCatalog/
GWTC-2 plot v1.0
LIGO-Virgo | Frank Elavsky, Aaron Geller | Northwestern

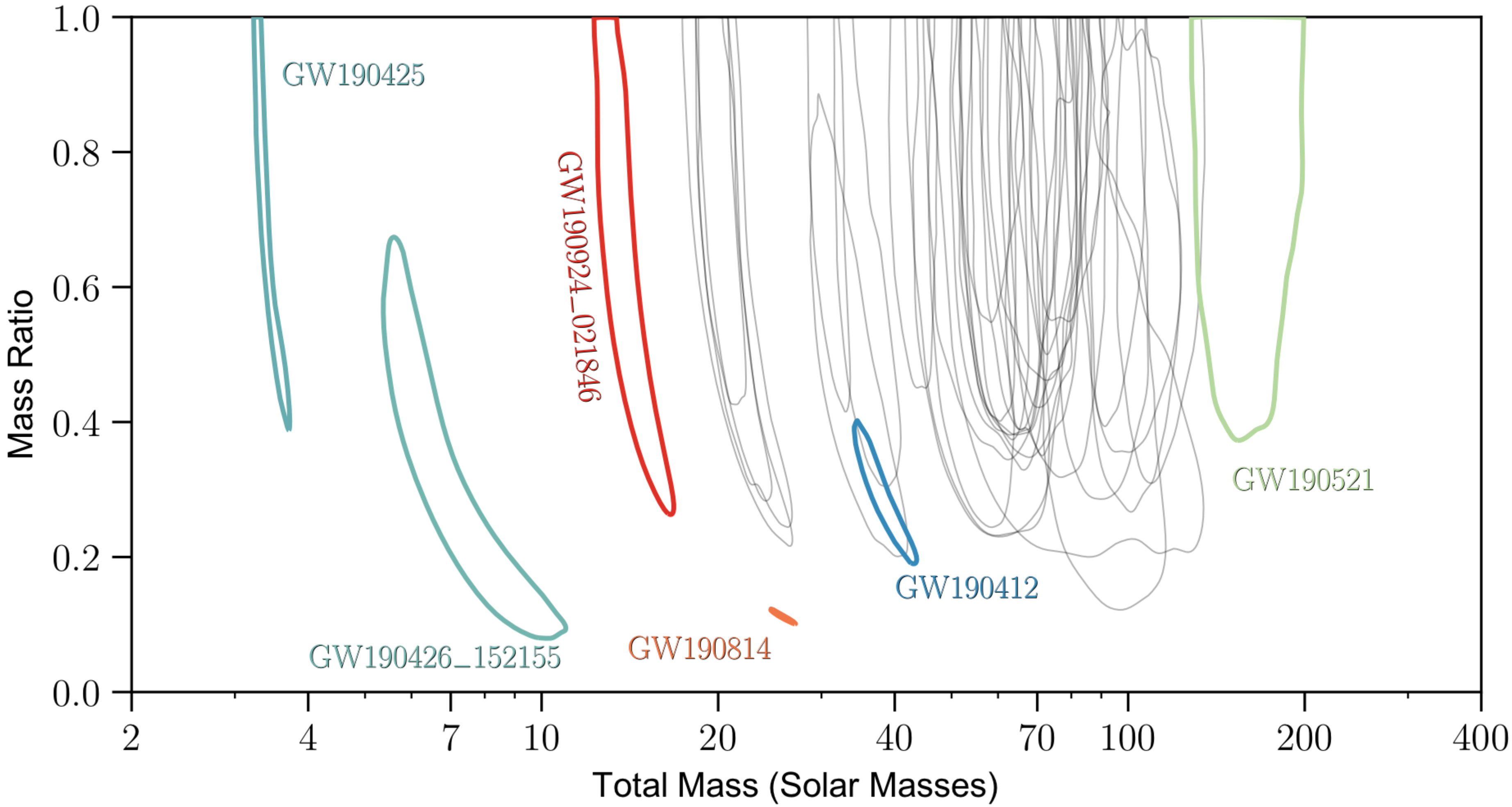

https://www.ligo.org/science/Publication-O3aCatalog/

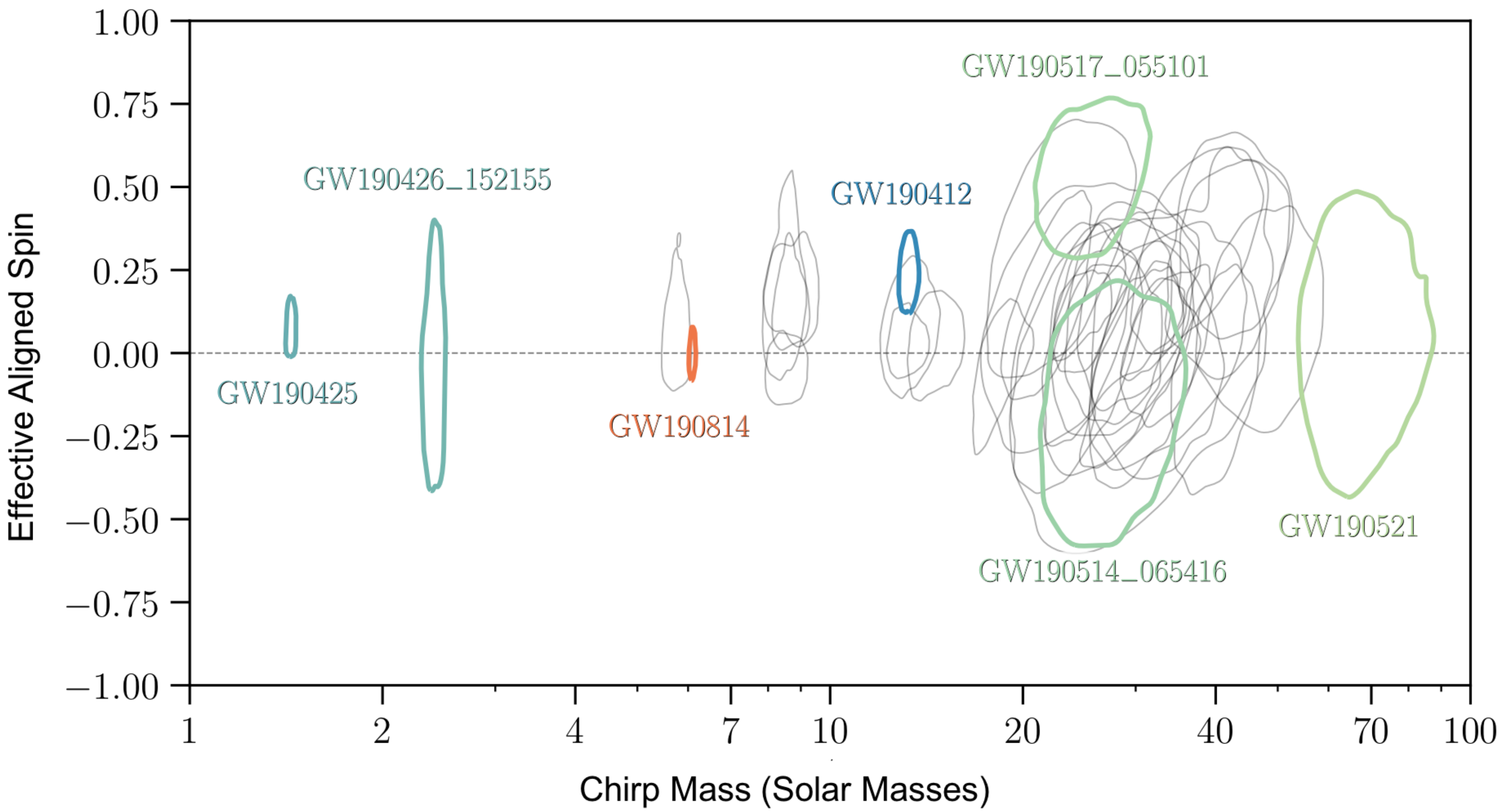

https://www.ligo.org/science/Publication-O3aCatalog/

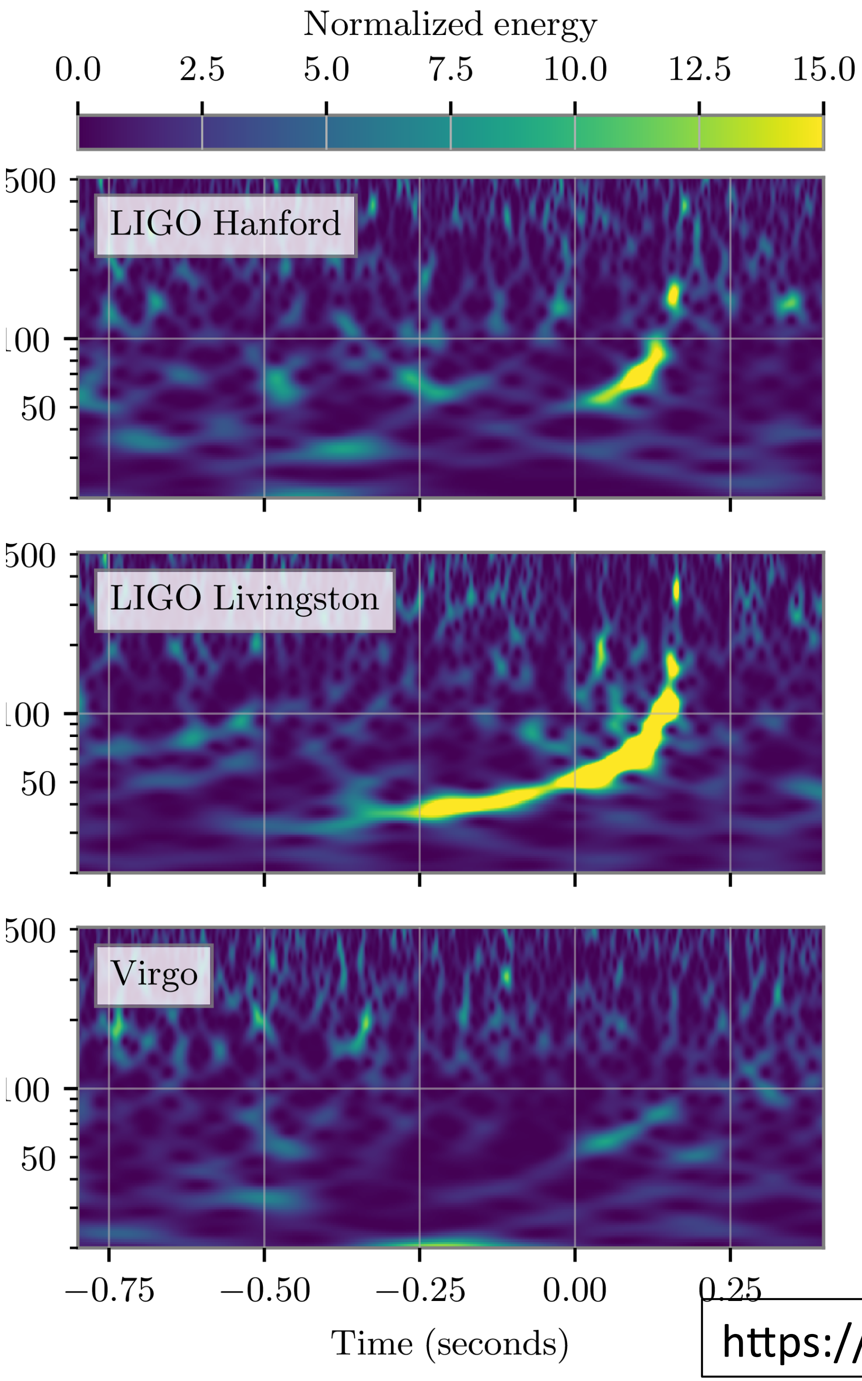

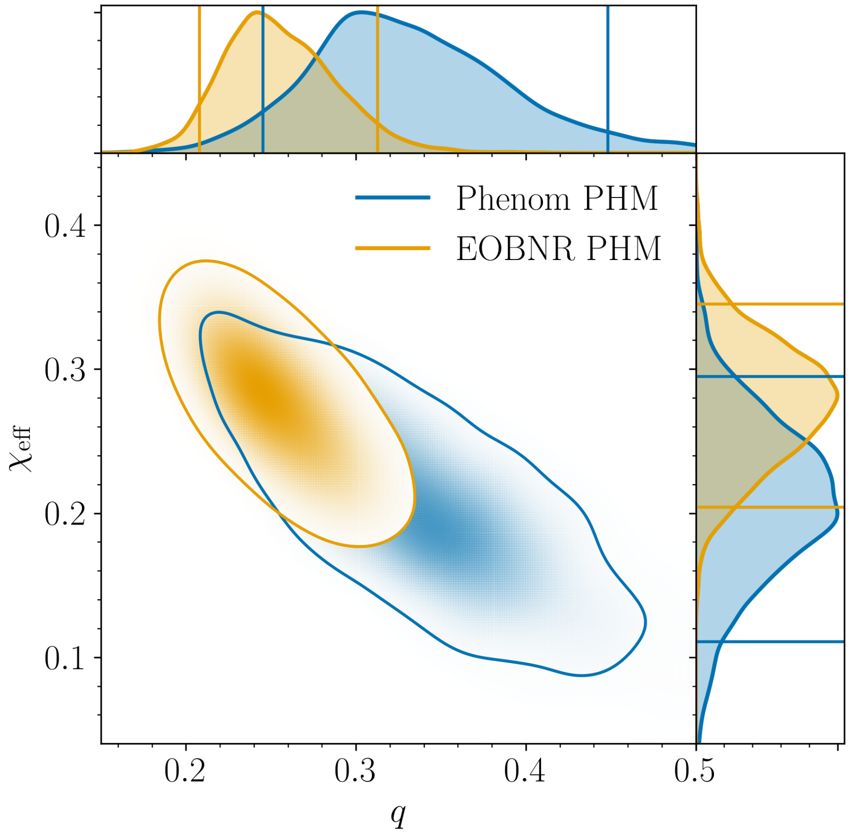

https://www.ligo.org/science/Publication-GW190412/

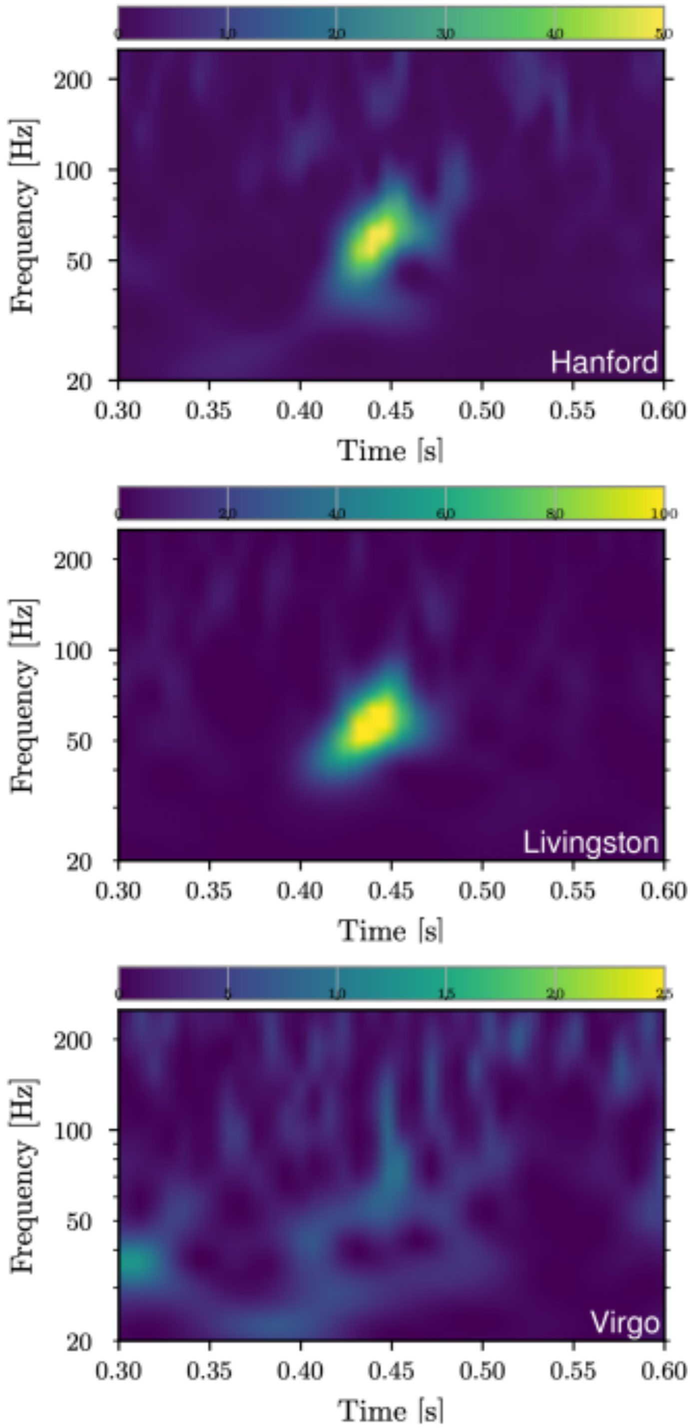

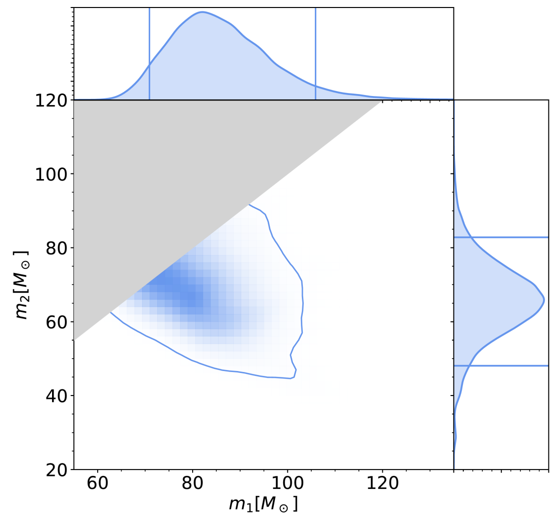

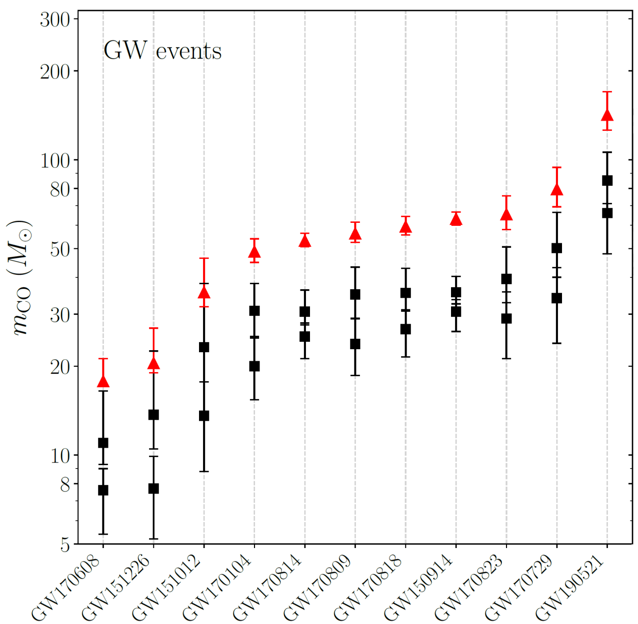

https://www.ligo.org/science/Publication-GW190521/

https://www.ligo.org/science/Publication-GW190425/

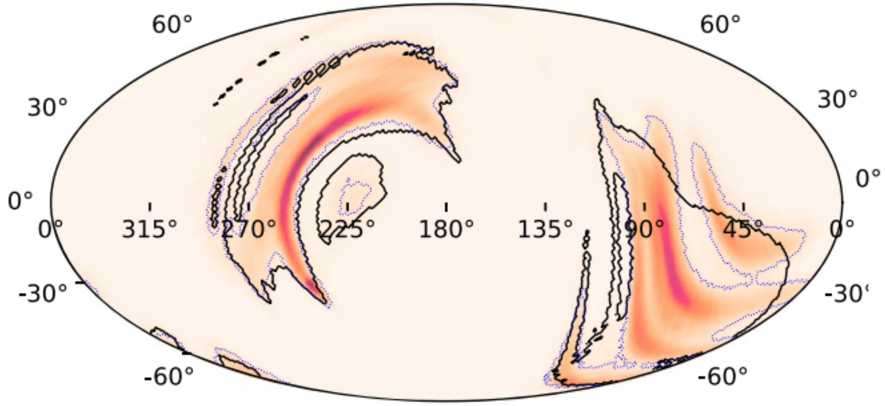

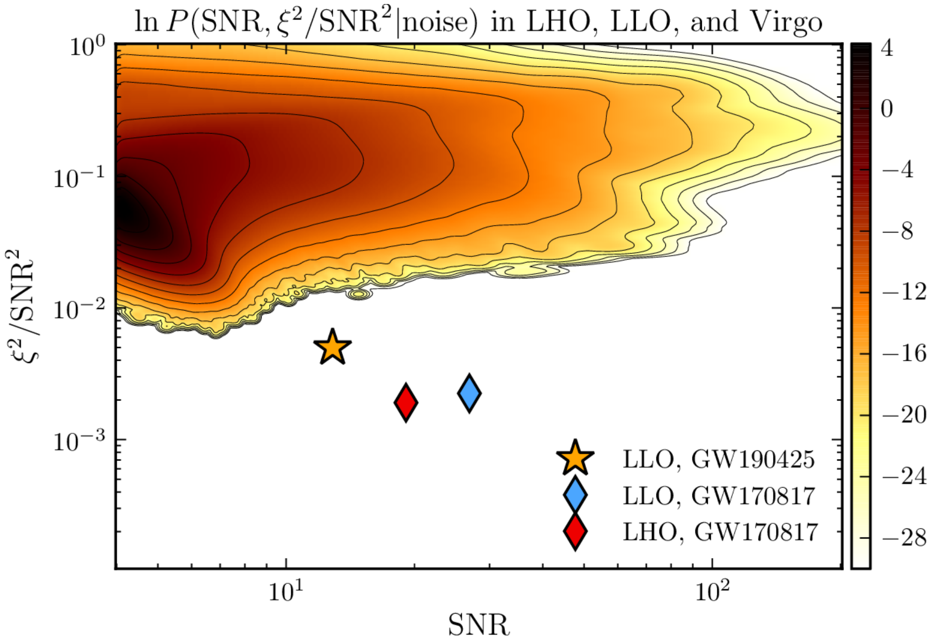

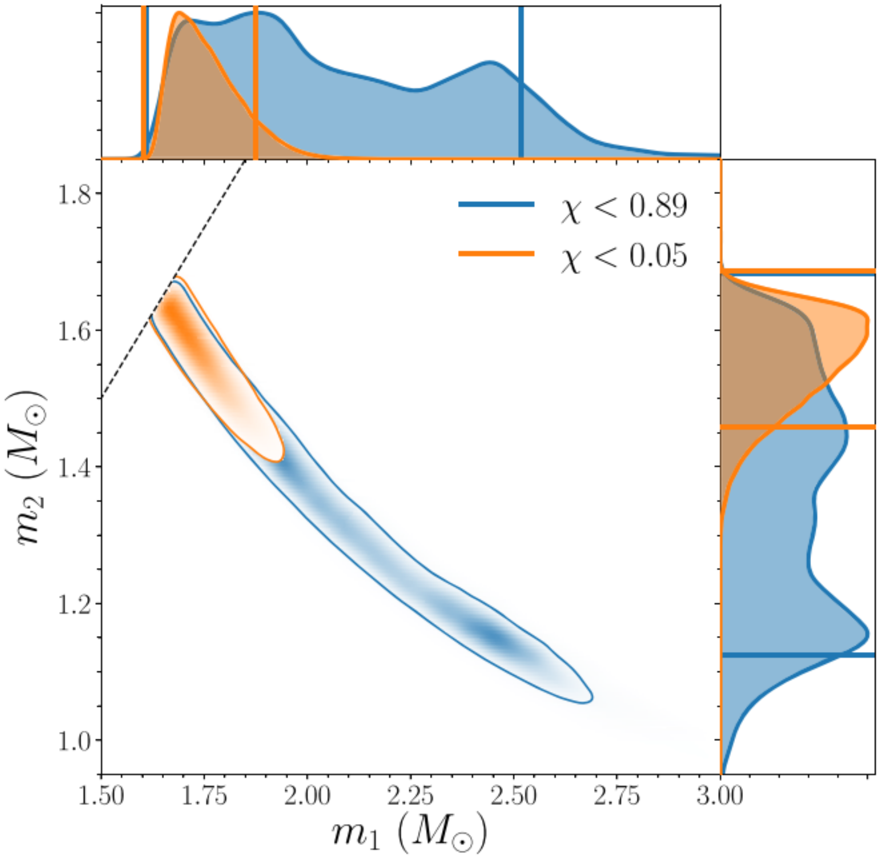

https://www.ligo.org/science/Publication-GW190425/

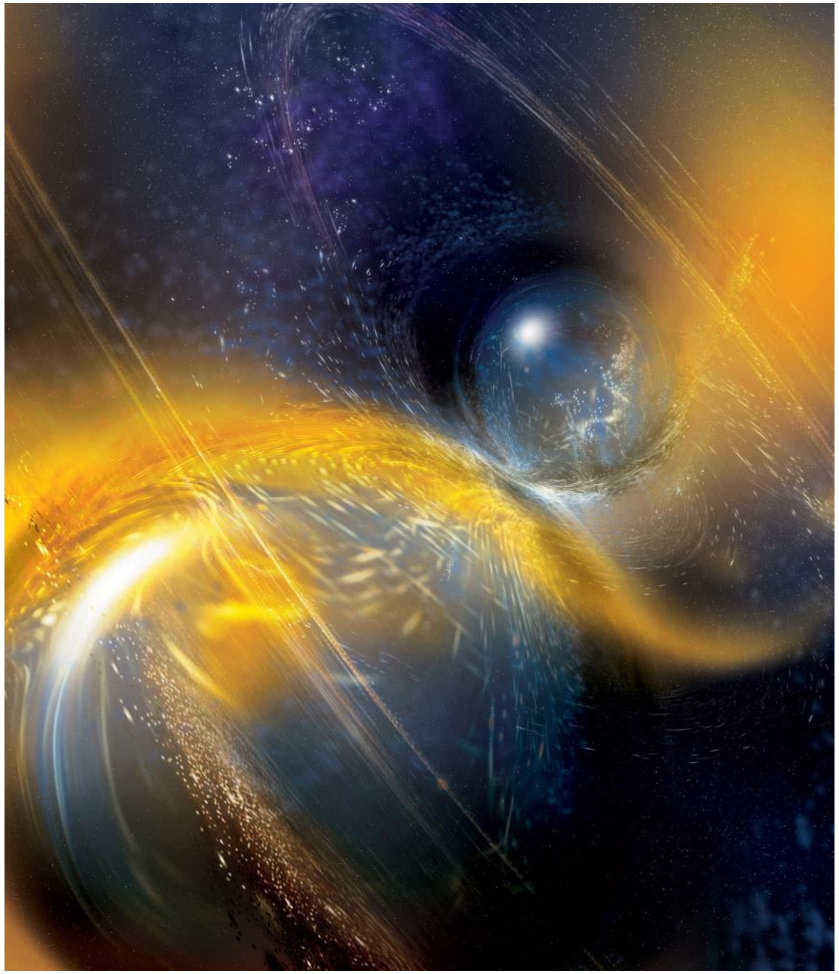

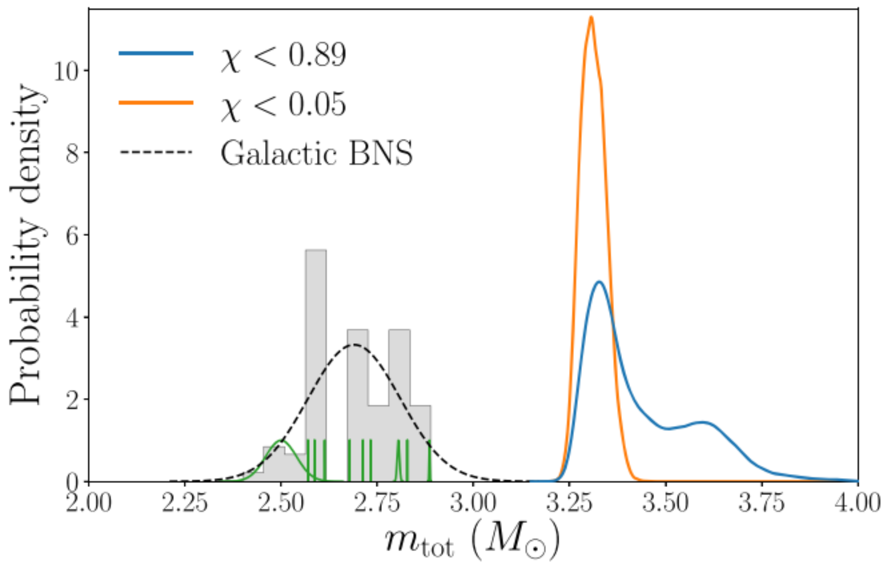

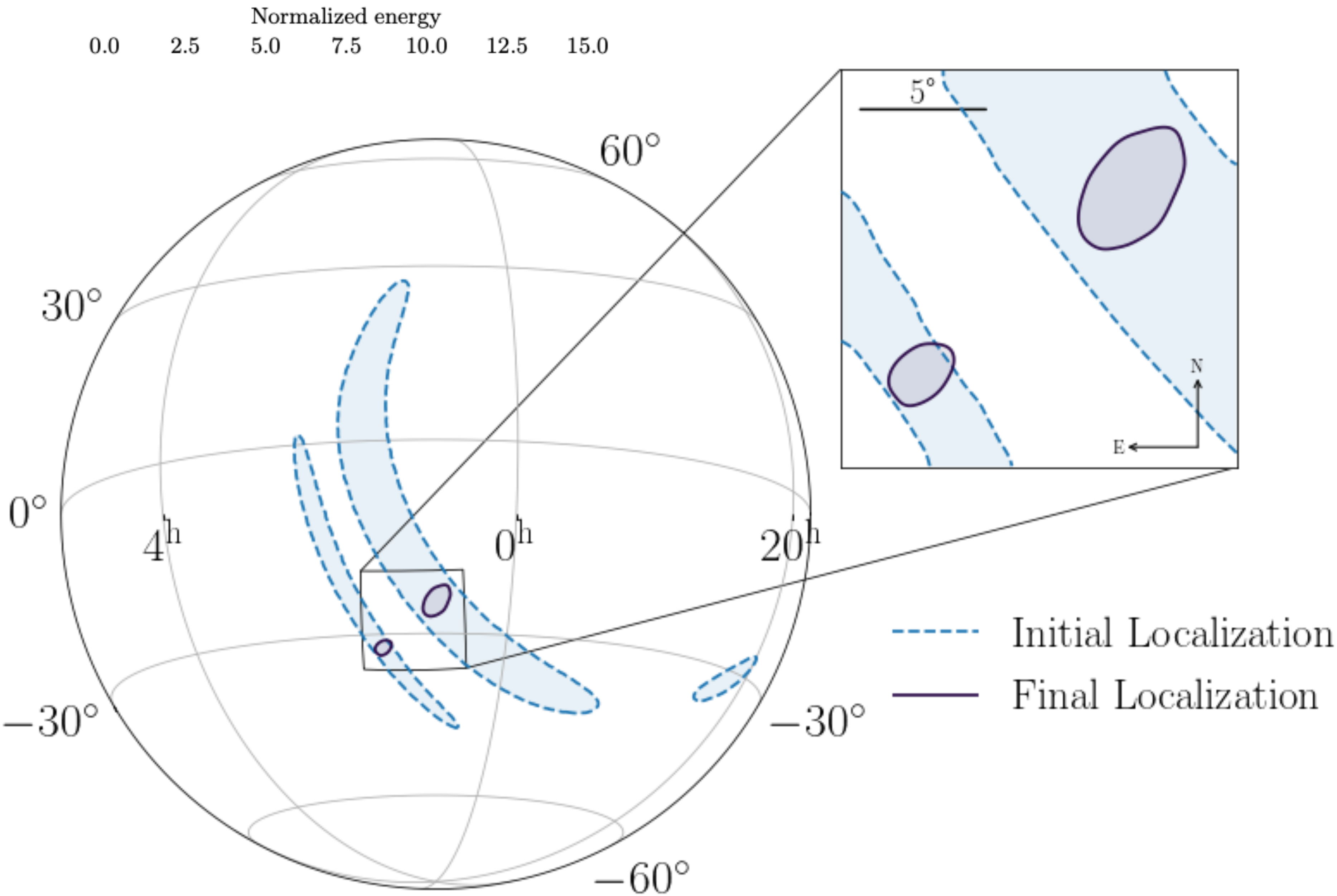

https://www.ligo.org/science/Publication-GW190814/

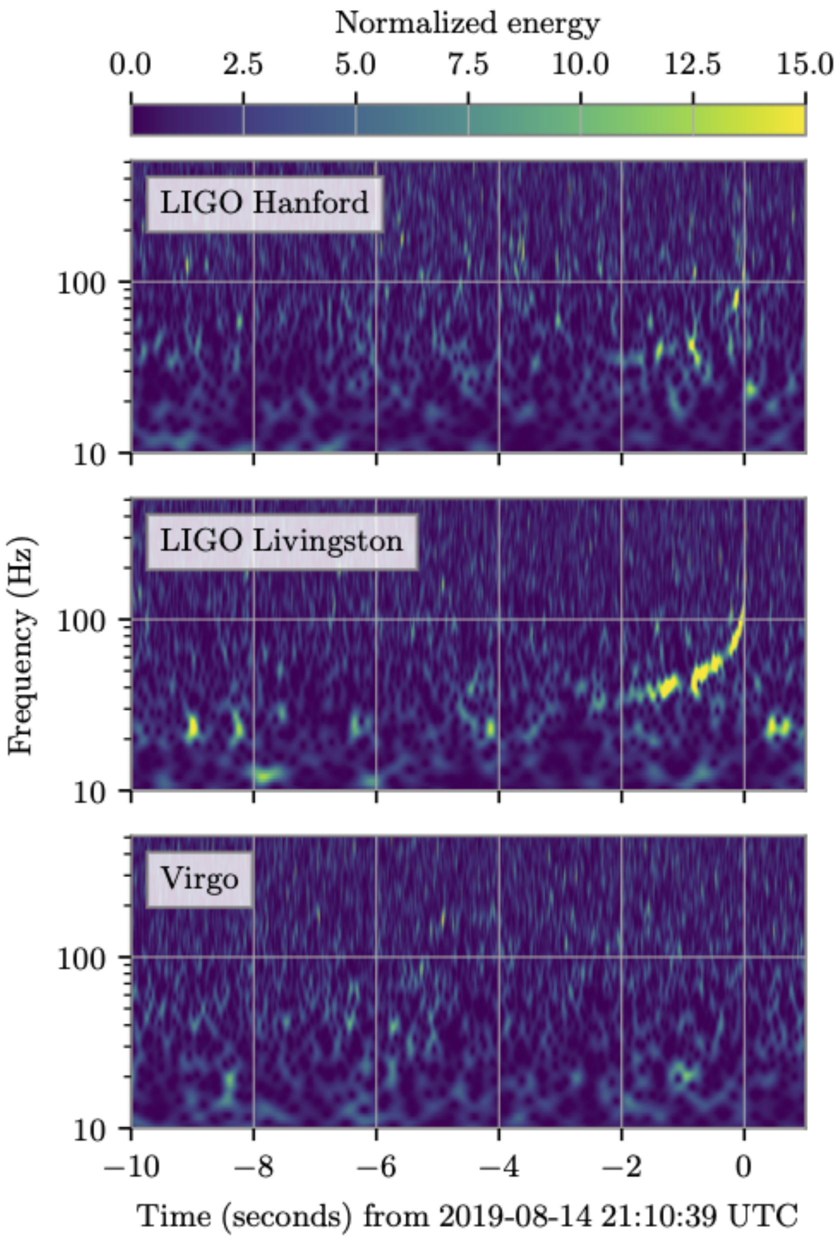

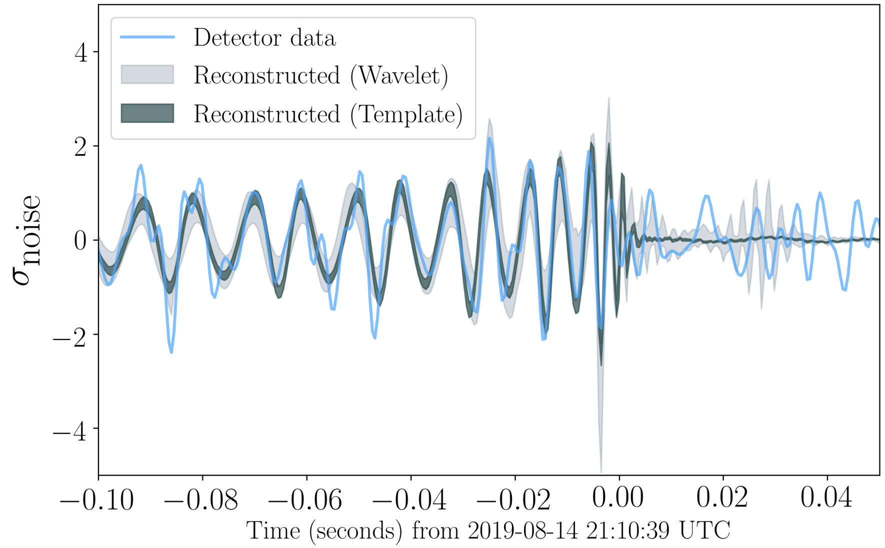

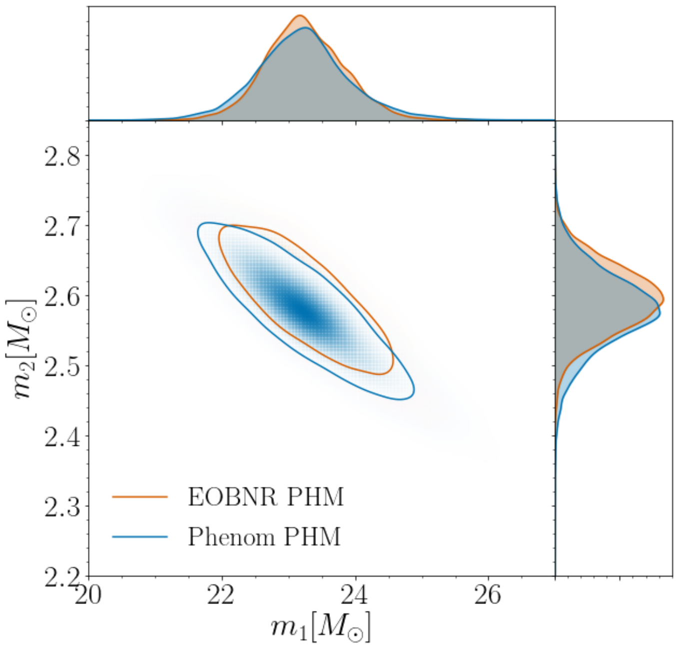

https://www.ligo.org/science/Publication-GW190814/

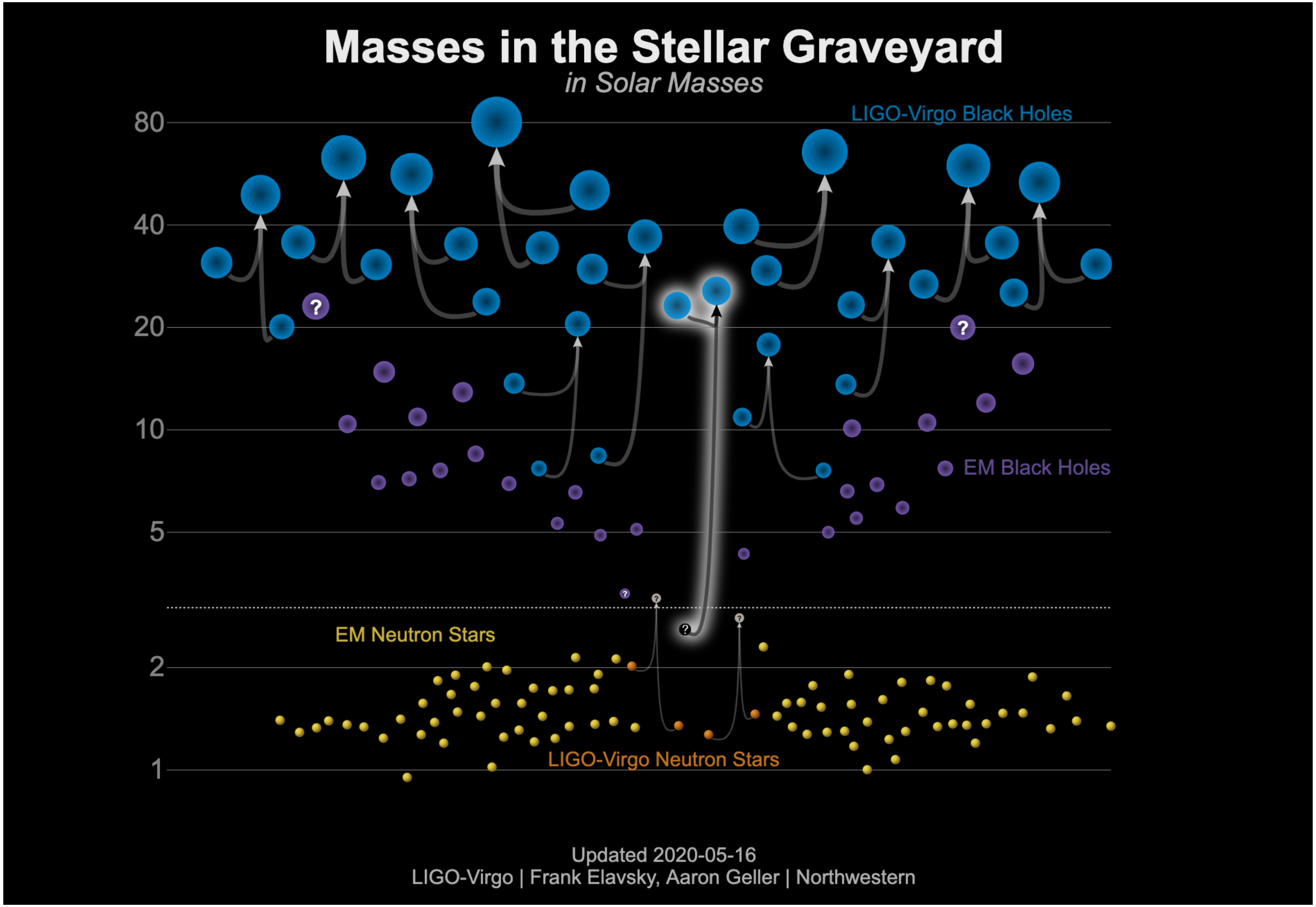
Masses in the Stellar Graveyard
in Solar Masses
LIGO-Virgo Black Holes
EM Black Holes
EM Neutron Stars
LIGO-Virgo Neutron Stars
80
40
20
10
5
2
1
Updated 2020-05-16
LIGO-Virgo | Frank Elavsky, Aaron Geller | Northwestern

LIGO-Virgo analyses for sources of gravitational waves

Sources can be transient or of continuous nature, and can be modeled or unmodeled

Coalescence of Compact Sources

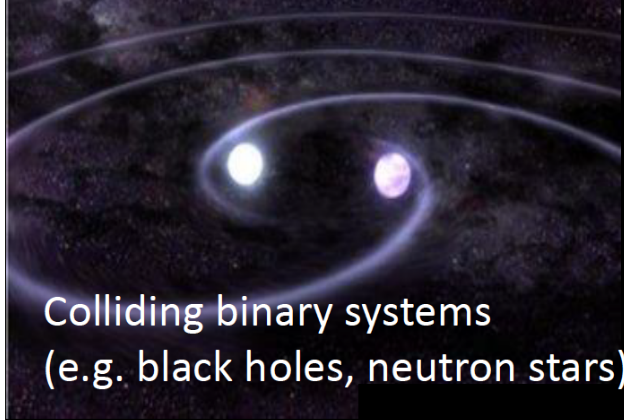

Colliding binary systems
(e.g. black holes, neutron stars)

Continuous Waves

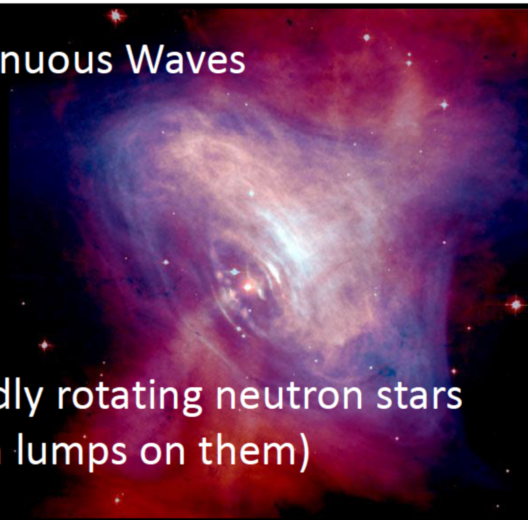

Rapidly rotating neutron stars
(with lumps on them)

Burst

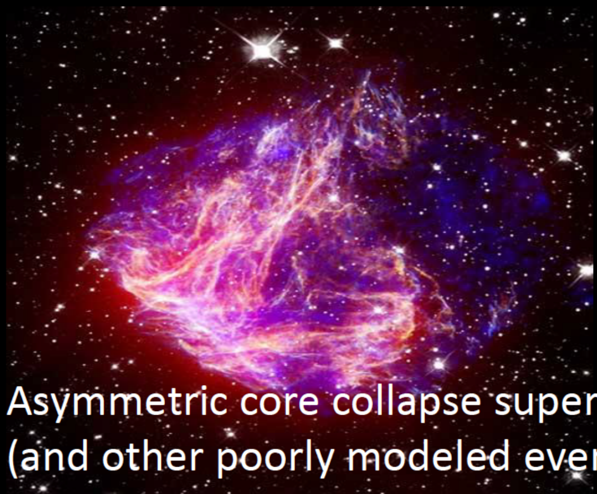

Asymmetric core collapse supernovae
(and other poorly modeled events)

Stochastic

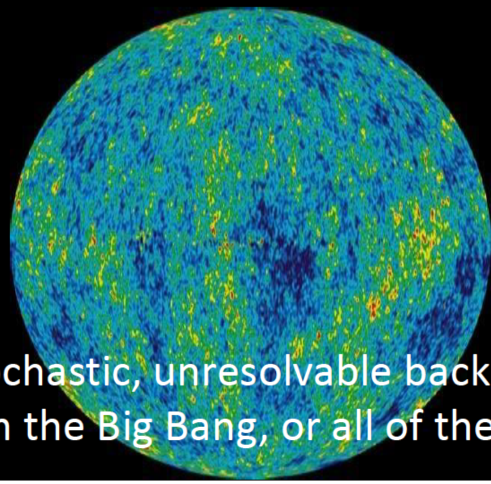

A stochastic, unresolvable background
(from the Big Bang, or all of the above)

Continuous Waves

Astrophysics

More than 2500 observed NSs (mostly pulsars) and O(10^8 –10^9) expected to exist in our galaxy
Sources must have some degree of non-axisymmetry originating from

- deformation due to elastic stresses or magnetic field not aligned to the rotation axis ($f_{GW} = 2f_r$)
- free precession around rotation axis ($f_{GW} \sim f_{rot} + f_{prec}$; $f_{GW} \sim 2f_{rot} + 2f_{prec}$)
- excitation of long-lasting oscillations (e.g. *r*-modes; $f_{GW} \sim 4f_r/3$)
- deformation due to matter accretion (e.g. LMXB; $f_{GW} \sim 2f_r$)

Source characteristics

Emission of quasi-monochromatic waves with a slowly decreasing intrinsic frequency
Constant amplitude, but weak, and persistent over years of data taking

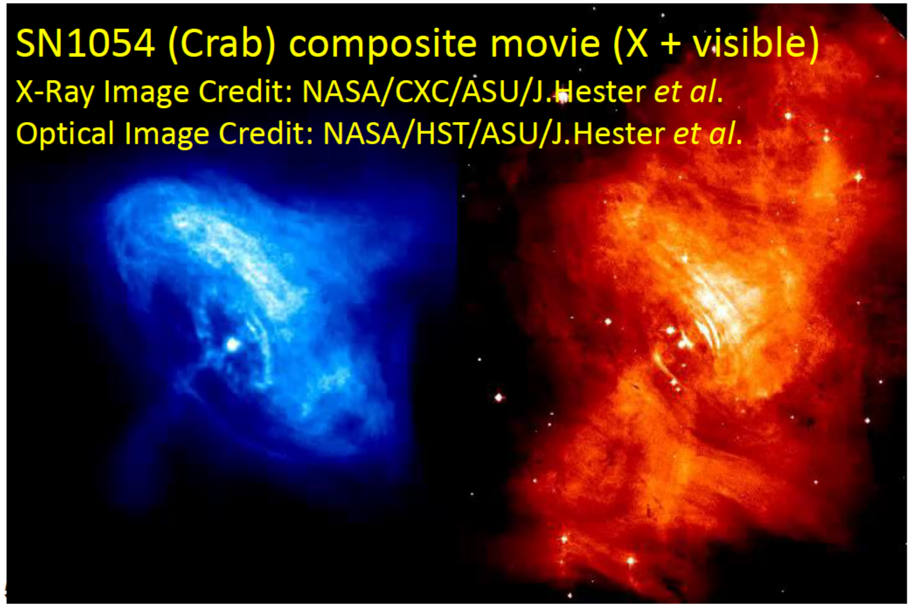

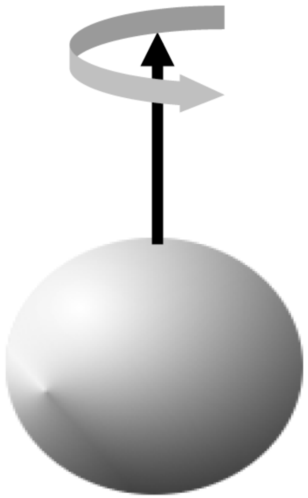

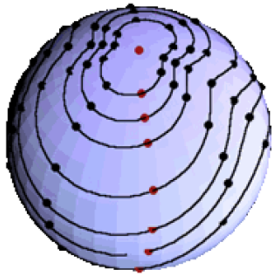

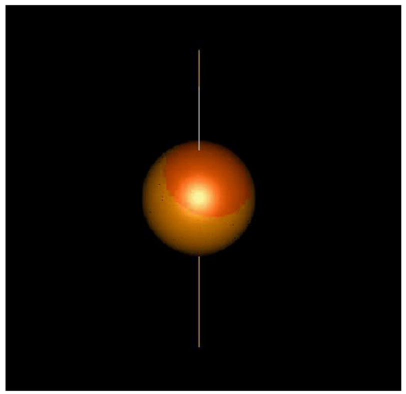

Continuous Waves analysis

Types of Continuous Waves searches

- Targeted searches: observed NSs with known source parameters as sky location, frequency & frequency derivatives (e.g. the Crab and Vela pulsars)
- Narrowband searches: observed NSs with uncertainties in rotational parameters. A small mismatch between the GW frequency (spindown) and the rotational star frequency (spindown) inferred from EM observations needs to be taken into account
- Directed searches: sky location is known while frequency and frequency derivatives are unknown (e.g. Cassiopeia A, SN1987A, Scorpius X-1, galactic center, globular clusters)
- All-sky searches: unknown pulsars => computing challenge (Einstein@Home – Cloud – Grid)

Papers

- First search for gravitational waves from known pulsars (LVC, ApJ 839, 12, 2017)
  - Analyzed 200 known pulsars (119 out of 200 are in binary systems)
  - Spindown limit beaten for 8 pulsars, including both Crab & Vela: For the Crab and Vela pulsars less than 2x10-3 and 10-2 of the spindown luminosity is being lost via GWs, respectively
- Narrowband search: LVC, PRD 96, 122006 (2017)
- Directed searches from Scorpius-X1 (LVC 2017: PRD 95, 122003; ApJ 847, 47, PRL 118, 121102)
- All-sky searches up to high frequencies (LVC, PRD 97, 102003, 2018)
- All-sky searches at low frequencies LVC, PRD 96, 122004, 2018)
- Search for non-tensorial polarizations (LVC, PRL 120, 031104, 2018)

Still to come: O2 results from targeted, narrowband, directed and all-sky searches

- See https://galaxy.ligo.caltech.edu/svn/cw/public/index.html

Stochastic GW Background

A stochastic background of gravitational waves has resulted from the superposition of a large number of independent unresolved sources from different stages in the evolution of the Universe

Astrophysical SGWB

All the sources since the beginning of stellar activity
Dominated by compact binary coalescences: BBHs, BNSs, BH-NSs

LIGO and Virgo have already published 10 BBHs and 1 BNS
Events are individual sources at z~0.07-0.2 for BBHs, 0.01 for BNS

Many individual sources at larger distances that contribute to SGWB
This could be the next milestone for LIGO/Virgo

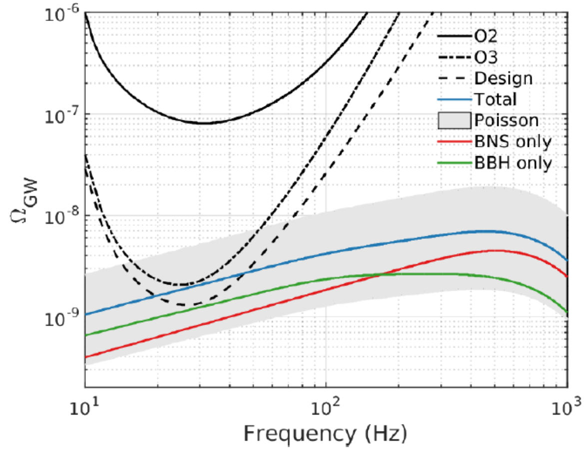

Abbott et al. PRL120.091101, 2017

Cosmological SGWB

Signatures of the early Universe
Inflation, cosmic strings, no phase transition in LIGO/Virgo

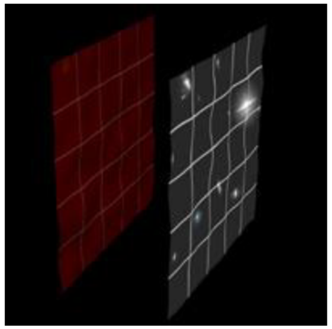

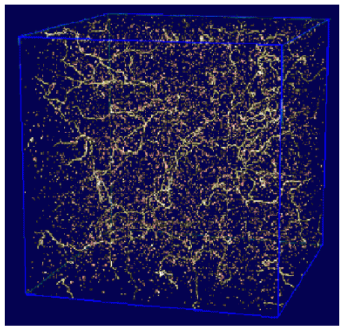

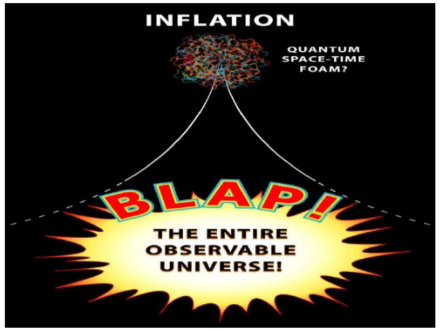

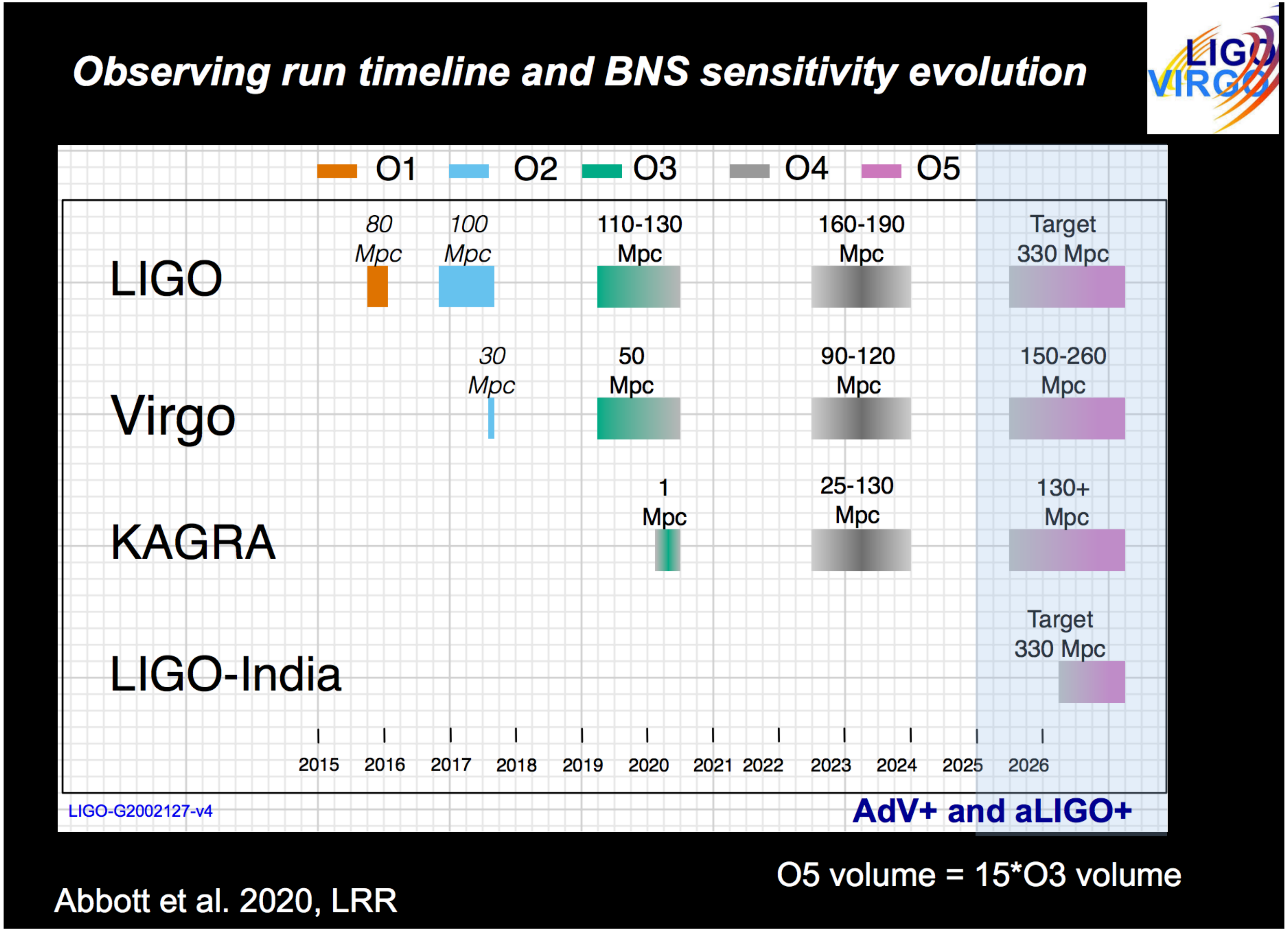

Branchesi 2021 (Theseus conference)


KAGRA inauguration
Signing of the MOA with LIGO and VIRGO
Toyama, October 4, 2019

Einstein Telescope and Cosmic Explorer

Realizing the next gravitational wave observatories is a coordinated effort with US to create a worldwide 3G network

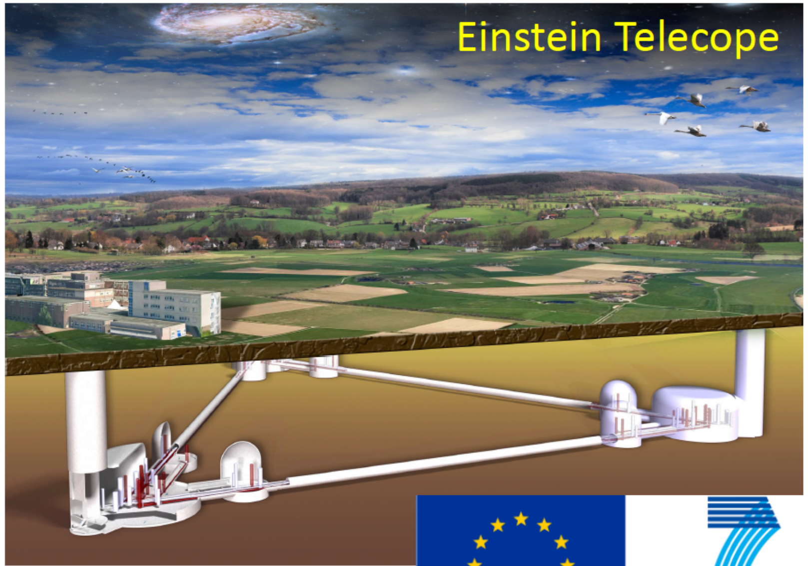

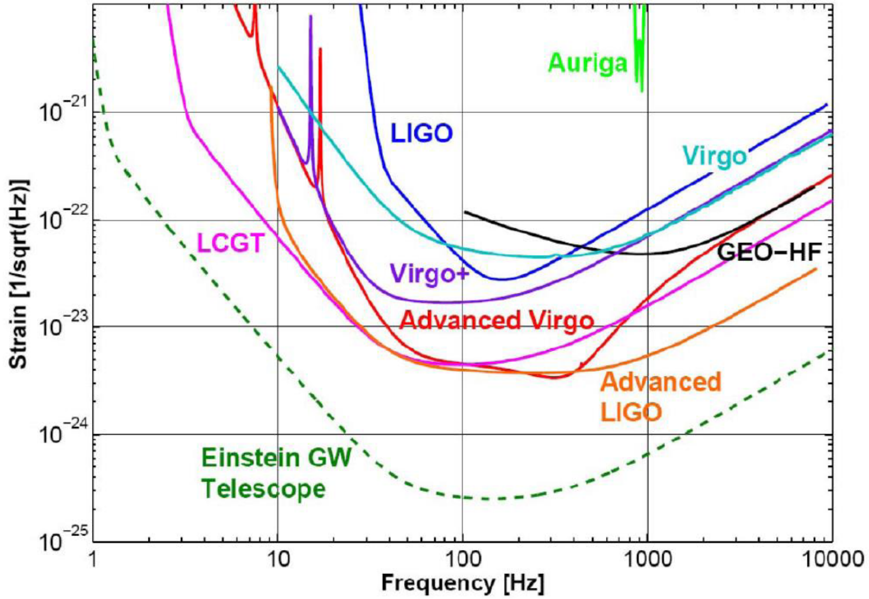

SEVENTH FRAMEWORK PROGRAMME

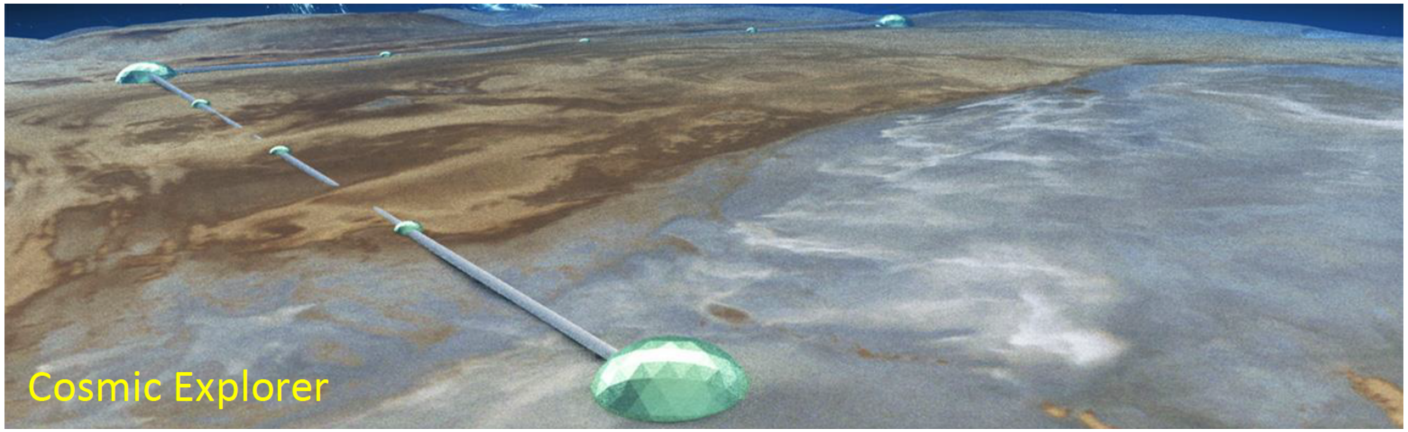

Einstein Telescope and Cosmic Explorer

Einstein Telescope will feature excellent low-frequency sensitivity and have great discovery potential

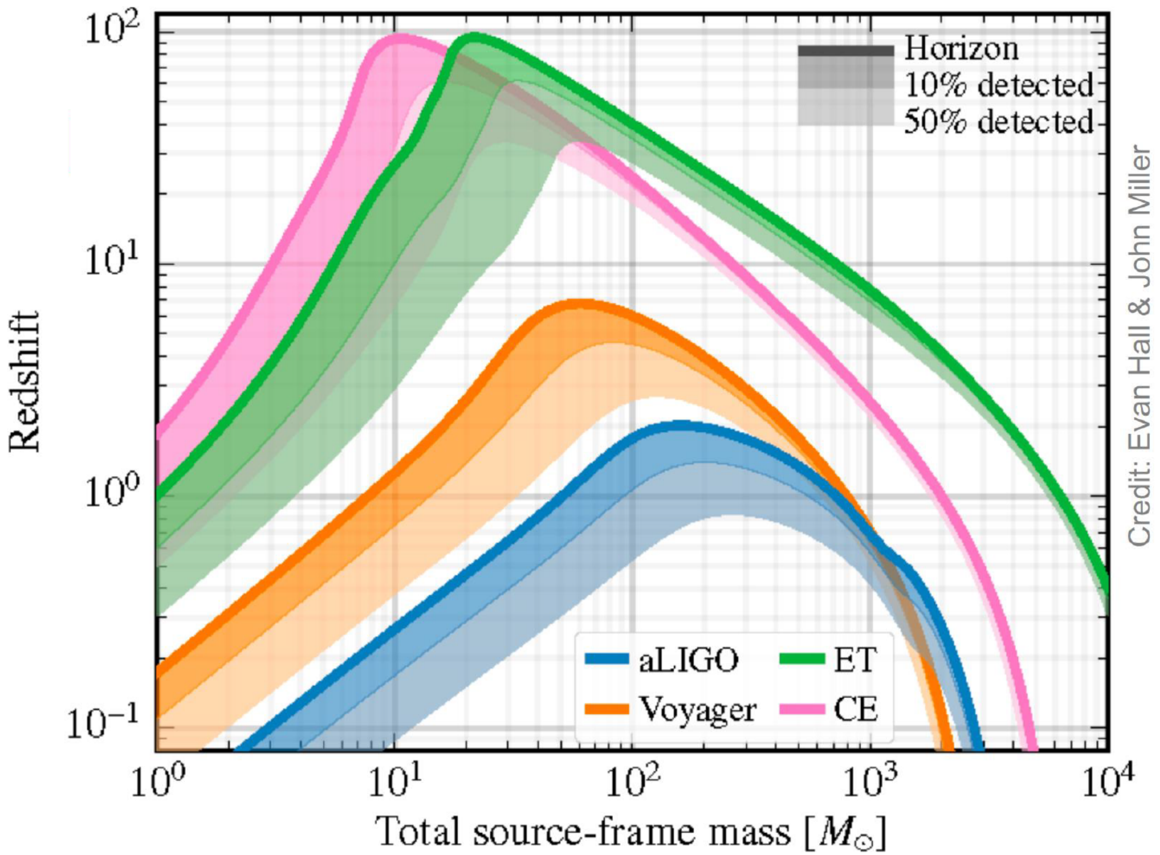

For science case, see https://www.dropbox.com/s/gihpzcue4qd92dt/science-case.pdf?dl=0

Einstein Telescope

Einstein Telescope can observe BBH mergers to red shifts of about 100. This allows a new approach to cosmography. Study primordial black holes, BH from population III stars (first metal producers), *etc*.

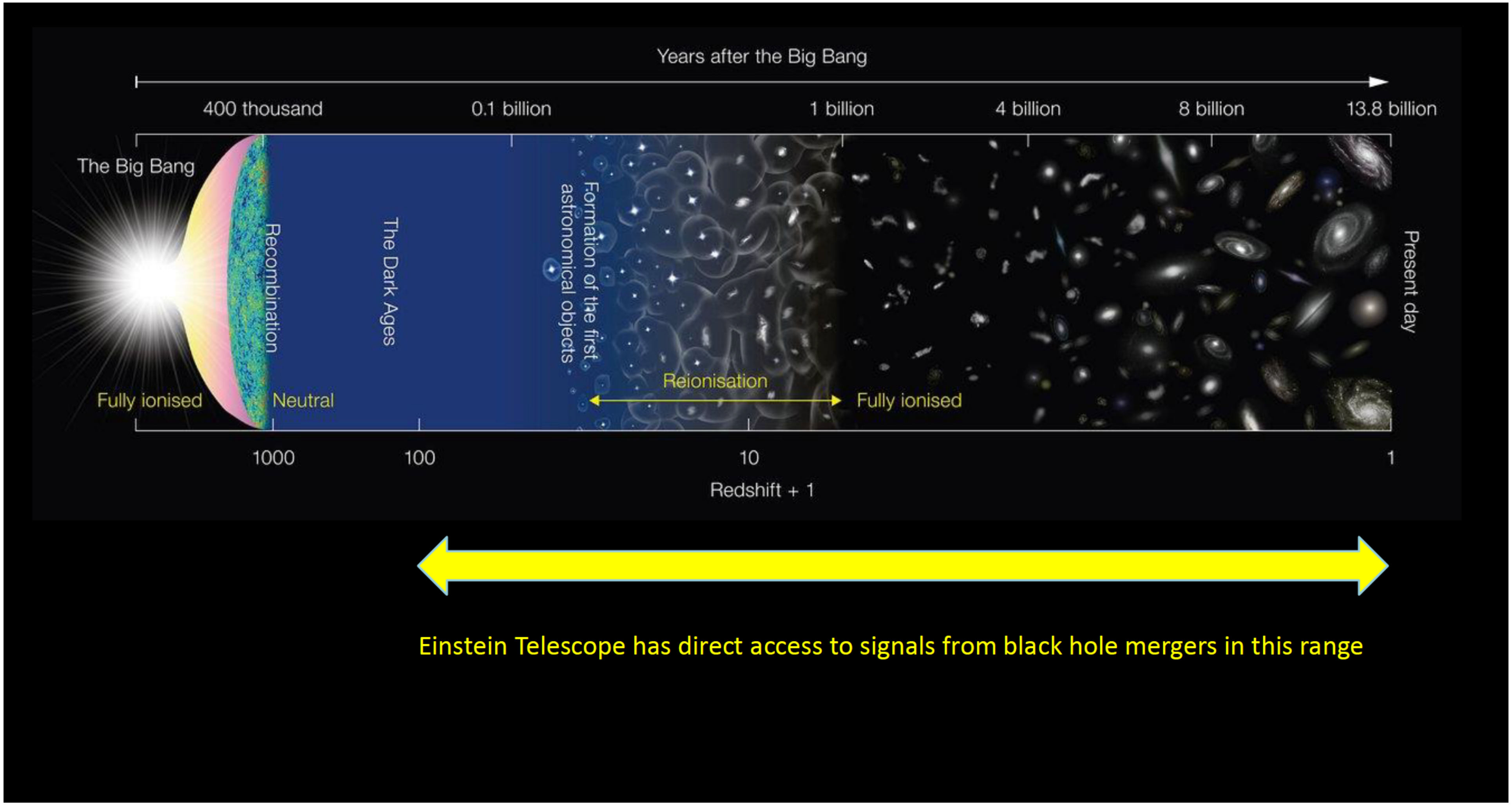

Einstein Telescope: an infrastructure for 50 to 100 years

ET will study events from the entire Universe. Gravitational waves will become a common tool just like conventional astronomy has been for the last four centuries

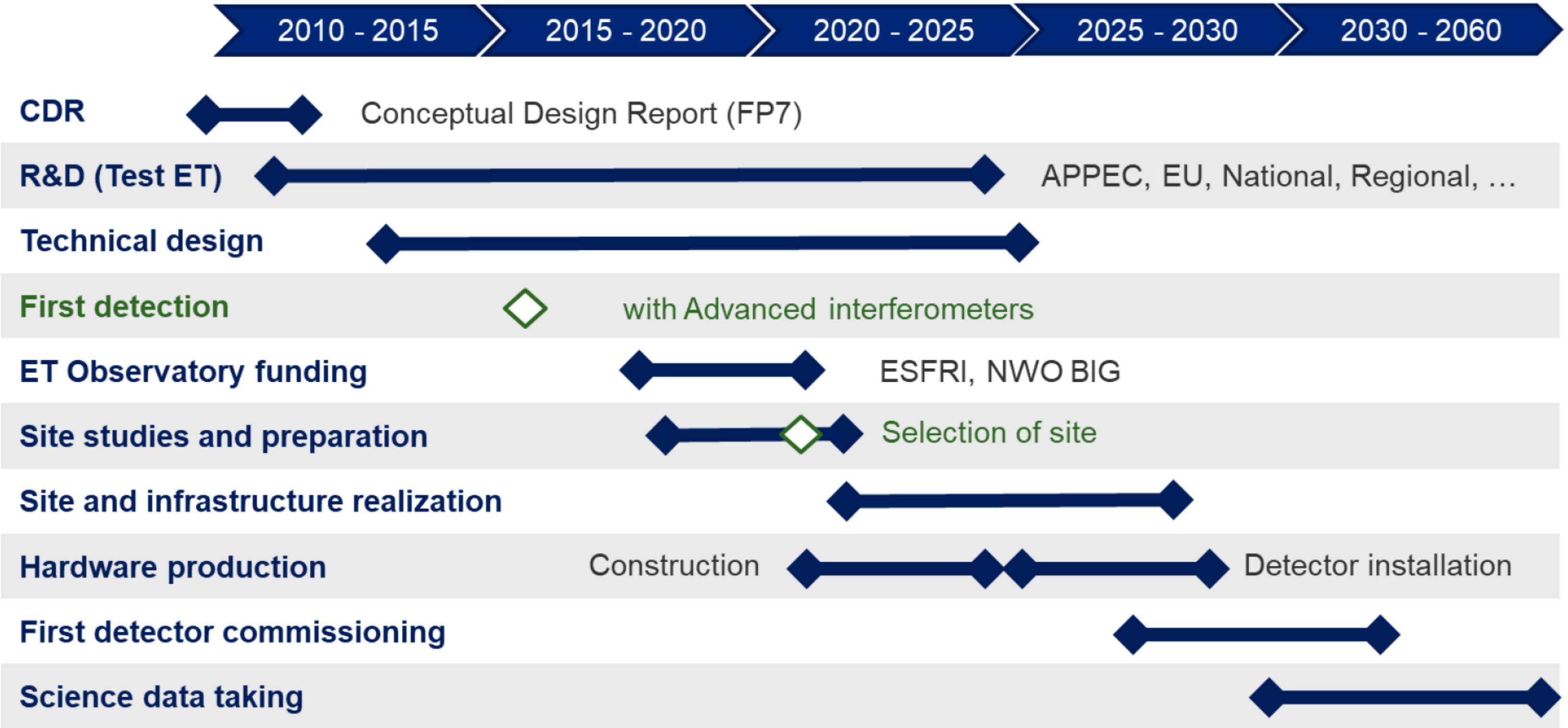

Einstein Telescope: cosmography

What is this mysterious dark energy that is tearing the Universe apart?
Use BNS and BBH as standard “candles” (so-called “sirens”)

Einstein Telescope: fundamental physics

What happened at the edge of a black hole?
Is Einstein's theory correct in conditions of extreme gravitation? Of does new physics await?

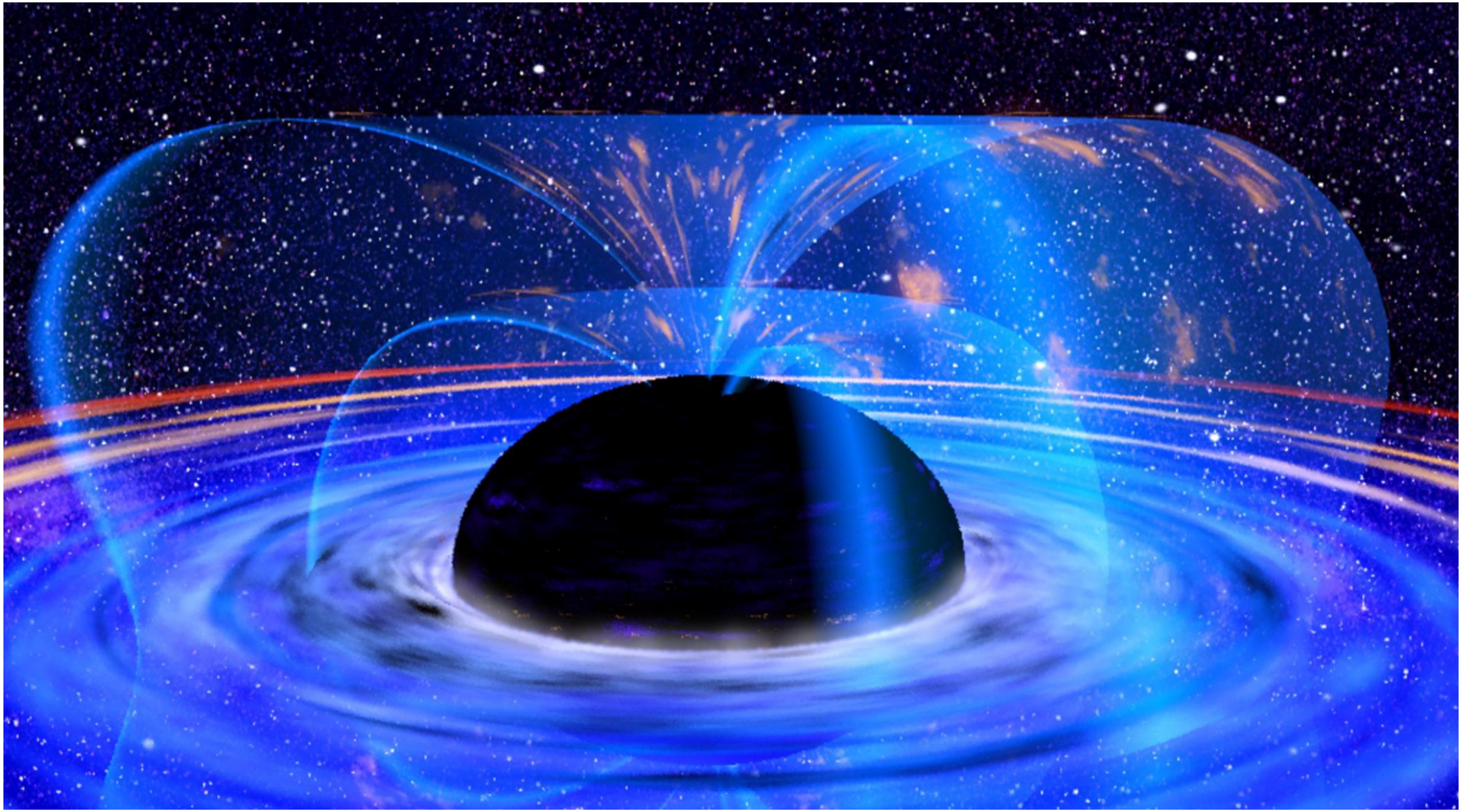

Observe intermediate-mass black holes

Globular clusters may host intermediate-mass black holes (IMBHs) with masses in the range 100 to 1000 solar masses

IMBH will be the most massive object in the cluster and will readily sink to the center

Binary with a compact-object companion will form. The binary will then harden through three-body interactions

Binary will eventually merge via an intermediate-mass-ratio inspiral (IMRI)

The number of detectable mergers depends on the unknown distribution of IMBH masses and their typical companions. Detect 300 events per year out to z = 1:5 for 100M (redshifted) primaries and 10M secondaries

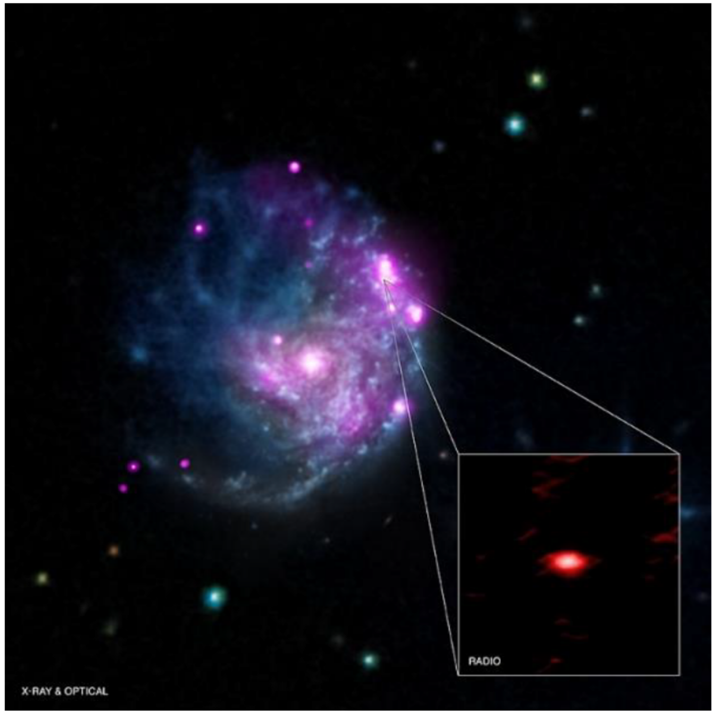

NGC 2276-3c: NASA's Chandra Finds Intriguing Member of Black Hole Family Tree
http://chandra.harvard.edu/photo/2015/ngc2276/

Provide early warning alerts hours in advance

A BNS system will stay in ET's sensitivity band for nearly 20 hours starting from 2 Hz, and a little less than 2 hours starting from 5 Hz. For the same lower frequency limits the duration of a BBH signal from a pair of 10 M BHs is 45 minutes and 4 minutes

It is of great importance to study spin-precession effects. Modulations encode the parameters of sources such as their masses, spins, and inclination of the orbit

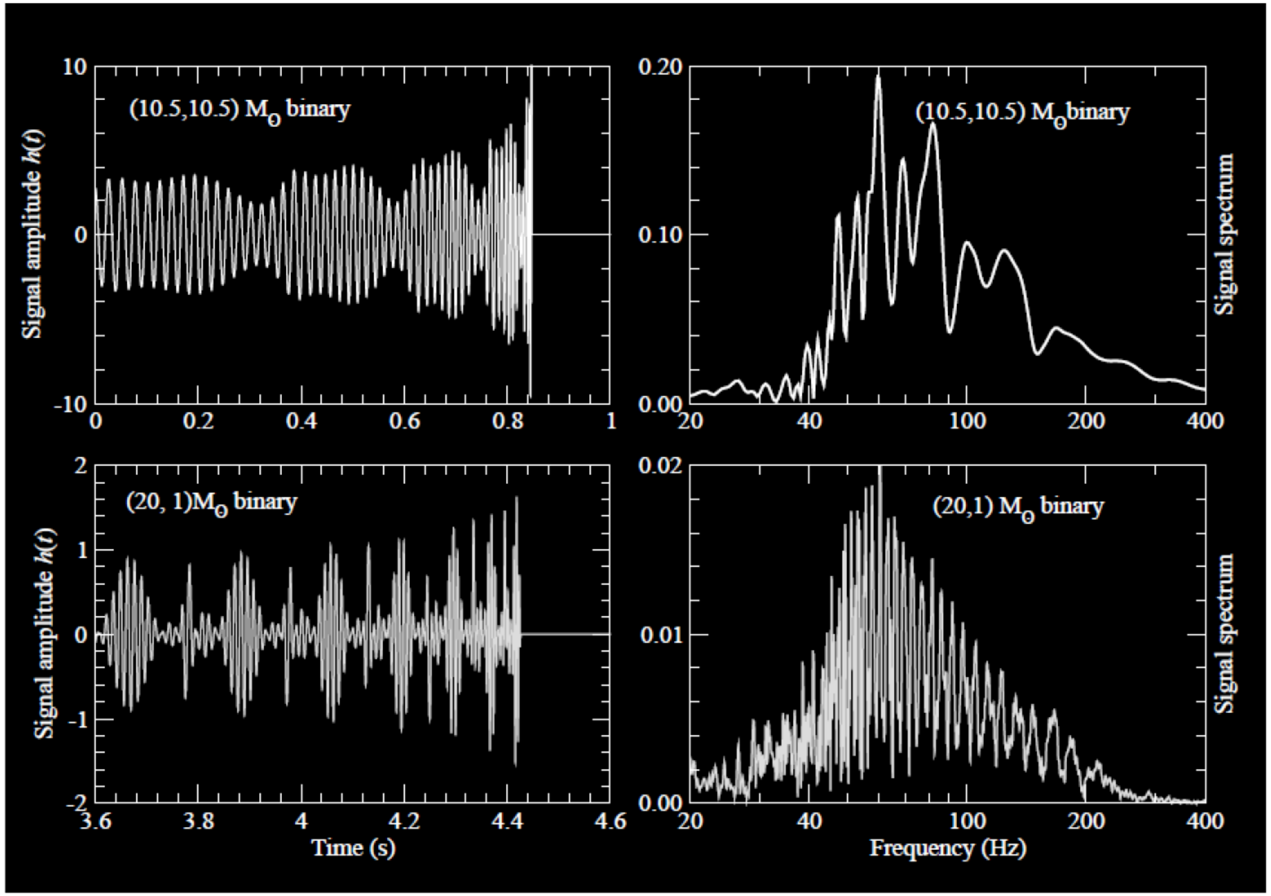

Physics of supernovae

Study progenitor mass, proto neutron star (NS) core oscillations, core rotation rate, mass accretion rate from shock, geometry of core collapse, effects of NS Equation of State, fate of collapse: NS or BH

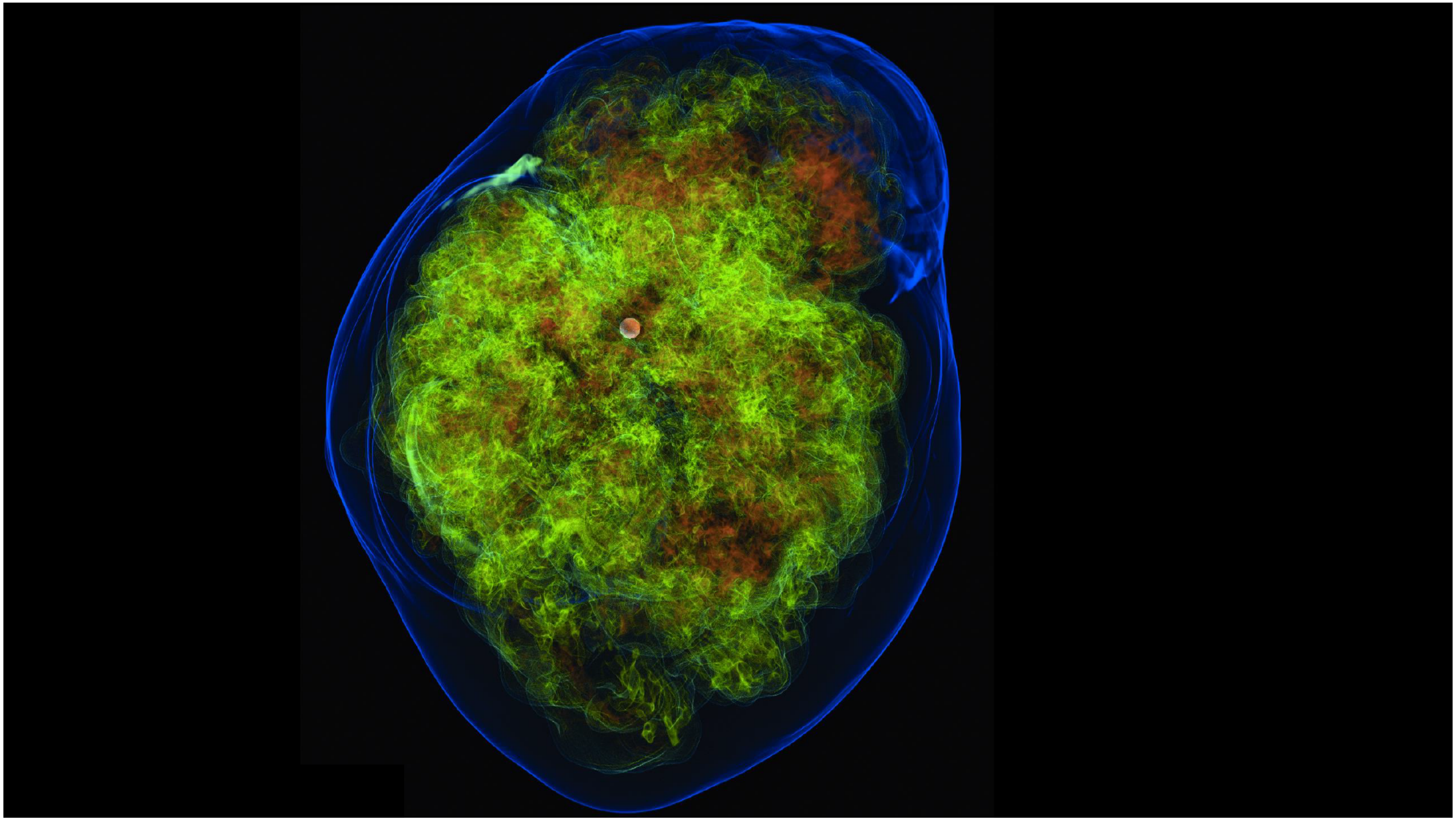

Physics of neutron stars

Deformation due to elastic stresses or magnetic field not aligned to the rotation axis, free precession around rotation axis, excitation of long-lasting oscillations (e.g. *r*-modes), deformation due to matter accretion (e.g. LMXB)

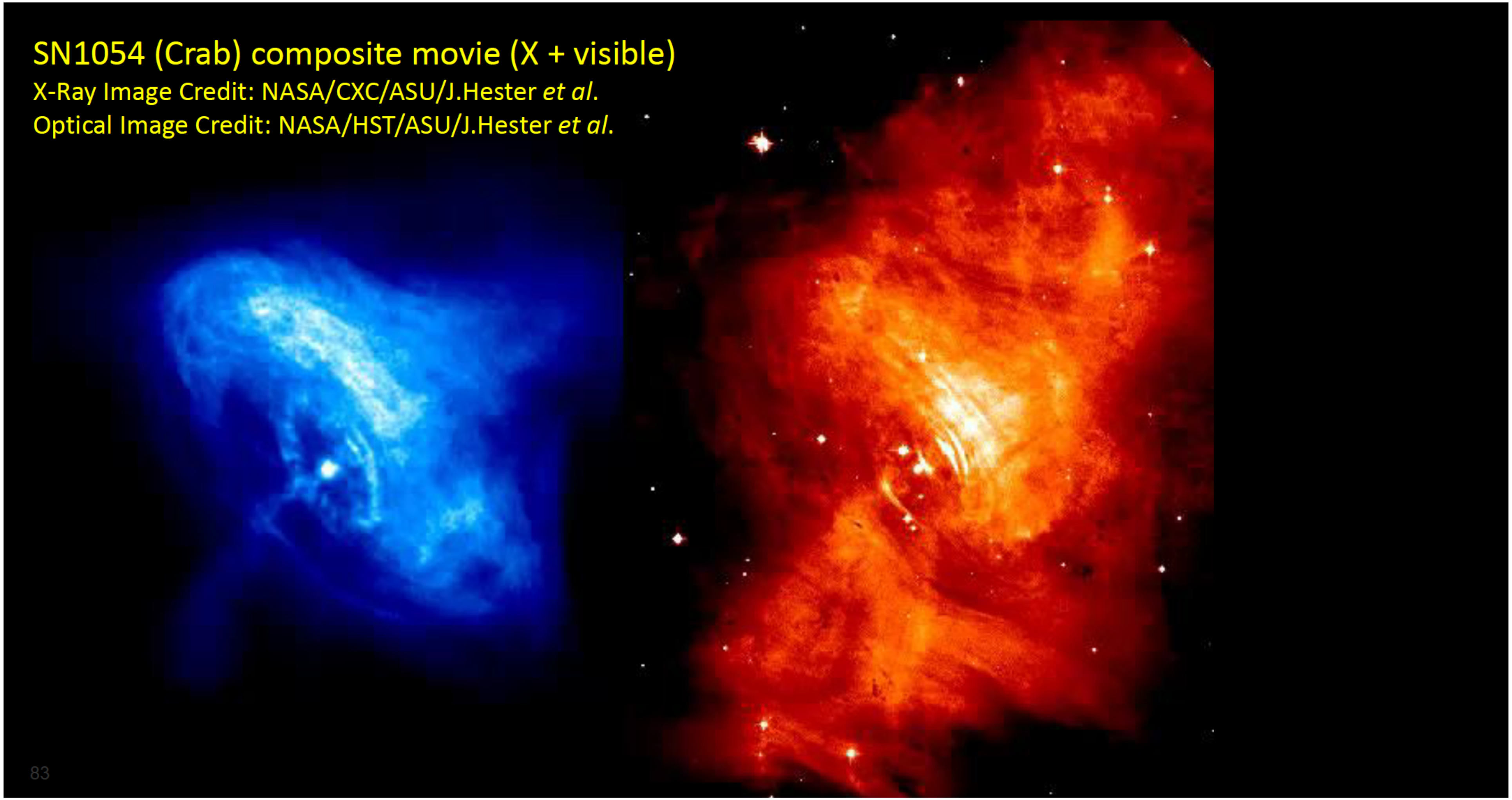

Physics from the early Universe

A stochastic background of gravitational waves may be observed from the earliest stages of the Universe

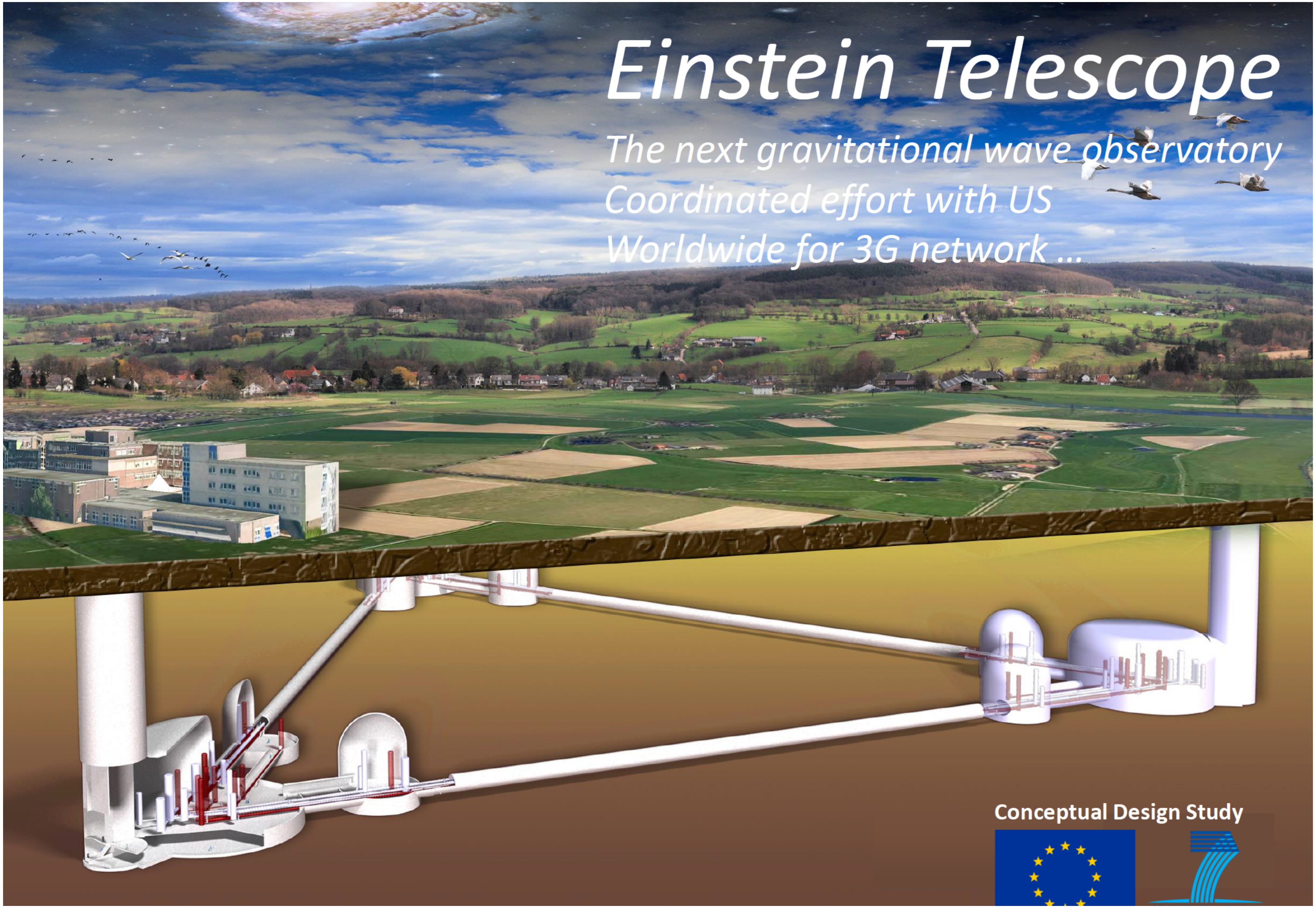

Einstein Telescope
The next gravitational wave observatory
Coordinated effort with US
Worldwide for 3G network ...
Conceptual Design Study

Bright future for gravitational wave research

LIGO and Virgo are operational. KAGRA in Japan joins this year, LIGO-India under construction. ESA launches LISA in 2034. Einstein Telescope and CE CDRs financed. Strong support by APPEC

Gravitational wave research

- LIGO and Virgo operational
- KAGRA to join this year
- LIGO-India under construction (2025)
- ESA selects LISA, NASA rejoins
- Pulsar Timing Arrays, such as EPTA and SKA
- Cosmic Microwave Background radiation

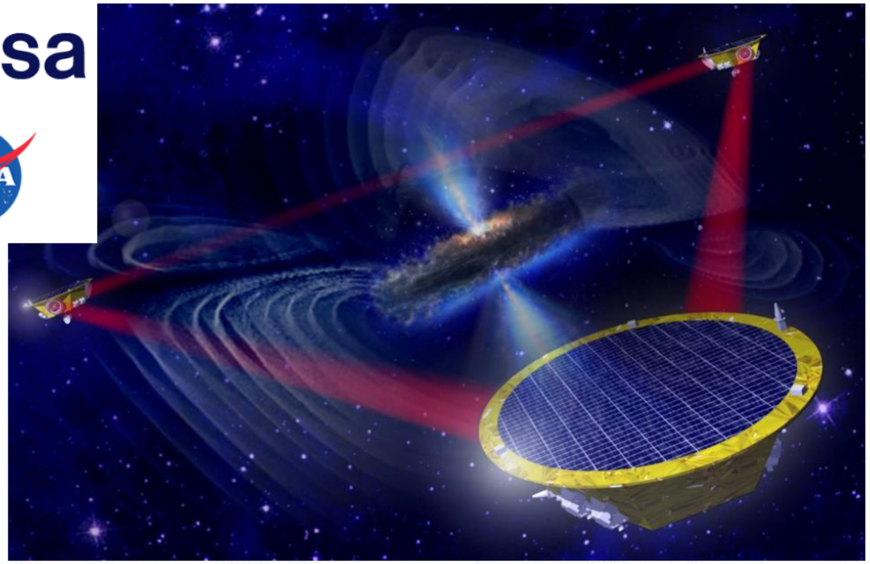

Einstein Telescope and Cosmic Explorer

- CDR ET financed by EU in FP7, CE by NSF
- APPEC gives GW a prominent place in the new Roadmap and especially the realization of ET

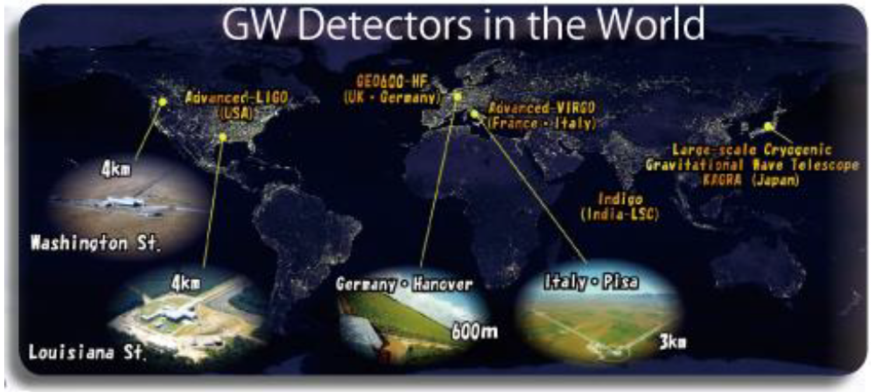

Next steps for 3G

- Organize the community and prepare a credible plan for EU funding agencies
- ESFRI Roadmap (2020)
- Support 3G: http://www.et-gw.eu/index.php/letter-of-intent

Astrofisica Nucleare e Subnucleare
Nuclear Astrophysics – I

Heavy element nucleosynthesis: the r process

Gabriel Martínez Pinedo

GSI

TECHNISCHE UNIVERSITÄT DARMSTADT

55th Karpacz Winter School of Theoretical Physics
ChETEC COST Action CA16117 training school
Artus Hotel, Karpacz, February 24 - March 2, 2019

HELMHOLTZ RESEARCH FOR GRAND CHALLENGES

SFB 1245

DFG

Nucleosynthesis beyond iron

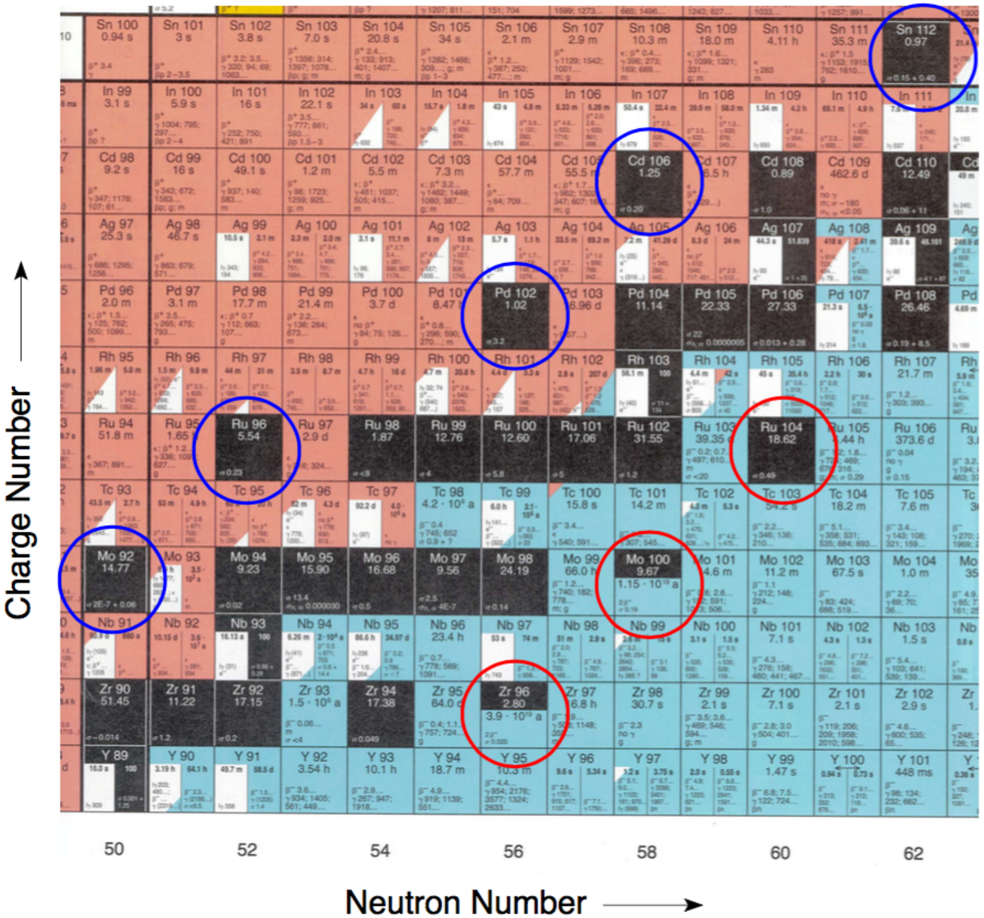

The stable nuclei beyond iron can be classified in three categories depending of their origin:

- s-process
- r-process
- p-process (γ-process)

Nucleosynthesis beyond iron

Three processes contribute to the nucleosynthesis beyond iron:
s-process, r-process and p-process (γ-process).

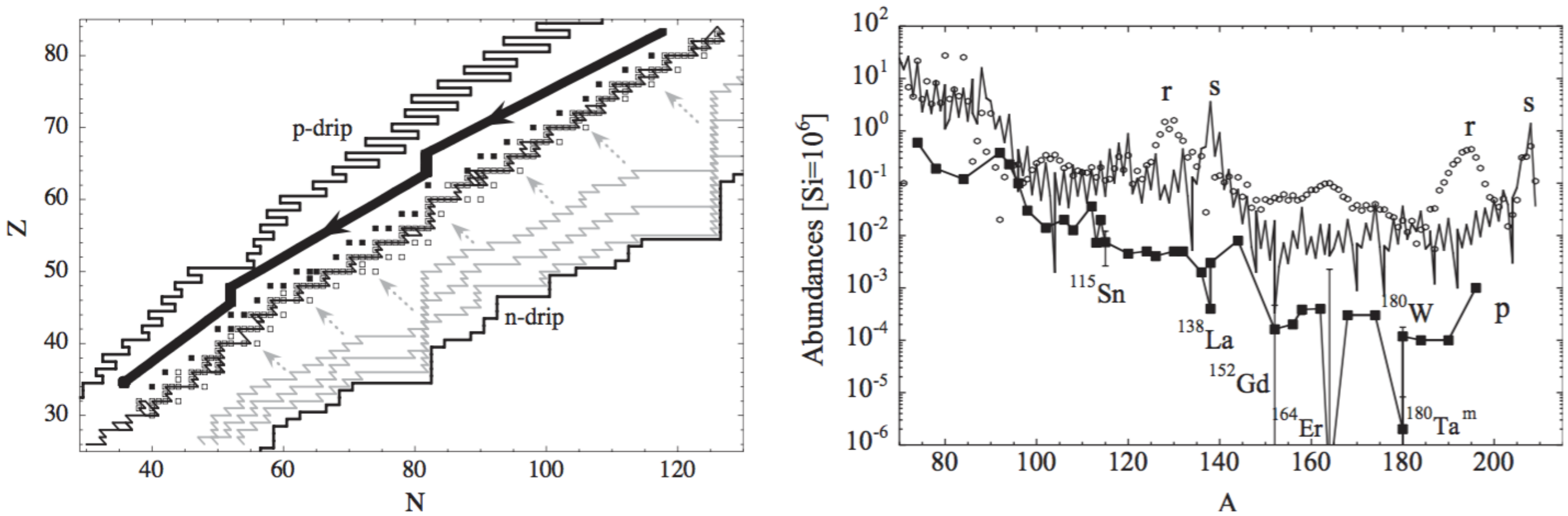

- s-process: relatively low neutron densities, $n_n = 10^{10-12}$ cm^{-3}, $\tau_n > \tau_\beta$
- r-process: large neutron densities, $n_n > 10^{20}$ cm^{-3}, $\tau_n < \tau_\beta$.
- p-process: photodissociation of s-process material.

Time evolution: metalicity

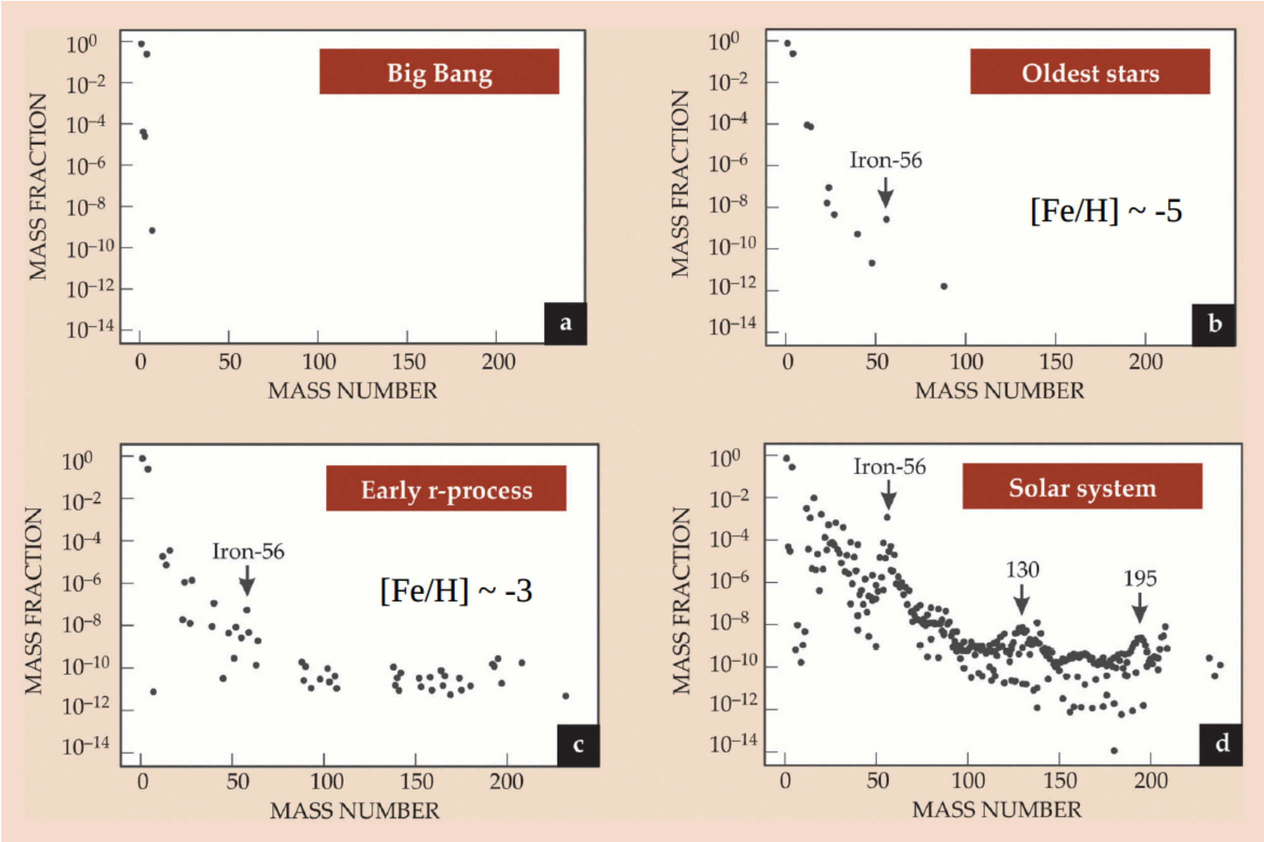

Astronomers use the metalicity:

$$[\mathrm{Fe/H}] = \log_{10}\left(\frac{N_{\mathrm{Fe}}}{N_{\mathrm{H}}}\right)_{*} - \log_{10}\left(\frac{N_{\mathrm{Fe}}}{N_{\mathrm{H}}}\right)_{\odot}$$

as a proxy for age.

Introduction: Summary

- The r process is a primary process operating in a site that produces both neutrons and seeds. Large neutron densities imply a site with extreme conditions of temperature and/or density.
- There is strong evidence that the bulk of r-process content in the Galaxy originates from a high yield/low frequency events.
- Neutron star mergers may account for most of the r-process material in the galaxy. However, due to the coalescent delay time they may not contribute efficiently at low metalicities. Magneto-rotational supernova may contribute at low metalicities.

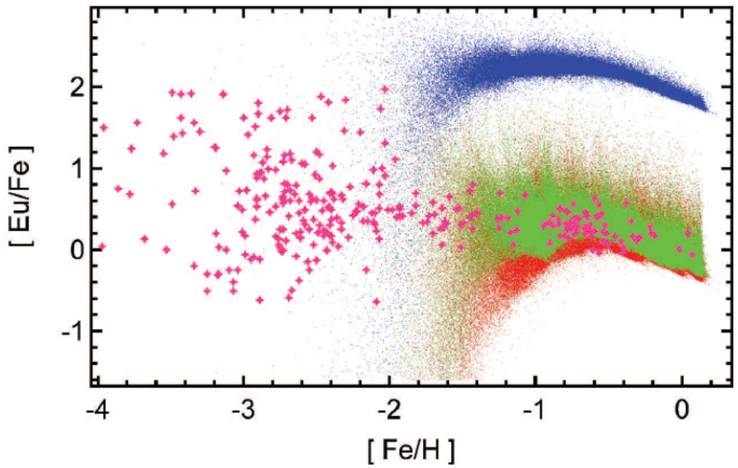

- Red dots: 10^8 yr coalescence time
- Green dots: 10^6 yr coalescence time
- Blue dots: larger merger probability.

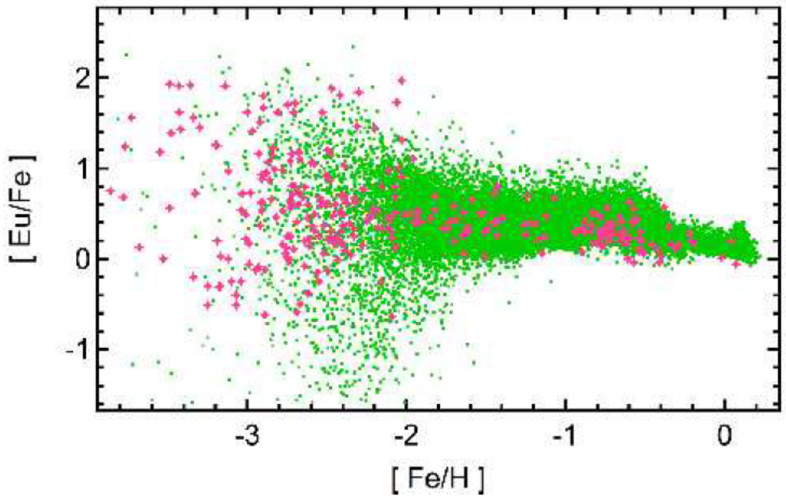

- Including MHD-jet supernovae

Wehmeyer, B., M. Pignatari, and F.-K. Thielemann , Mon. Not. Roy. Astron. Soc. 452, 1970 (2015)

Types of reactions

In order to dissentangle changes in the density (hydrodynamics) from changes in the composition (nuclear dynamics), the abundance is introduced:

$$Y_a = \frac{n_a}{n}, \quad n \approx \frac{\rho}{m_u} = \text{Number density of nucleons (constant)}$$

- $\sum_i Y_i Z_i = Y_e$ (charge neutrality)

R-process sites

- Any r-process site should be able to produce both the "seed" nuclei where neutrons are captured and the neutrons that drive the r-process. The main parameter describing the feasibility of a site to produce r-process nuclei is the neutron-to-seed ratio: n_n/n_{seed}.
- If the seed nuclei have mass number A_{seed} and we have n_n/n_{seed} neutrons per seed, the final mass number of the nuclei produced will be $A = A_{\text{seed}} + n_n/n_{\text{seed}}$.
- For example, taking $A_{\text{seed}} = 90$ we need $n_n/n_{\text{seed}} = 100$ if we want to produce the 3rd r-process peak ($A \sim 195$) and $n_n/n_{\text{seed}} = 150$ to produce U and Th.

R-process sites

In an astrophysical site there are only two possible ways to achieve large neutron-to-seeds:

1. Let us consider high temperature neutron-rich matter with high entropy that it is ejected at high velocities. As the material expands α particles will be formed. However, the build up of heavy nuclei by 3-body reactions becomes very unefficient by two reasons: 1) Too many photons per nucleon due to the high entropy, 2) Too litle time to produce heavy nuclei due to the fast expansion. It means that we will have an α-rich freeze out with a few heavy nuclei produced and many neutrons left ($Y_\alpha \approx Y_e/2$, $Y_n \approx 1 - 2Y_e$). This is commonly denoted as “high entropy” r-process
2. Let us consider matter very high density matter with low entropies. Due to the high densities electrons have large fermi energies and will drive the composition very neutron rich. At some point the neutron drip line is reached and nuclei start to “drip” neutrons. This is the situation in the crust of neutron stars where densities are 10^{12-13} g cm^{-3} and $Y_e \sim 0.05$: $Y_n = 1 - \langle A\rangle Y_e/\langle Z\rangle$, $Y_s = Y_e/\langle Z\rangle$; $Y_n/Y_s = \langle Z\rangle/Y_e - \langle A\rangle$; $Y_n/Y_s \sim 500 - 2000$. This is commonly denoted as “low entropy” r-process.

r-process nucleosynthesis relevant parameters

Independently of the astrophysical site the nucleosynthesis is sensitive to a few parameters that determine the neutron-to-seed ratio and the heavier elements that can be produced:

$$A_f = A_i + n_s, \quad n_s = n_n/n_{\text{seed}} \sim s^3/(Y_e^3 \tau_{\text{dyn}})$$

Y_e The lower the value of Y_e more neutrons are available and the larger n_s

entropy Large entropy $s \sim T^3/\rho$, means low density and high temperature (large amount of photons). Both are detrimental to the build up of seeds by 3-body reactions.

expansiton time scale The faster the matter expands, smaller τ_{dyn}, the less time one has to build up seeds

Neutron star mergers: Short gamma-ray bursts and r-process

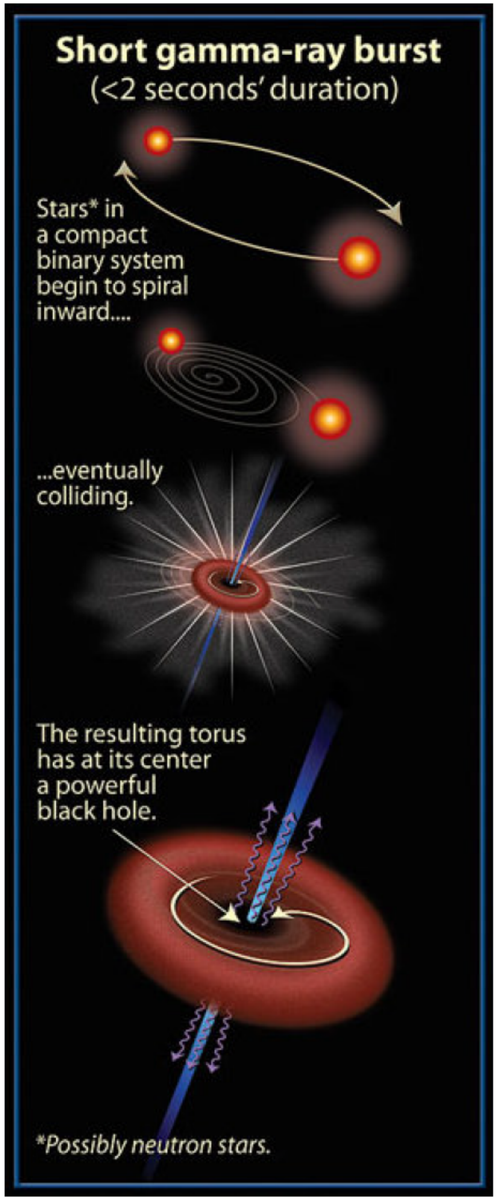

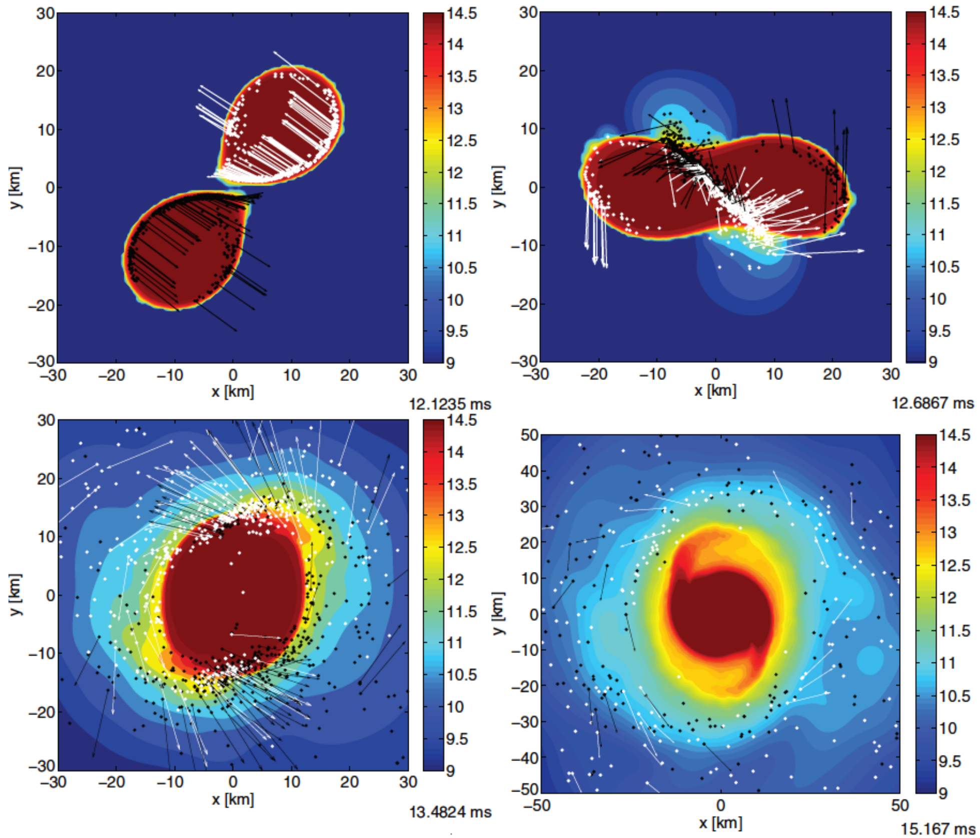

Basuswein, Goriely, Janka, ApJ 773, 78 (2013)

- Mergers are associated with short-gamma ray bursts.
- They are also promising sources of gravitational waves.
- Observational signatures of the r-process?

Merger channels and ejection mechanism

In mergers we deal with a variety of initial configurations (netron-star neutron-star vs neutron-star black-hole) with additional variations in the mass-ratio. The evolution after the merger also allows for further variations.

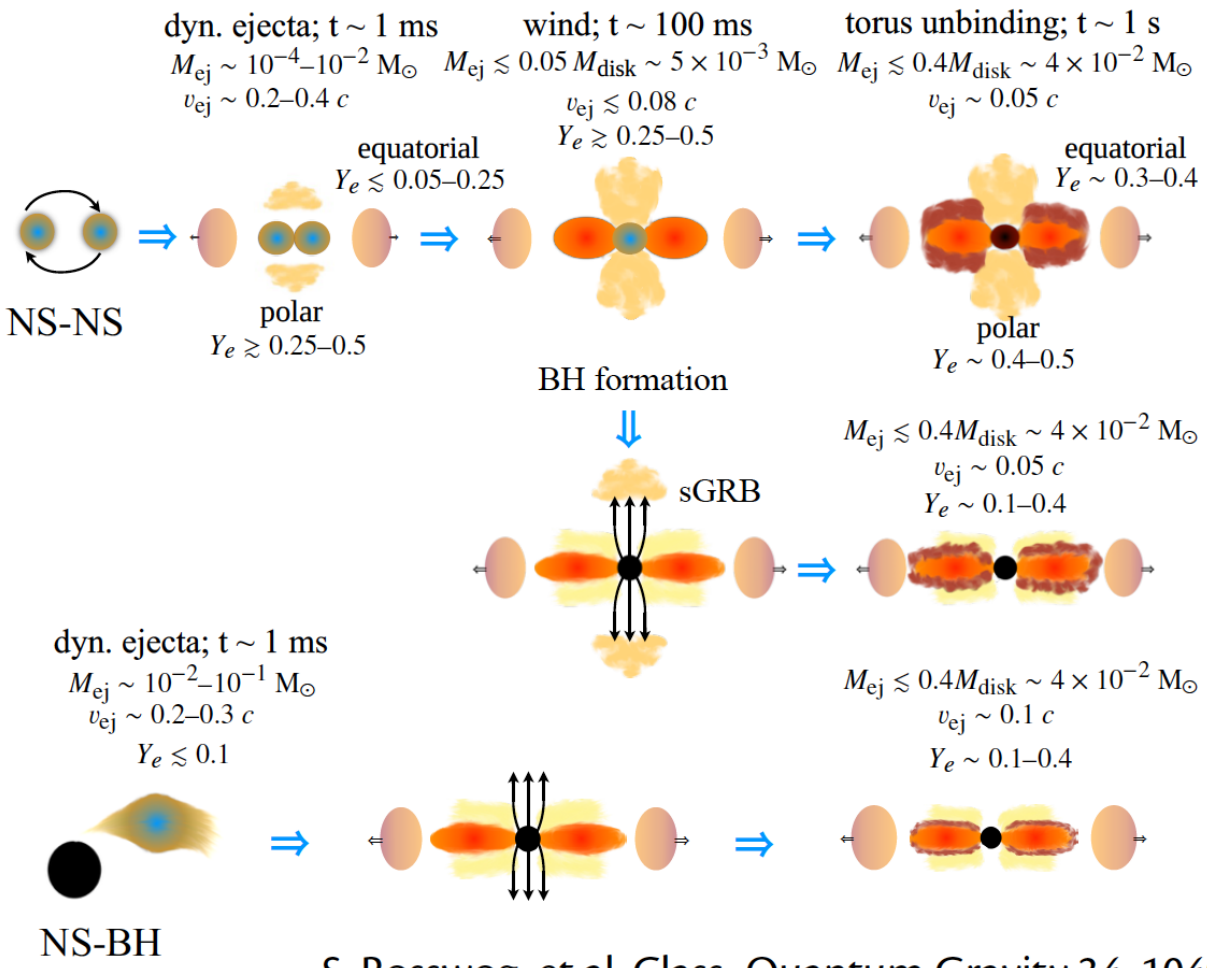

S. Rosswog, et al, Class. Quantum Gravity 34, 104001 (2017).

Dependence nucleosynthesis on Y_e

Nucleosynthesis depends on neutron richness of ejecta

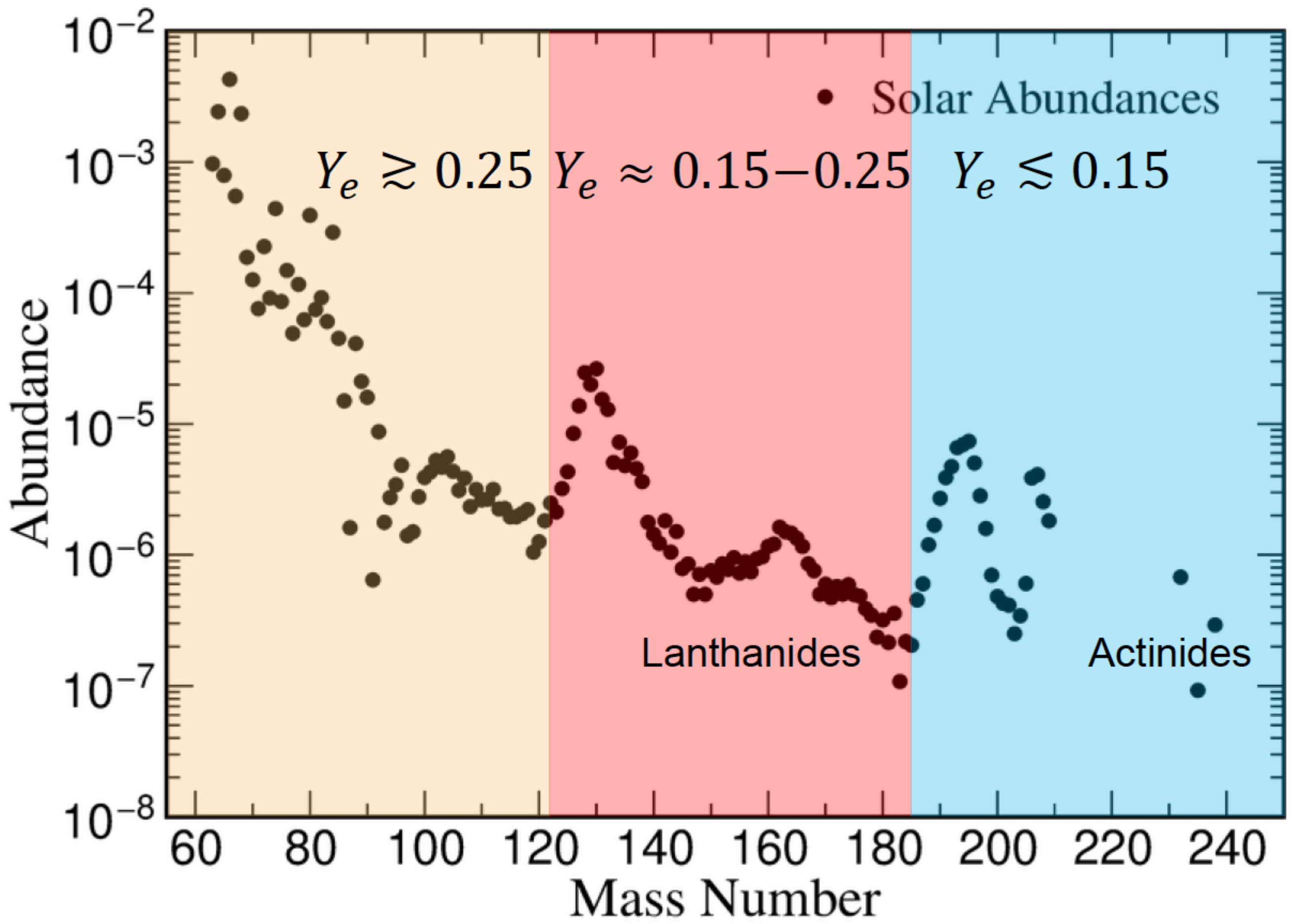

The relevant nuclear physics depends on the particular conditions.

Post-merger Nucleosynthesis (NS remnant)

An Hypermassive neutron star produces large neutrino fluxes that drive the composition to moderate neutron rich ejecta.

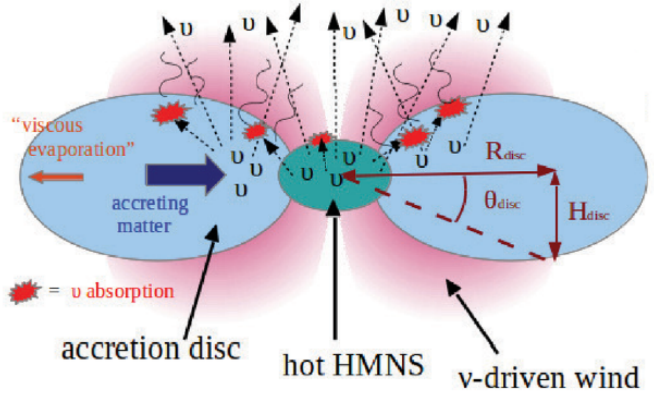

Perego, *et al*, MNRAS 443, 3134 (2014)

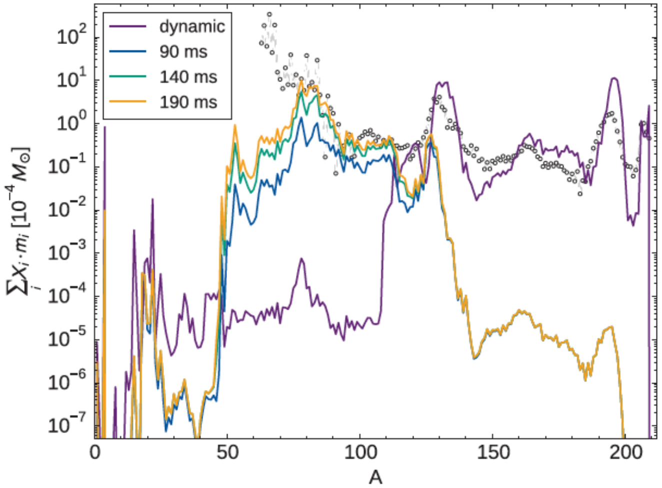

Martin, *et al*, ApJ 813, 2 (2015)

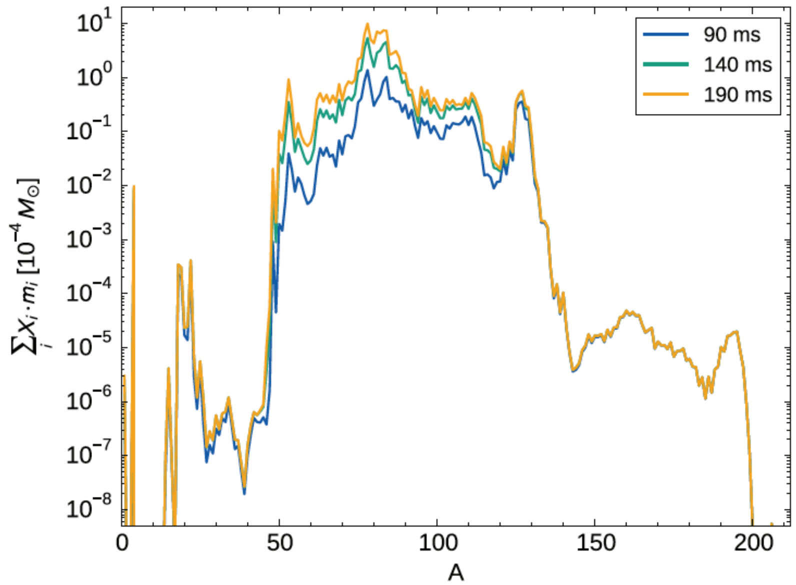

Only nuclei with $A < 120$ are produced (no lanthanides, blue kilonova).

See also Lippuner et al, MNRAS **472**, 904 (2017)

AT 2017 gfo: electromagnetic signature from r process

In-situ signature of r process nucleosynthesis

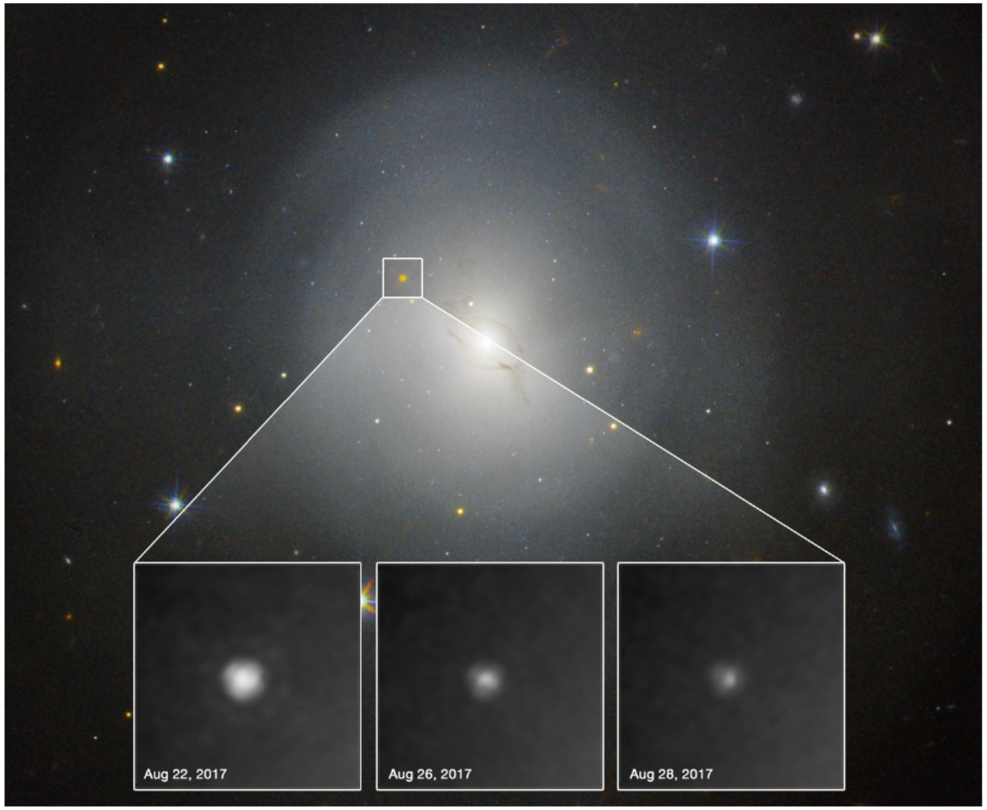

NASA and ESA. N. Tanvir (U. Leicester), A. Levan (U. Warwick), and A. Fruchter and O. Fox (STScI)

- Novel fastly evolving transitent
- Signature of statistical decay of fresly synthesized r process nuclei

AT 2017 gfo: interpretation

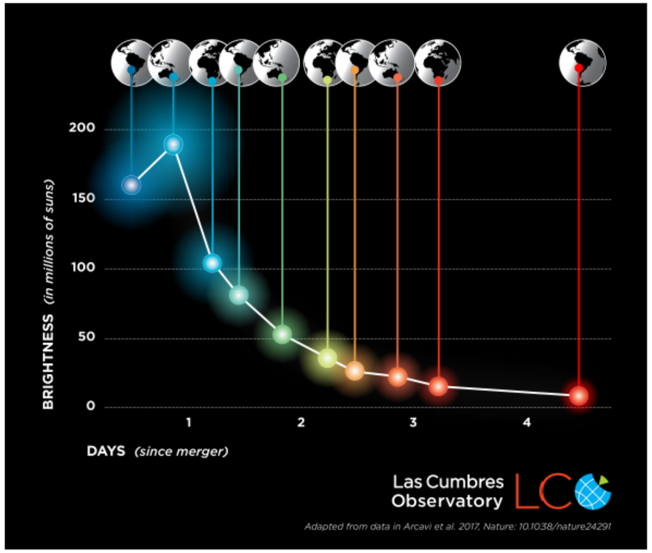

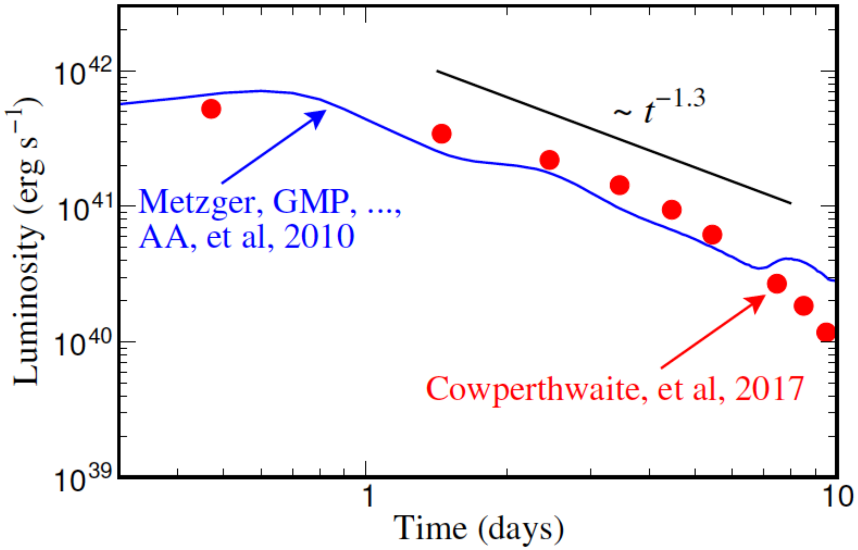

- Time evolution determined by the radioactive decay of r-process nuclei
- Two components:
  - blue dominated by light elements ($Z < 50$)
  - Red due to presence of Lanthanides ($Z = 57$–71) and/or Actinides ($Z = 89$–103)
- Likely source of heavy elements including Gold, Platinum and Uranium

Two components model

Kasen et al, Nature 551, 80 (2017)

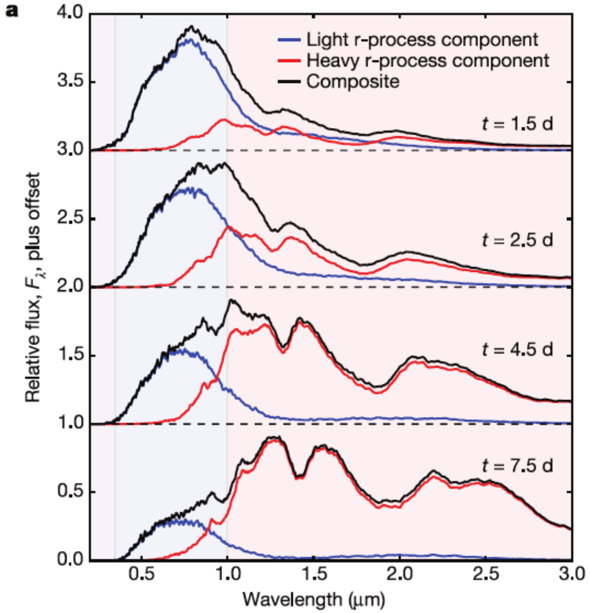

- Blue component from polar ejecta subject to strong neutrino fluxes (light r process)
  $$M = 0.025\,M_\odot, v = 0.3c, X_{\rm lan} = 10^{-4}$$
- Red component disk ejecta after NS collapse to a black hole (includes both light and heavy r process)
  $$M = 0.04\,M_\odot, v = 0.15c, X_{\rm lan} = 10^{-1.5}$$

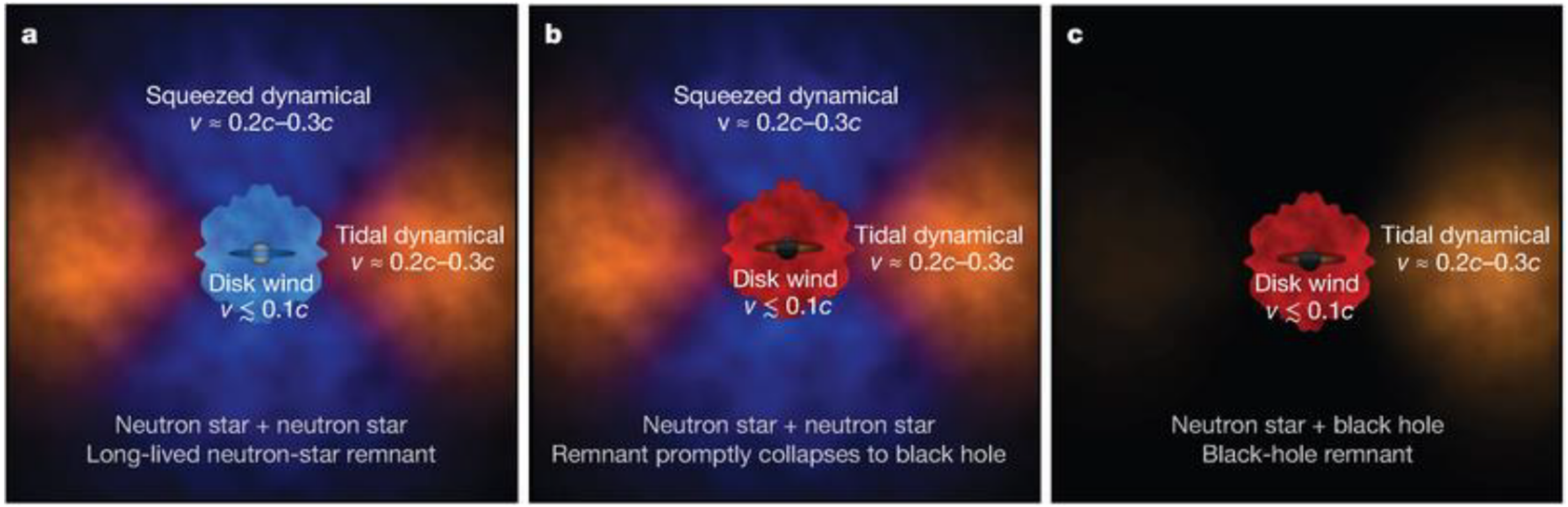

Summary

- Heavy elements are observed at very early times in Galactic history. Produced by a primary process that creates both neutrons and seeds.
- Neutron star mergers are likely the site where the "main r process" takes place.
- Radioactive decay of r-process ejecta produces an electromagnetic transient observed for the first time after GW170817.
- Observations of Blue and Red kilonova components show that both light ($A \lesssim 120$) and heavy ($A \gtrsim 120$) elements are produced. No direct evidence of individual elements.
    - How can we determine composition?
    - What were the heavier elements produced in the merger?
    - How does the nucleosynthesis depends on merging system?
    - What is the contribution of mergers to light r process elements?

Bibliography:

Cowan, *et al.*, *Making the Heaviest Elements in the Universe: A Review of the Rapid Neutron Capture Process*, arXiv:1901.01410 [astro-ph.HE]

Astrofisica Nucleare e Subnucleare

“MeV” Astrophysics

Coded Mask Imaging

The Coded Mask Technique

is the worst possible way of making a telescope

Except when you can 't do anything better !

- Wide fields of view
- Energies too high for focussing, or too low for Compton/Tracking detector techniques
- Very good angular resolution
- The best energy resolution

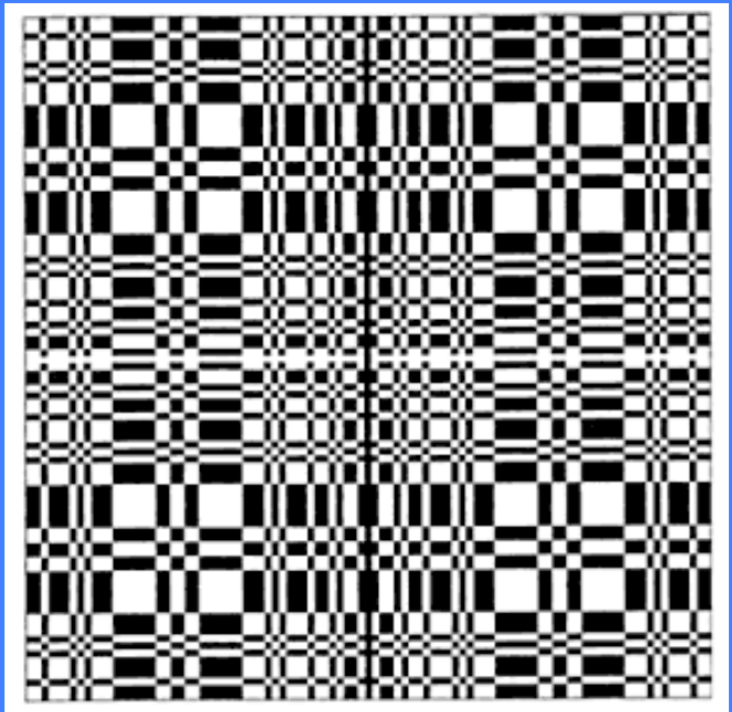

Mask of IBIS (15 keV – 10 MeV) onboard *INTEGRAL*

Coded Mask Imaging

The Coded Masks for Integral

JEM-X

Energy: 3-100 keV
535mm dia
0.5mm Tungsten
3.3 mm pitch
Resolution 3 arc min

IBIS

Energy: 15-10000 keV
1064 mm square
16 mm Tungsten
11.2 mm pitch
Resolution 12 arc min

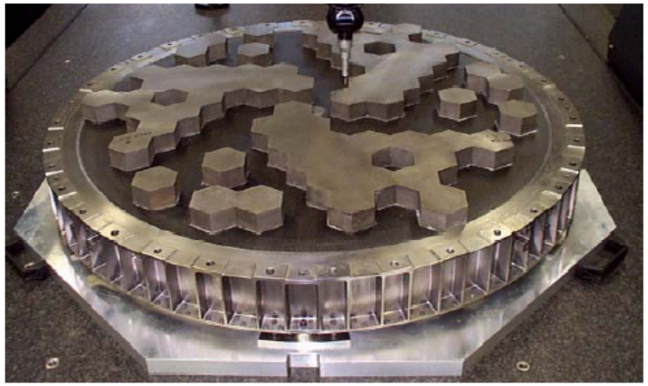

SPI

Energy: 20-8000 keV
770 mm dia
3 cm thick Tungsten
60 mm pitch
Resolution ~ 2.5°

INTEGRAL

INTEGRAL, the International Gamma-Ray Astrophysics Laboratory
Fine spectroscopy (E/dE=500) and fine imaging (angular resolution of 12' FWHM)
Energy range 15 keV to 10 MeV
plus simultaneous X-ray (3-35 keV) and optical (550 nm) monitoring capability
Two main g-ray instruments: SPI (spectroscopy) and IBIS (imager)

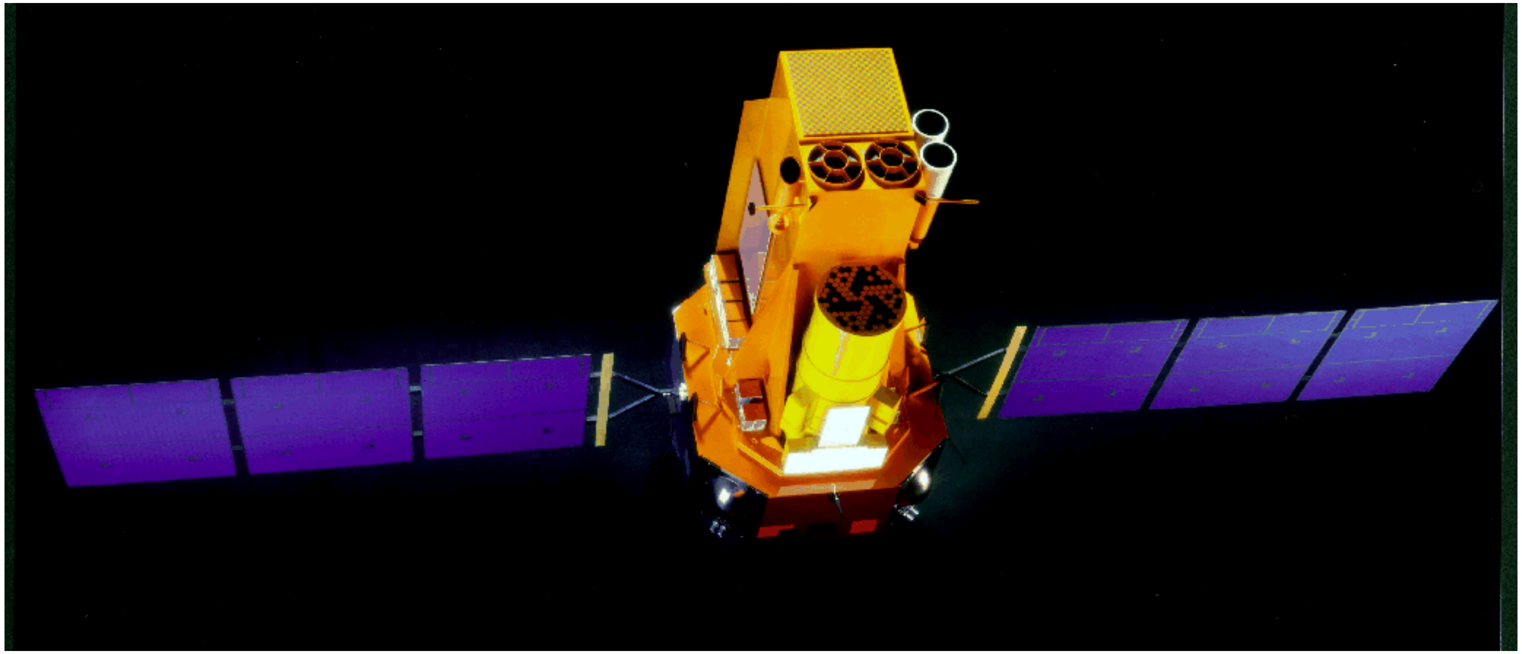

http://integral.esa.int

INTEGRAL

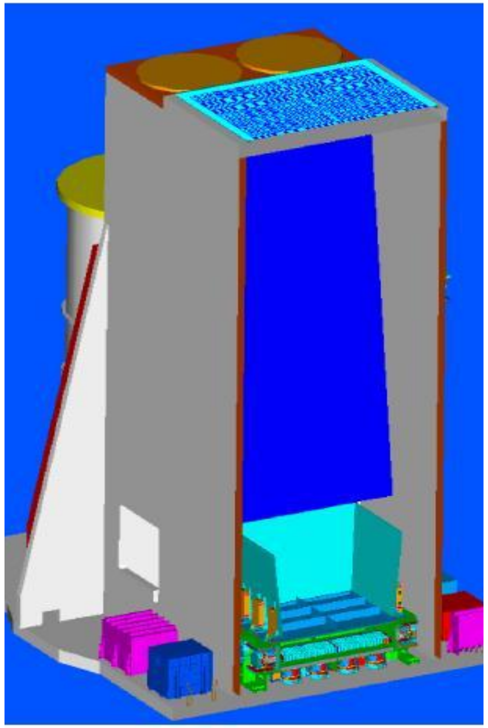

Imager IBIS

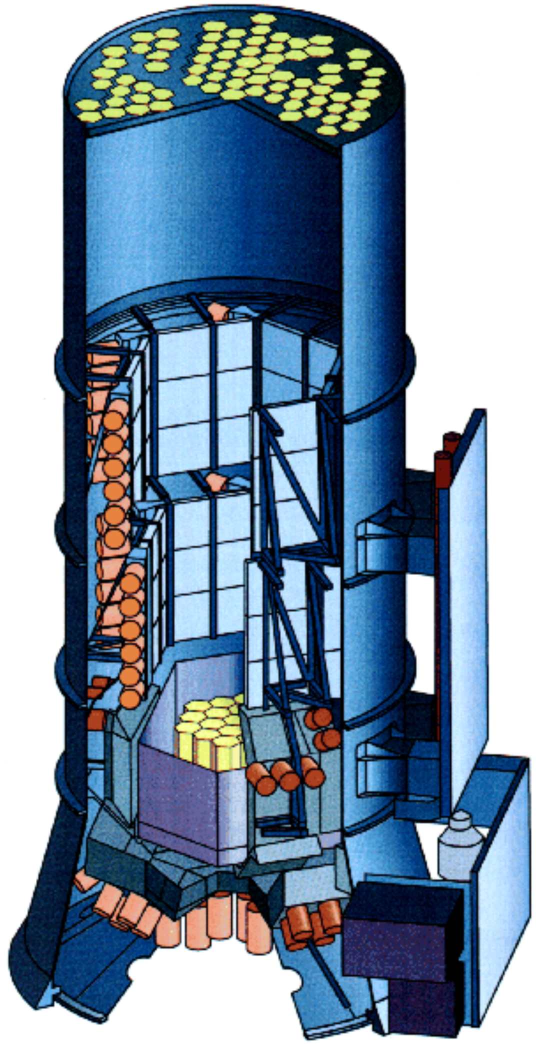

Spectrometer SPI

IBIS

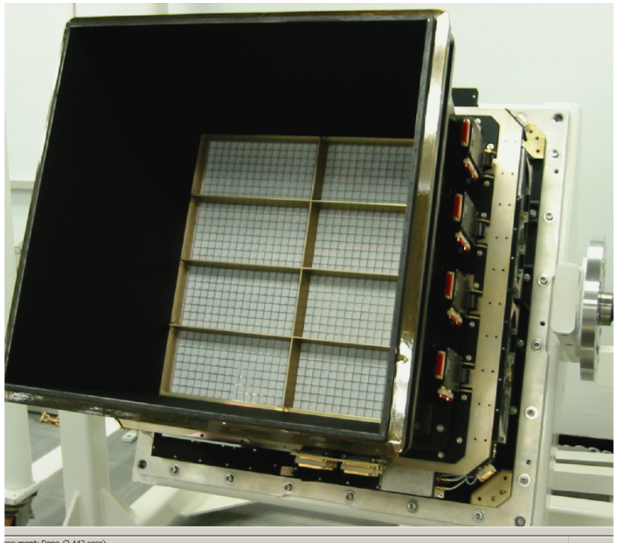

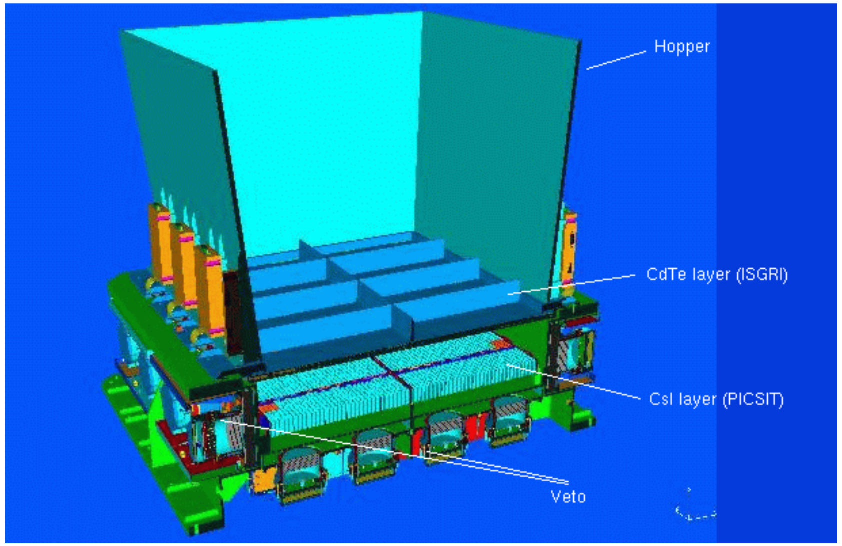

The Imager IBIS (Imager on Board the Integral Satellite) provides diagnostic capabilities of fine imaging (12 arcmin FWHM), source identification and spectral sensitivity to both continuum and broad lines over a broad (15 keV - 10 MeV) energy range. The Imager will exploit simultanesously with the other instruments on Integral celestial objects of all classes ranging from the most compact galactic systems to extragalactic objects.
A tungsten coded-aperture mask (located at 3.2 m above the detection plane) is optimised for high angular resolution. As diffraction is negligible at gamma-ray wavelengths, the angular resolution obtainable with a coded mask telescope is limited by the spatial resolution of the detector array. The Imager design takes advantage of this by utilising a detector with a large number of spatially resolved pixels, implemented as physically distinct elements.
The detector uses two planes, one 2600 cm^2 front layer of CdTe pixels, each (4x4x2) mm (width x depth x height), and a 3000 cm^2 layer of CsI pixels, each (9x9x30) mm. The CdTe array (ISGRI) and the CsI array (PICsIT) are separated by 90 mm. The detector provides the wide energy range and high sensitivity continuum spectroscopy required for Integral. The division into two layers allows the paths of the photons to be tracked in 3D, as they scatter and interact with more than one element. Events can be categorised and the signal to noise ratio improved by rejecting those which are unlikely to correspond to real (celestial) photons, e.g. towards the high end of the energy range.
The aperture is restricted by a lead shielding tube and shielded in all other directions by an active BGO scintillator veto.

SPI

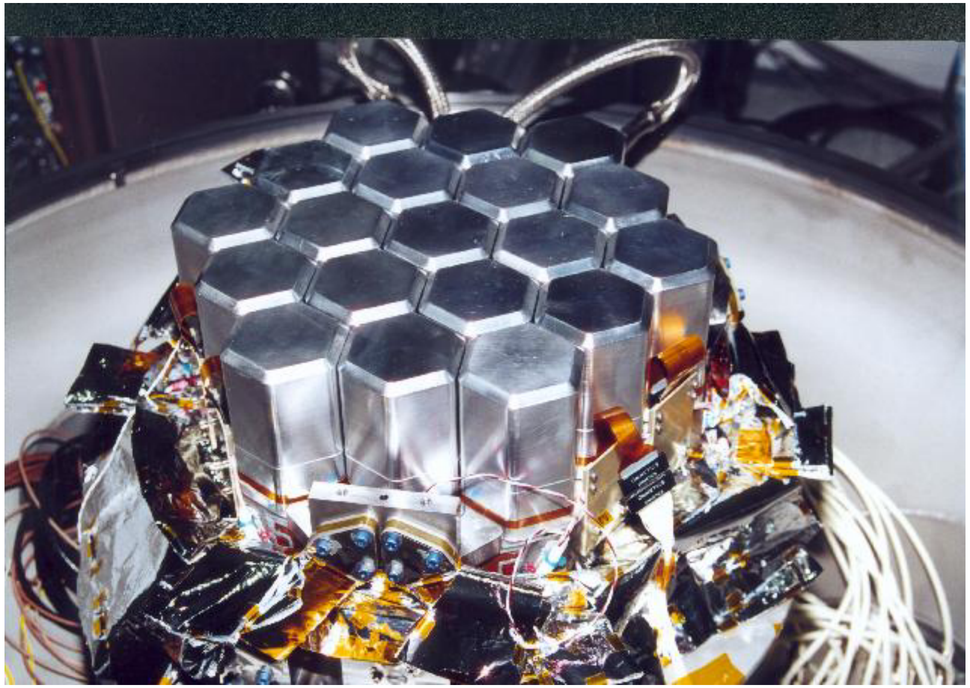

The spectrometer SPI (SPectrometer on INTEGRAL) will perform spectral analysis of gamma-ray point sources and extended regions in the 18 keV - 8 MeV energy range with an energy resolution of 2.2 keV (FWHM) at 1.33 MeV. This will be accomplished using an array of 19 hexagonal high purity Germanium detectors cooled by a Stirling cooler system to an operating temperature of 85 K. A hexagonal coded aperture mask is located 1.7 m above the detection plane in order to image large regions of the sky (fully coded field of view = 16 degrees) with an angular resolution of 2.5 degrees. In order to reduce background radiation, the detector assembly is shielded by a veto (anticoincidence) system which extends around the bottom and side of the detector almost completely up to the coded mask. The aperture (and hence contribution by cosmic diffuse radiation) is limited to ~ 30 degr. A plastic veto is provided below the mask to further reduce the 511 keV background.

Gamma Spectroscopy

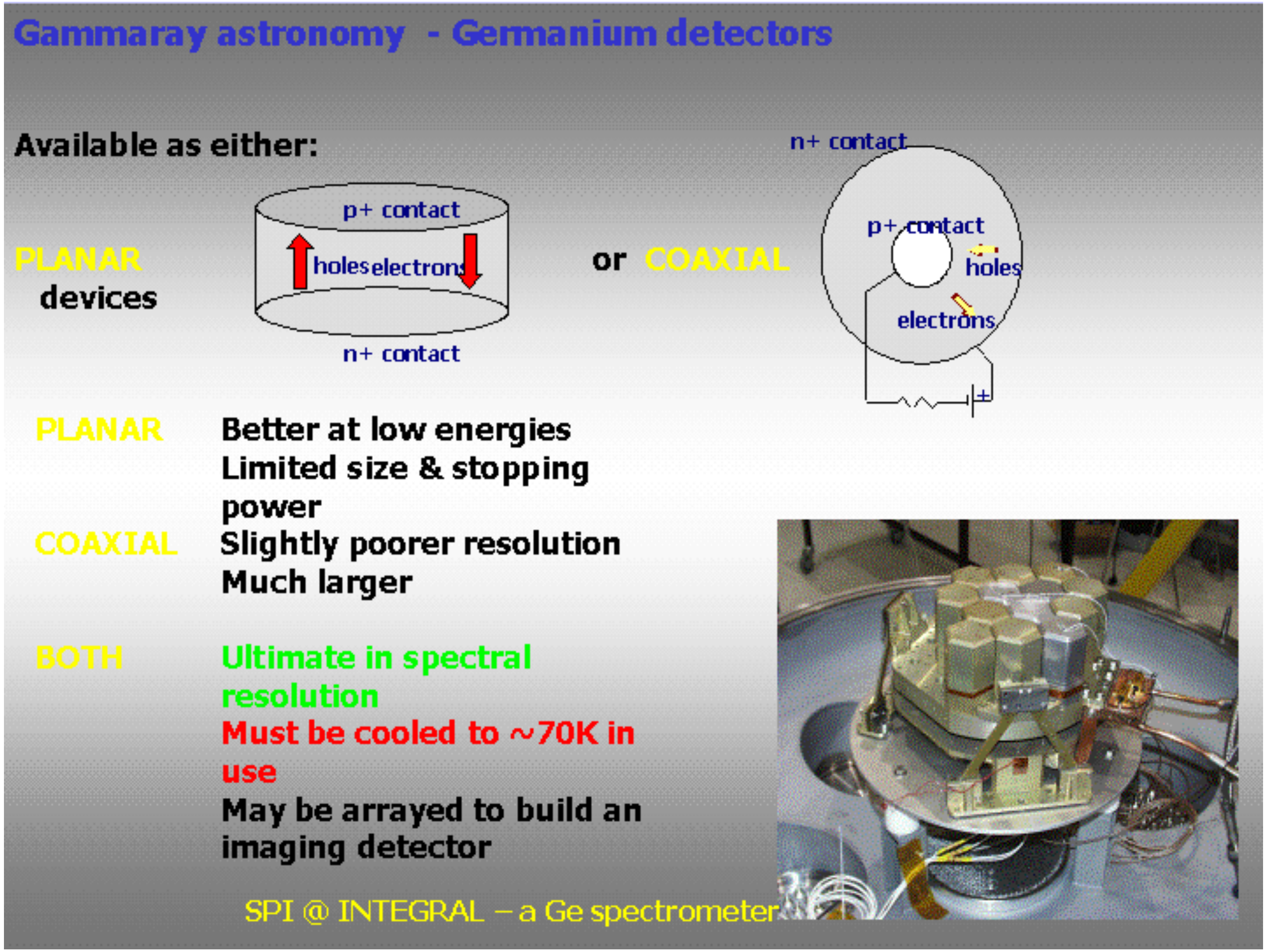

Gamma Spectroscopy

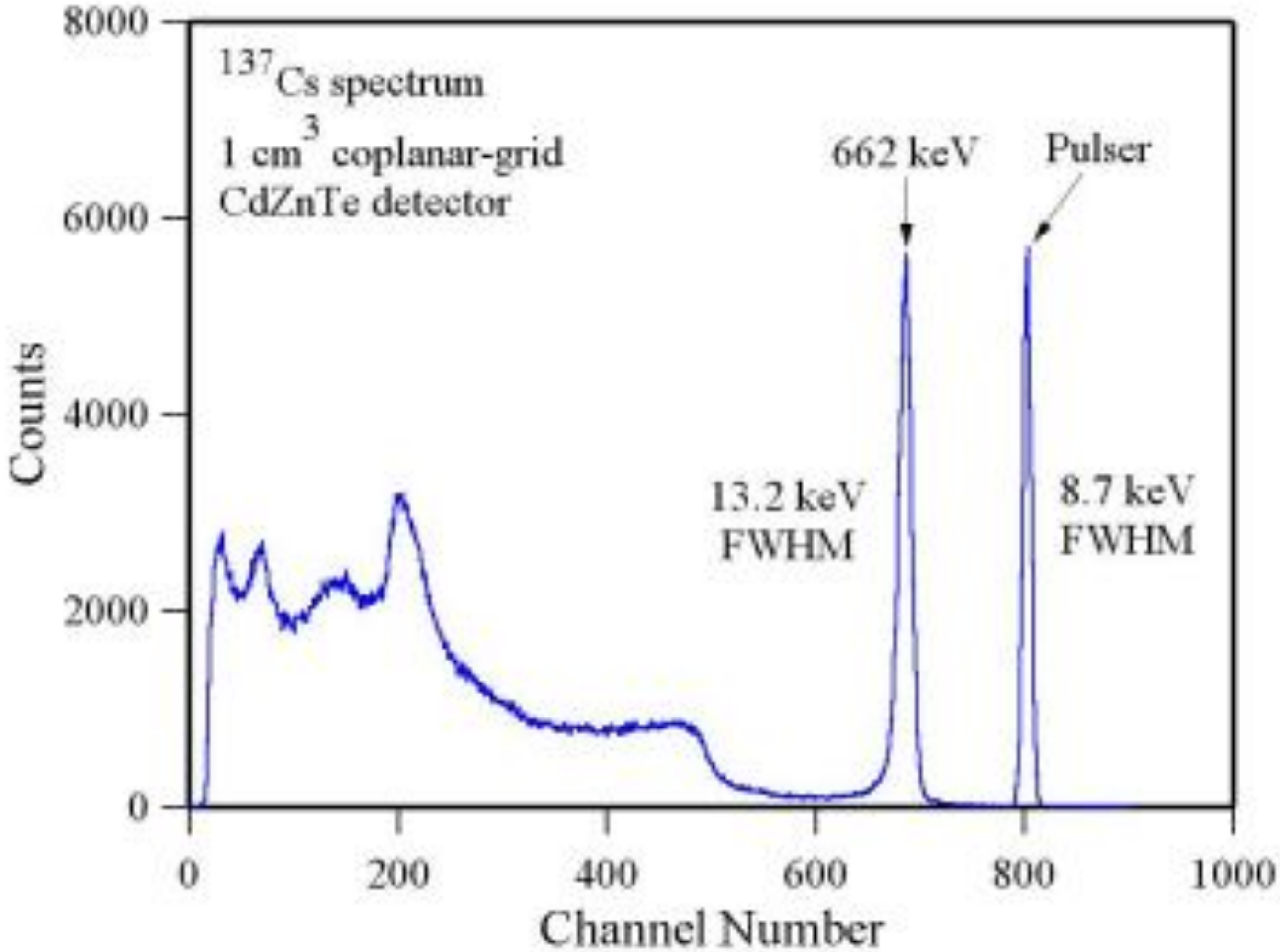

Rivelatori al Germanio

· Good response to high-energy photons

• Germanium is the best choice for high-energy (E > 100 keV – 10 MeV) spectroscopy

Very thin surface dead layers may give Ge an advantage where response from 1 keV - 100's of keV is desired

• Disadvantages (compared to compound semiconductors or scintillation detectors)

Requires cooling (complexity and cost)

Surfaces sensitive to contamination (handling/packaging more difficult)

For fine (Dx < 1 mm) position-sensitive detectors, segmented contact technology not well developed.

Examples CdTe: *Integral*/IBIS (SPI)

Rivelatori a stato solido a temperatura ambiente: Cd(Zn)Te – Cadmium Zinc Telluride (CZT)

- **Energy gap (1.4-2.2 eV)**
  - **Non necessaria criogenia (a differenza del Ge)**

- **Alta ρ (~6 g cm^{-3}) per massimizzare l'efficienza**

- **Alto Z (48, 52) per effetto fotoelettrico:**
  - **10 volte il μ_{Compt} fino a 110 keV (60 il Ge, 25 il Si);**
  - **Single site ok per imaging**

- **Facilmente segmentabile a piccole dimensioni:**
  - **$\Rightarrow$ risoluzione spaziale**

Examples CdTe: *Integral*/IBIS (ISGRI) – *Swift*/BAT

INTEGRAL

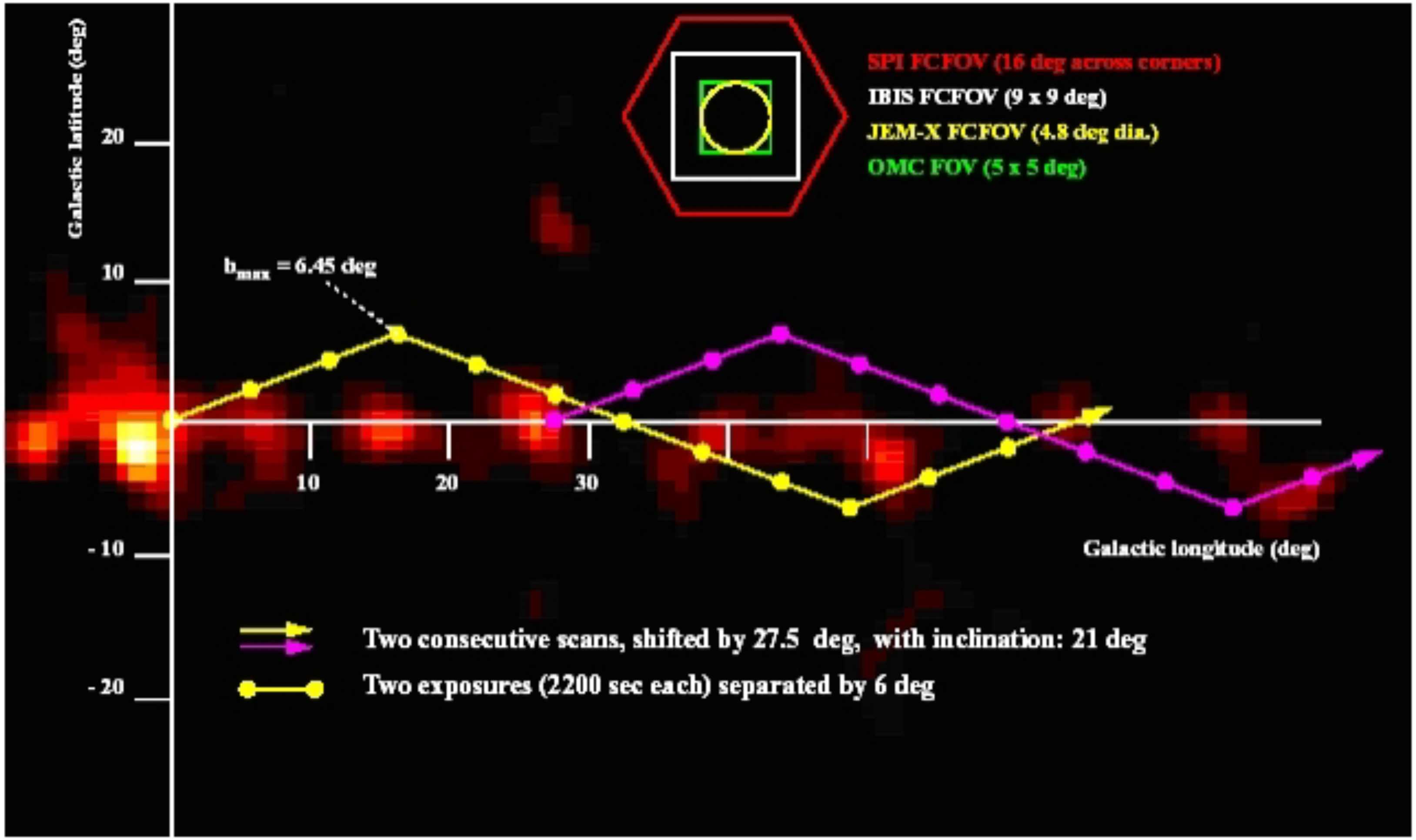

SPI FCFOV (16 deg across corners)
IBIS FCFOV (9 x 9 deg)
JEM-X FCFOV (4.8 deg dia.)
OMC FOV (5 x 5 deg)
Galactic latitude (deg)
20
10
- 10
- 20
b_{max} = 6.45 deg
10
20
30
Galactic longitude (deg)
Two consecutive scans, shifted by 27.5 deg, with inclination: 21 deg
Two exposures (2200 sec each) separated by 6 deg

INTEGRAL

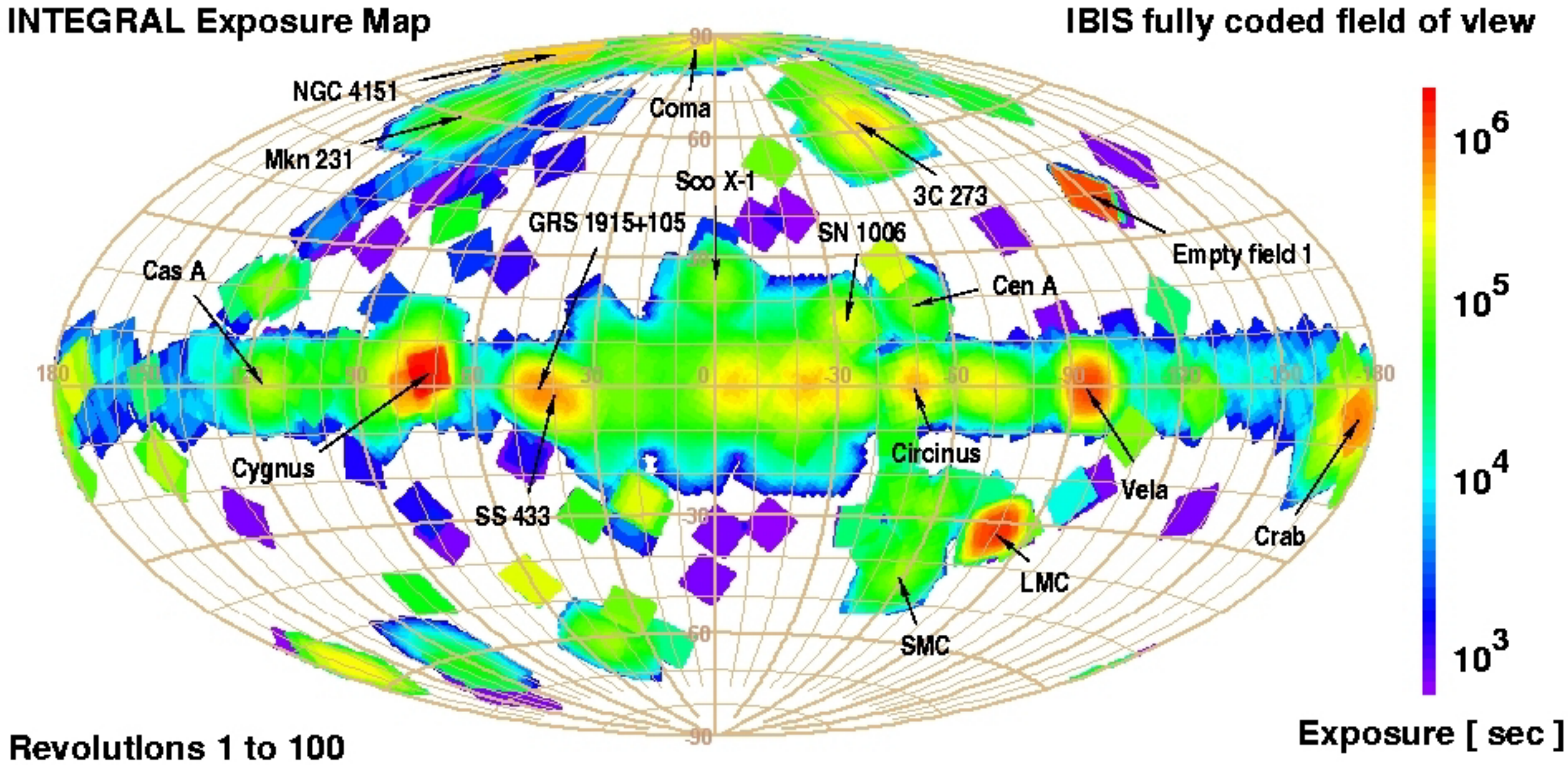
INTEGRAL Exposure Map
IBIS fully coded field of view
NGC 4151
Coma
Mkn 231
3C 273
Sco X-1
GRS 1915+105
SN 1006
Empty field 1
Cas A
Cen A
Cygnus
Circinus
Vela
SS 433
LMC
Crab
SMC
Revolutions 1 to 100
Exposure [sec]
10^6
10^5
10^4
10^3

INTEGRAL

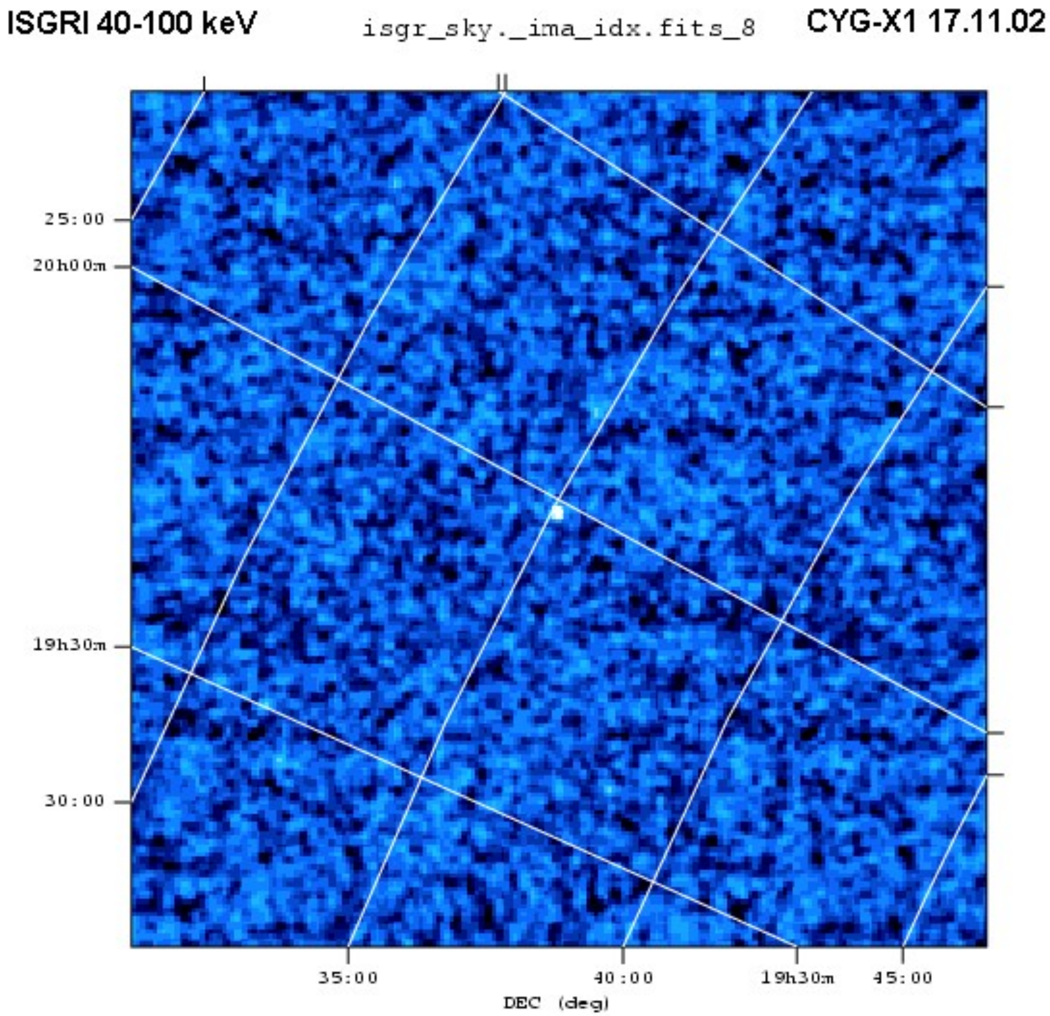

ISGRI 40-100 keV
isgr_sky._ima_idx.fits_8
CYG-X1 17.11.02
25:00
20h00m
19h30m
30:00
35:00
40:00
19h30m
45:00
DEC (deg)

INTEGRAL Science Objectives

Outline INTEGRAL Science Objectives

The scientific goals of Integral are addressed through the use of high resolution spectroscopy with fine imaging and accurate positioning of celestial sources in the gamma-ray domain. The following list of topics will be addressed by Integral:

- Compact Objects *(White Dwarfs, Neutron Stars, Black Hole Candidates, High Energy Transients and Gamma-Ray Bursts)*
- Extragalactic Astronomy *(Galaxies, Clusters, AGN, Seyferts, Blazars, Cosmic Diffuse Background)*
- Stellar Nucleosynthesis *(Hydrostatic Nucleosynthesis (AGB, WR Stars), Explosive Nucleosynthesis (Supernovae, Novae))*
- Galactic Structure *(Cloud Complex Regions, Mapping of continuum and line emission, ISM, CR distribution)*
- The Galactic Centre
- Particle Processes and Acceleration *(Transrelativistic Pair Plasmas, Beams, Jets)*
- Identification of High Energy Sources *(Unidentified Gamma-Ray Objects as a Class)*
- PLUS: Unexpected Discoveries

Gamma-Ray Astrophysics before INTEGRAL

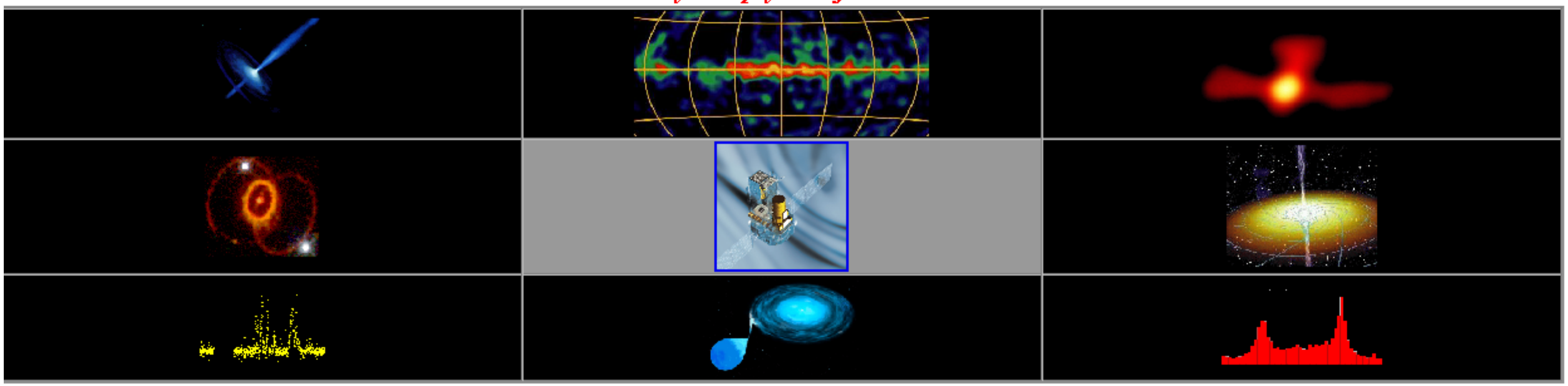

INTEGRAL

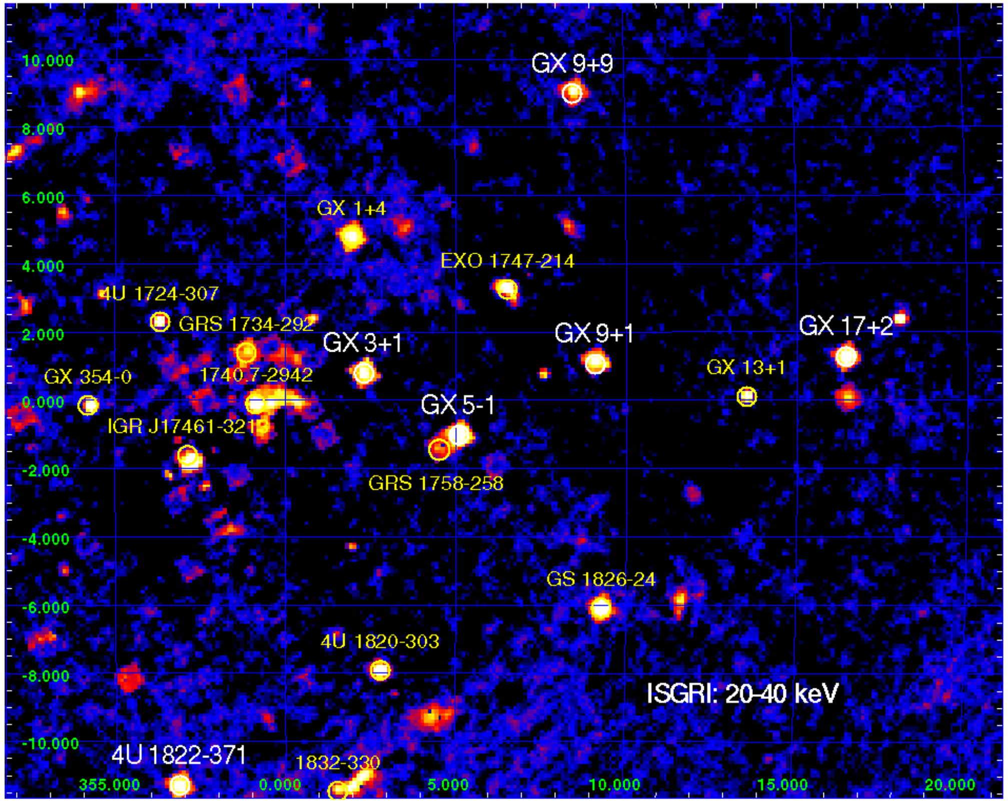

The image is an IBIS/ISGRI image of the Galactic Centre in the 20-40 keV band.
The analysis of IBIS/ISGRI data is based on GCDE (Galactic Center Deep Exposure) and GPS (Galactic Plane Scan) data from revolution 30 to 64 i.e. January 11th to April 22nd, 2003 for a total of one thousand pointings (about 2 Msec exposure)

INTEGRAL

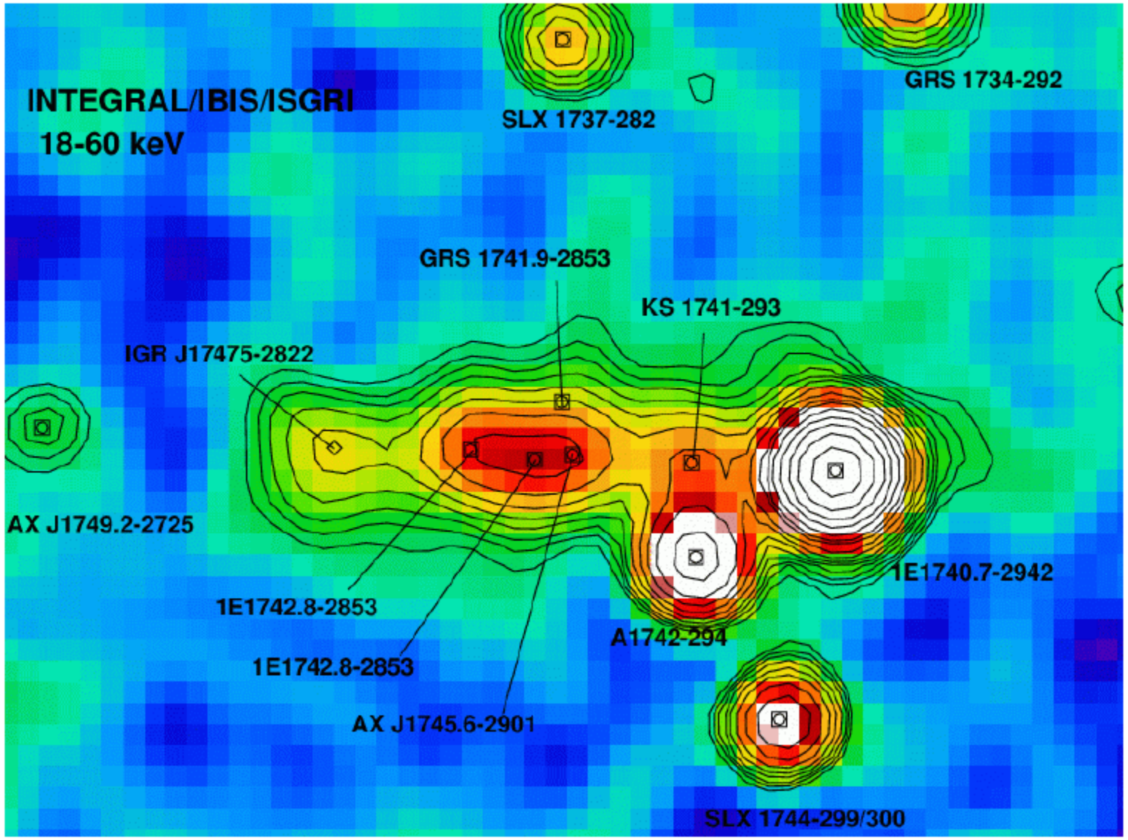

INTEGRAL views a Compton mirror at the Galactic Centre. M. Revnivtsev et al. report on the association of IGR J17475-2822, recently discovered by INTEGRAL, with the giant molecular cloud Sgr B2 in the Galactic Center region. Data from different observatories strongly support the idea that the hard X-ray emission of Sgr B2 is Compton scattered and reprocessed radiation emitted in the past by the Sgr A* source, the supermassive black-hole candidate in the center of our Galaxy. The IBIS/ISGRI image (18-60 keV) shows the inner 3.5 degree by 2.5 degree region of the center of the Galaxy. Contours represent signal-to-noise levels starting at S/N = 5 and increasing with a factor 1.4. The image has a total effective exposure time of 2.3 Ms.

INTEGRAL

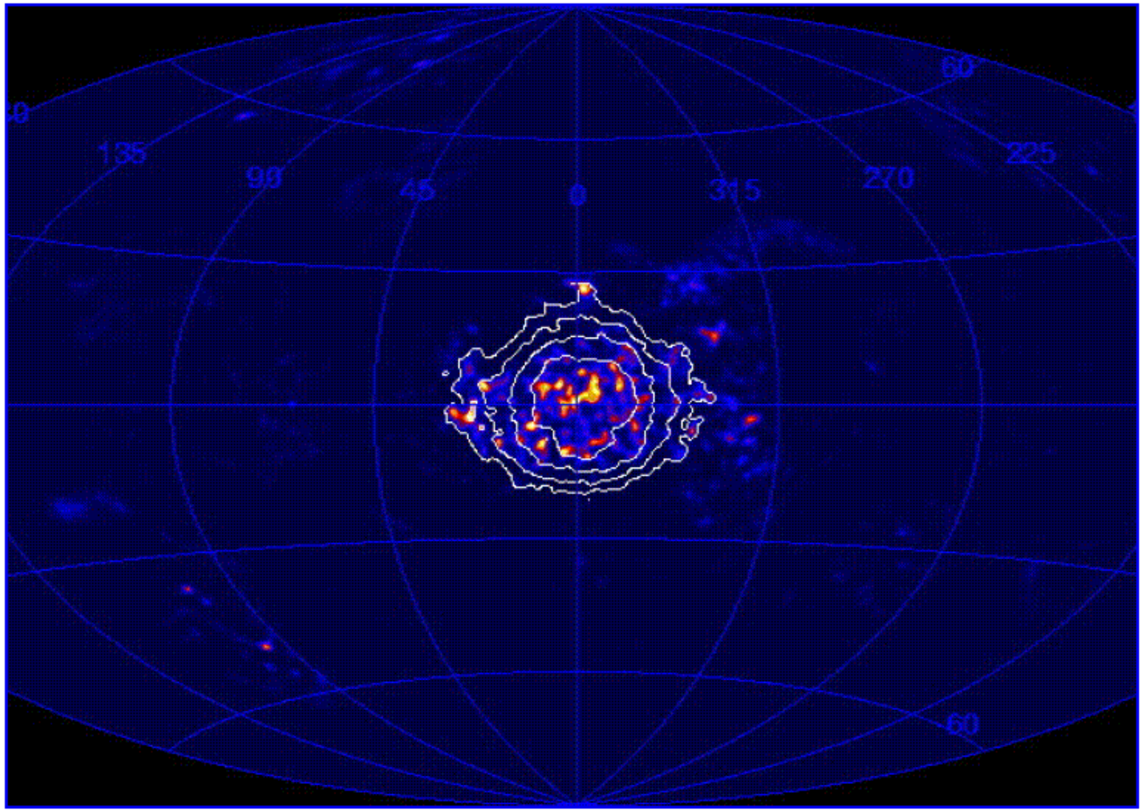

The SPI instrument onboard INTEGRAL has performed a search for 511 keV emission (resulting from positron-electron annihilation) all over the sky. The figure represents the results of this search: the all-sky map in galactic co-ordinates shows that 511 keV emission is - so far - only seen towards the center of our Galaxy. The SPI data are equally compatible with galactic bulge or halo distributions, the combination of a bulge and a disk component, or a combination of a number of point sources. Such distributions are expected if positrons originate either from low-mass X-ray binaries, novae, Type Ia supernovae, or possibly light dark matter.

INTEGRAL

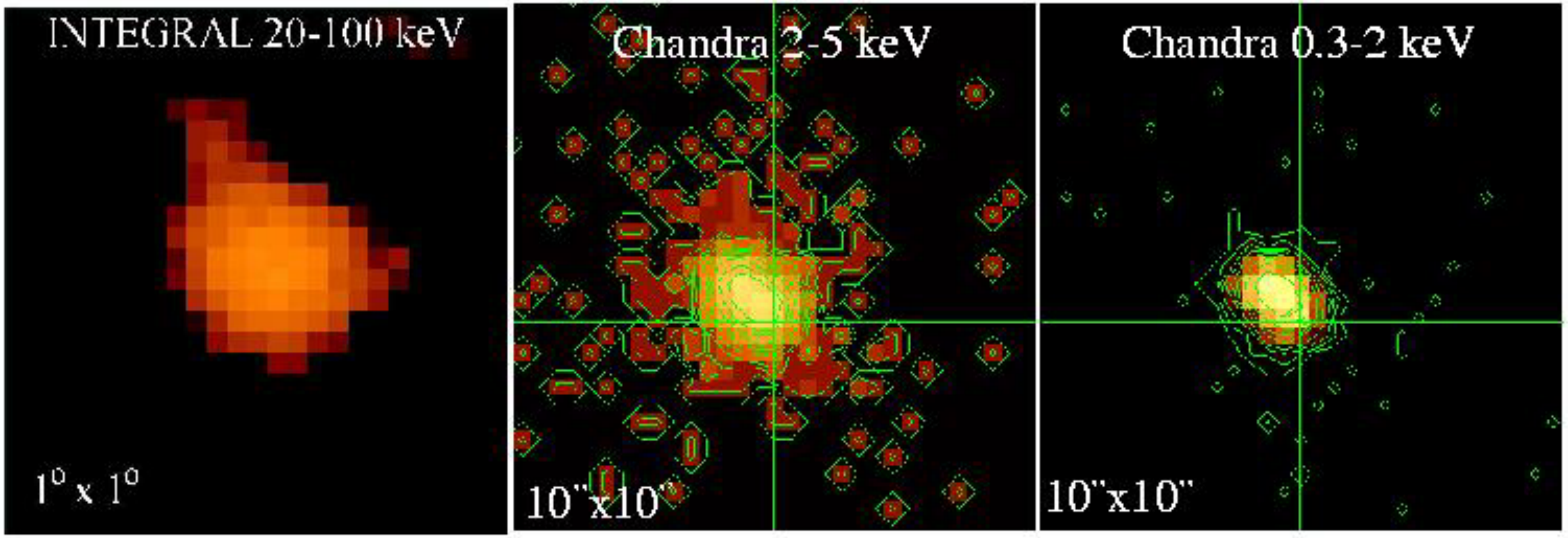

The blazar PKS 1830-211 is one of the most distant objects observed so far by INTEGRAL, it was reported as an ISGRI source in the galactic centre region. The source is clearly detected in 20-100 keV band. The image from IBIS/ISGRI is shown in the left panel. Notwithstanding its high redshift (z=2.507) it is a bright X-ray source, due to gravitational lensing by an intervening galaxy at z=0.89. Radio observations show two compact components separated by about 1 arcsecond; this effect (just at the limit of the angular resolution of Chandra), is clearly visible in the elliptically shaped Chandra images (central and right panels).

By assuming a magnification factor due to the lensing of the order of 10, the bolometric luminosity of PKS 1830-211 is huge: about 10^48 erg/s! The spectrum can be modelled adding an external source of low energy photons scattered up to gamma-ray energies by relativistic electrons. As observed in some high redshift quasars, Chandra spectra of PKS 1830-211 show evidence of absorption below 5 keV (rest frame). This effect could be due either to the lens galaxy at z=0.89 or to an intrinsic warm (ionized) gas at redshift of the source.

INTEGRAL

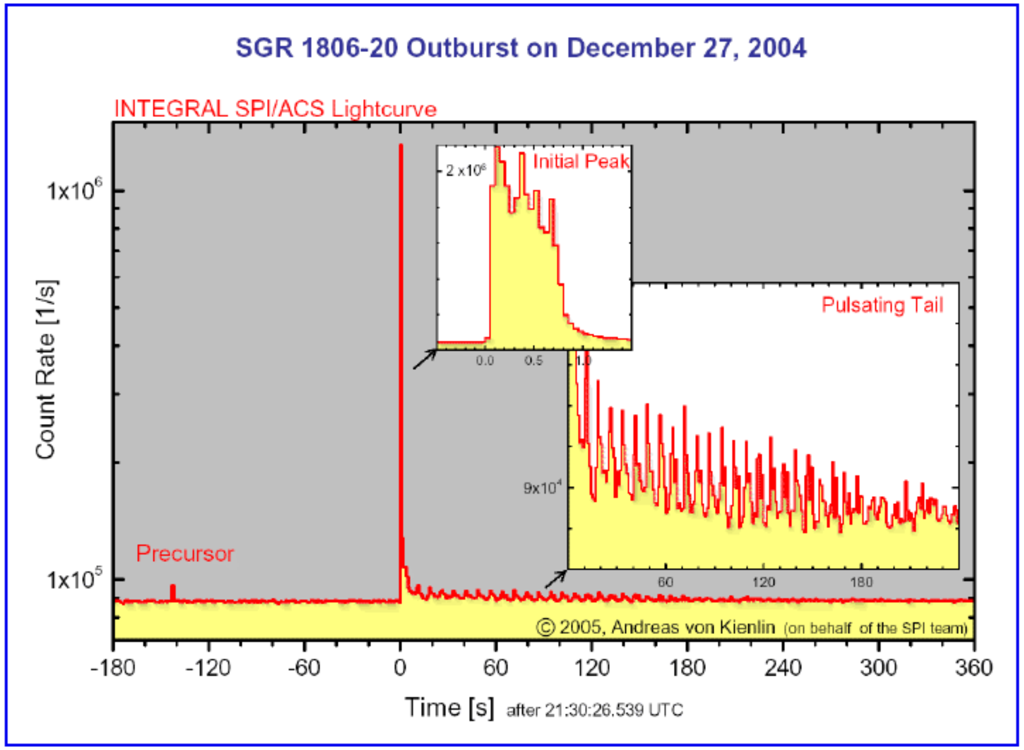

SGR 1806-20 which belongs to the class of soft gamma-ray repeaters (SGR) is believed to be a rotating neutron star with a super-strong magnetic field (10^15 Gauss); a so-called magnetar. The tremendous outburst of SGR 1806-20 on December 27, 2004 as seen by the large anticoincidence shield (ACS) of the INTEGRAL-spectrometer SPI is shown in the figure. The mean veto count rate of the ACS (~88000 counts/s) is interrupted at 21:30:26.539 UTC (T=0) by a steep count-rate increase (about a factor 25) for about 0.7 s. This outburst is thought to be caused by a large-scale rearrangement to a state of lower energy of a magnetar's super-strong magnetic field ($10^{\wedge 15}$ Gauss), which is the current model for soft gamma-ray repeaters. The ~300 s long pulsating tail with a period of 7.56 s is clearly seen and can be explained by a trapped fireball which is co-rotating with the neutron star (magnetar). The initial peak is proceeded at T= -143 s by a small precursor, which could be shown via triangulation to originate from the position of SGR 1806-20.

INTEGRAL

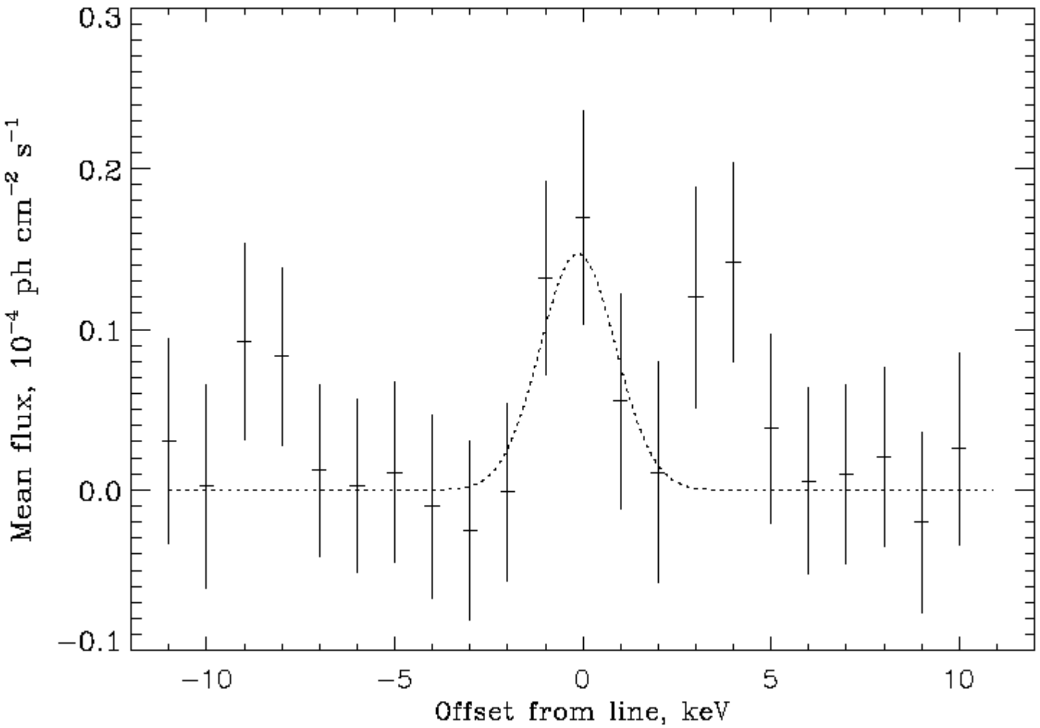

The SPI instrument on board INTEGRAL has observed the ^{60}Fe lines (at 1173 and 1333 keV) from the inner galaxy. The picture shows the combined ^{60}Fe signal from the two lines. The line flux is 3.7 ± 1.1 x 10^5 cm^{-2} s^{-1} per line.
The origin of the iron line is believed to be core-collapse supernovae which seed the interstellar medium with isotopes such as ^{60}Fe. From other SPI measurements of the ^{26}Al line the ratio $^{60}Fe/^{26}Al$ = 0.11 ±0.03 is derived, which is substantially smaller than predictions (0.40) for massive stars. This ratio supports the idea that there is an extra source of ^{26}Al in addition to the core-collapse supernovae.

INTEGRAL

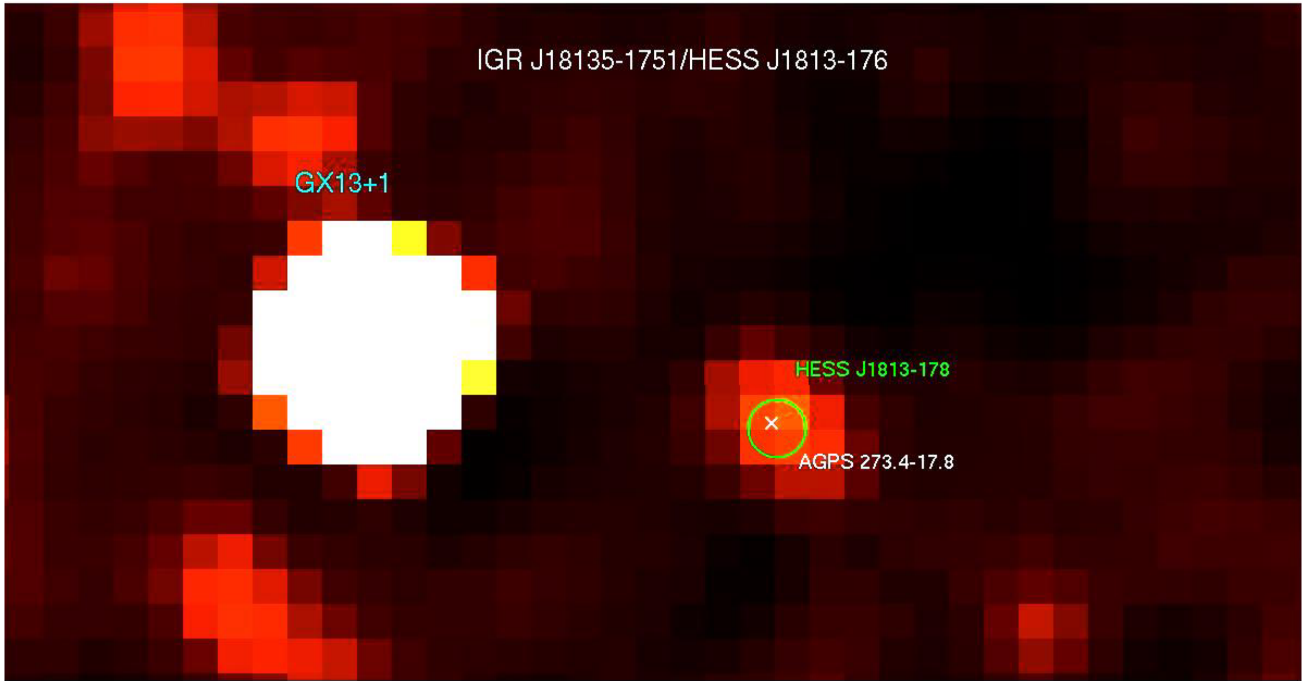

INTEGRAL has discovered, using the IBIS instrument, a new gamma-ray source (IGR J18135-1751). This source is remarkable, since it coincides spatially with one of the ten objects which have been seen during the first survey at TeV energies of the inner part of the galaxy: HESS J1813-178. This source is a powerful ultra-high energy emitter in the 0.2-10 TeV range. The X-ray counterpart (AGPS273.4-17.8) of the INTEGRAL source has an absorbed spectrum and is thought to be either a pulsar wind nebula or a supernova remnant. This picture shows the IBIS/ISGRI 20-100 keV image of IGR J18135-1751 as well as the position of HESS J1813-178 (green circle) and AGPS273.4-17.8 (white cross). The white spot on the left is the saturated image of the bright LMXB GX 13+1.

INTEGRAL

The central regions of our Galaxy, the Milky Way, as seen by INTEGRAL in gamma rays. With its superior ability to see faint details, INTEGRAL reveals the individual sources that comprised the foggy, soft gamma-ray background seen by previous observatories. The brightest 91 objects seen in this image were classified by INTEGRAL as individual sources, while the others appear too faint to be properly characterized at this stage.

INTEGRAL

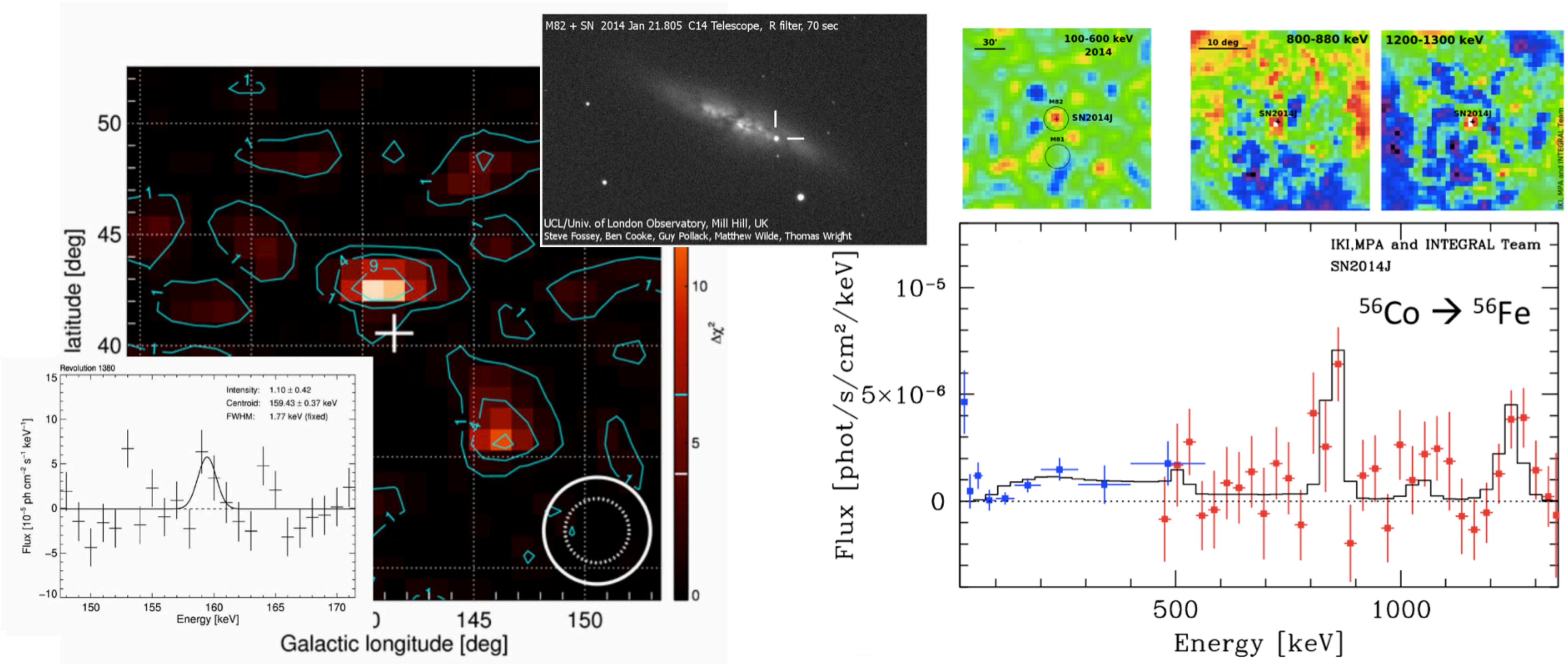

INTEGRAL for the first time, confirms by direct measurement of the primary gamma-ray lines the ^{56}Ni origins of SN light. The INTEGRAL measurements of this sufficiently-nearby SN provide a unique opportunity to compare the direct gamma-rays from the SN's energy source with the more-indirect other radiation. This will help astrophysicists to refine their models on how in fact these explosions do occur, because the explosion details affect how much new nuclei are created, and how they move and interact with the remainder of the exploding star. These observations constitute a reference in SNIa science, and thus an important scientific legacy for years to come.

INTEGRAL

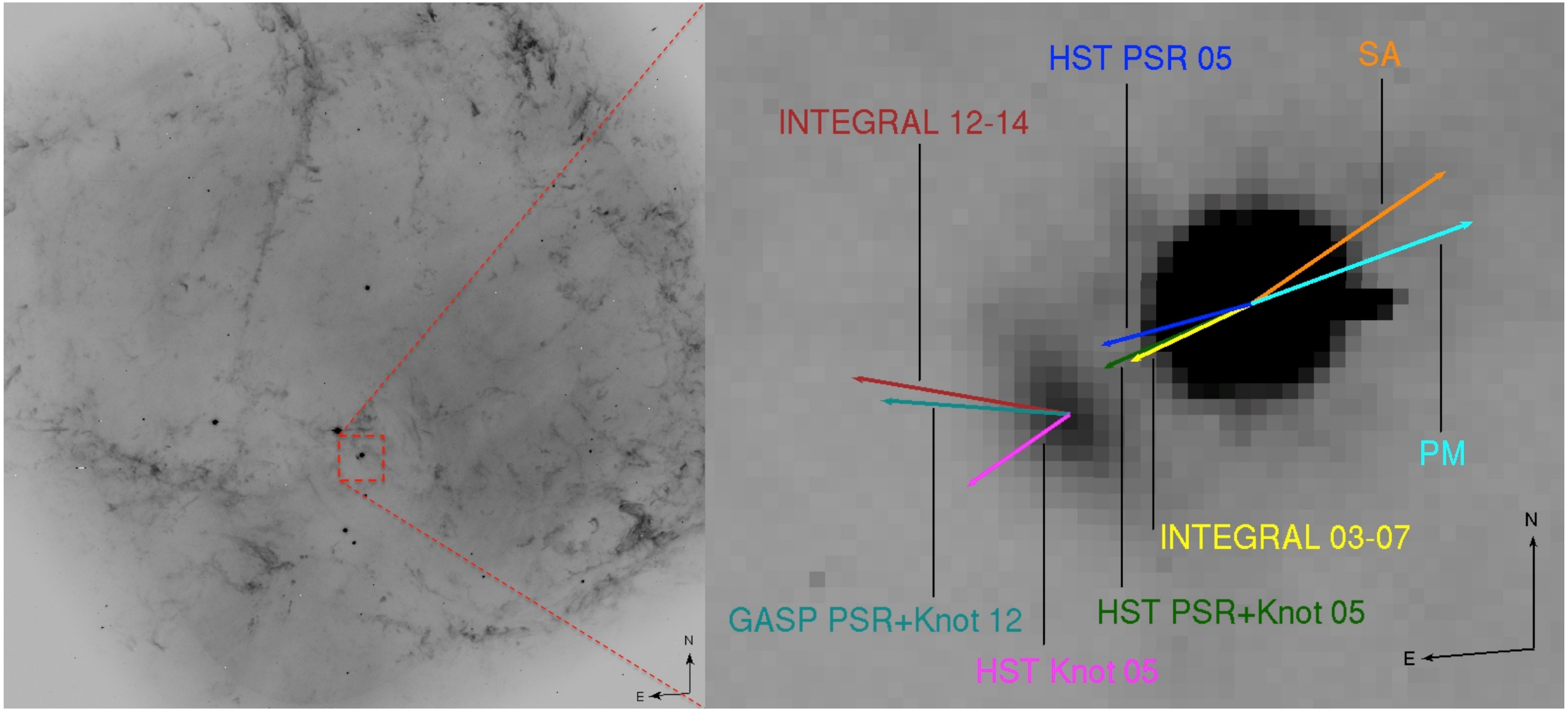

On the left, this HST image shows the inner part of the Crab nebula with the Crab pulsar and its near-by knot located 0.65" (1300 AU) south-east of the pulsar inside the red box. On the right, a zoomed view of the image is shown. The arrows indicate at different periods in time the polarization angle in the optical (HST in 2005 and GASP in 2012) and in hard X-rays (Integral in the period 2003-2007 and 2012-2014). Also indicated are the directions of the proper motion (PM) and spin axis (SA) of the pulsar.

INTEGRAL

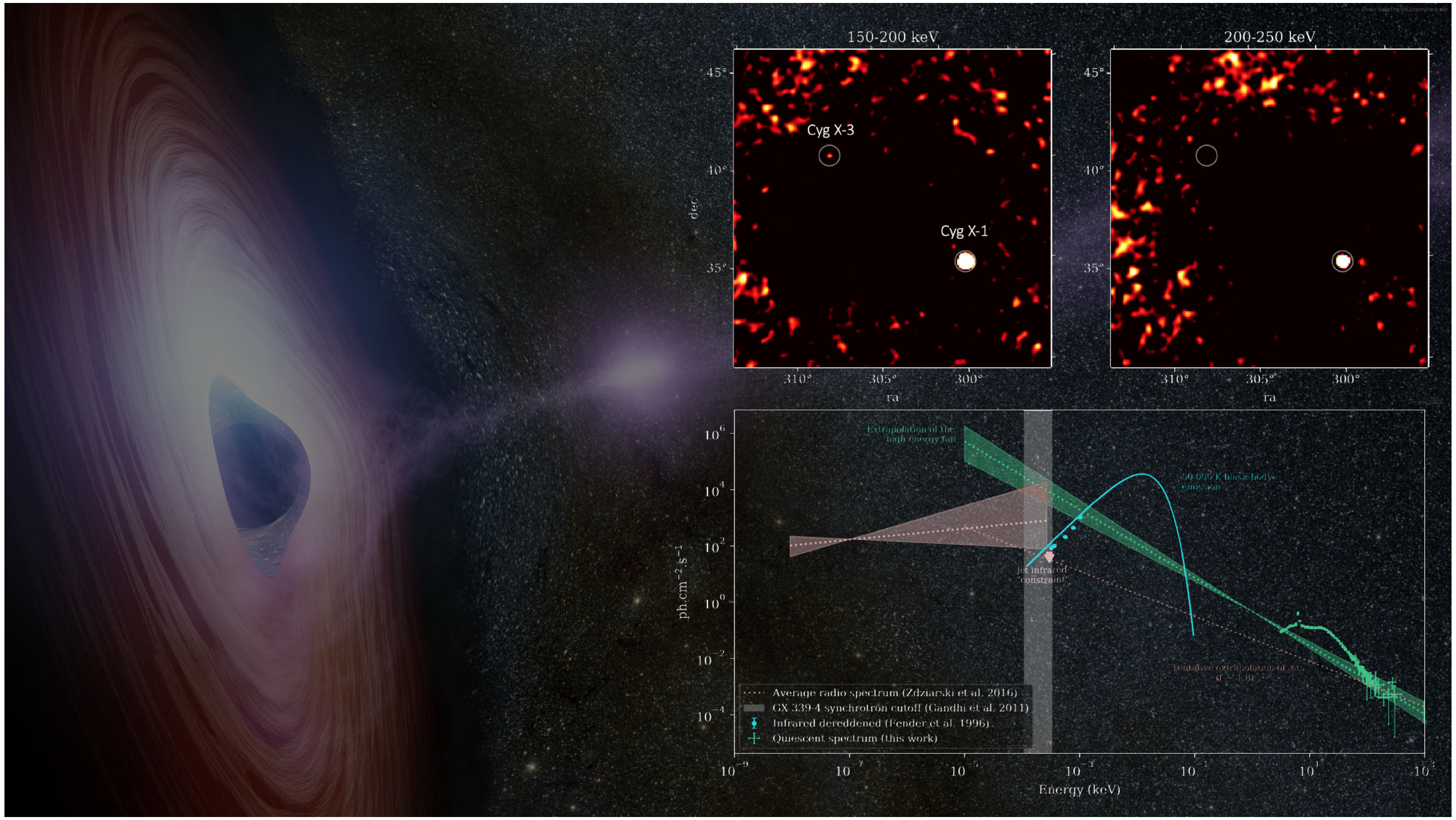

Cygnus X-3 is one of the first discovered X-ray binaries and the only bright compact binary system known to host a Wolf-Rayet star as a companion. The intense stellar wind created by this companion is one of the reasons why Cygnus X-3 exhibits a very peculiar spectral behavior. Indeed, it shows a wider variety of states than the two canonical ones usually observed in other standard X-ray binaries. Despite the fact that the source is well known since many years, very little is known about its spectral behavior beyond 50 keV. This lack of knowledge is especially due to the source being very faint at these energies. Thanks to INTEGRAL, it is possible to explore more than 16 years of observations, and so to probe the sky region of Cygnus X-3 with the best sensitivity ever. As shown at the top of the figure, one can detect the source up to 200 keV. Moreover, one can create six X-ray spectra from 3 to 200 keV, one for each observed spectral state of the source.

INTEGRAL

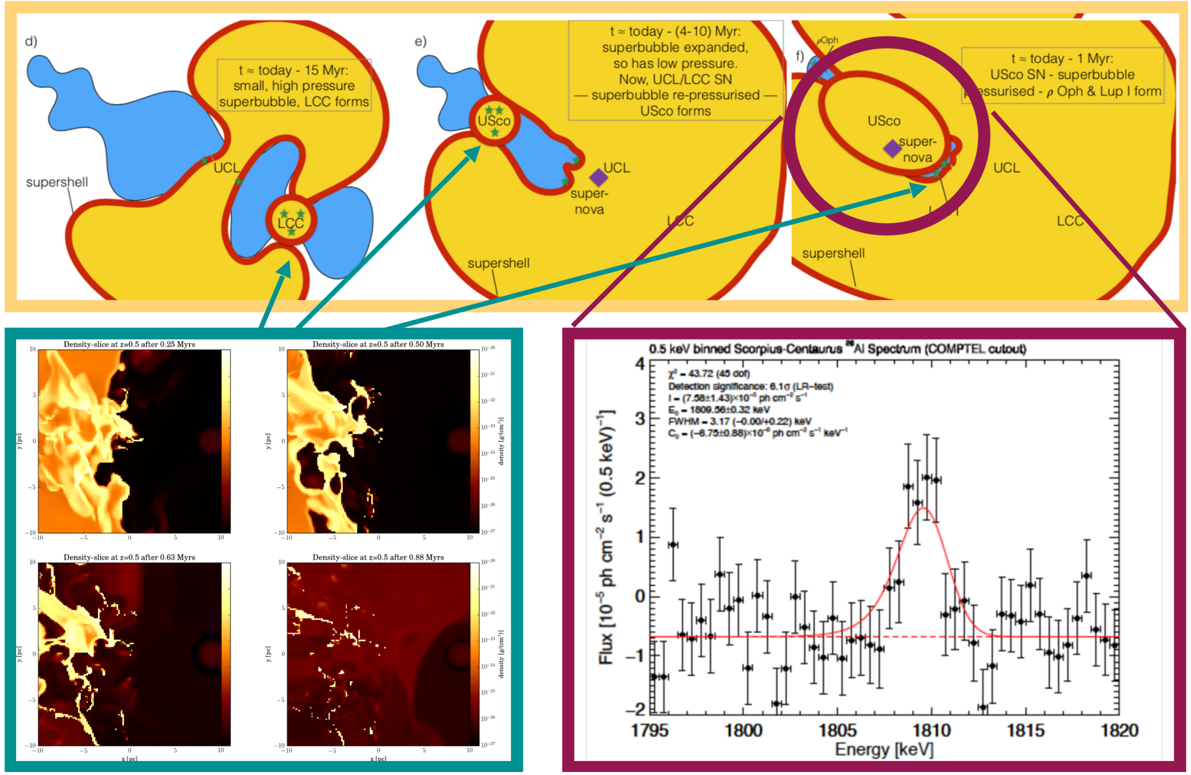

^{26}Al is uniquely produced by massive stars. These stars eject ^{26}Al through their winds and supernova explosions, which have a huge impact on the surrounding interstellar medium. Due to its short, in astronomical terms, decay time of a million years, ^{26}Al serves as evidence of very recent massive star activity. The detection of ^{26}Al towards the Scorpius-Centaurus region, therefore, provides a key piece of evidence in the reconstruction of the history of this massive star forming region.

Groups of stars first start to form in the densest part of a cloud, which in general may have a filamentary/elongated structure. The massive star activity forms a bubble of hot gas, which would be ^{26}Al enriched from massive-star ejecta. Gas may be compressed locally, leading to more star formation, but may also quickly escape along the minor axis of the cloud. In the tenuous medium around the cloud, the overpressured bubble could progress much more quickly than through the dense cloud, and thus reach and compress far-away regions of the cloud. The details of cloud compression and fragmentation of such a superbubble have been simulated and are shown in the bottom left part of the image. The ^{26}Al signal detected by INTEGRAL/SPI is independent proof for massive-star activity within approximately the last million years, and a key part of the study of how massive-star feedback works.

Galactic Sources

Accretion disk formation

Matter circulates around the compact object:

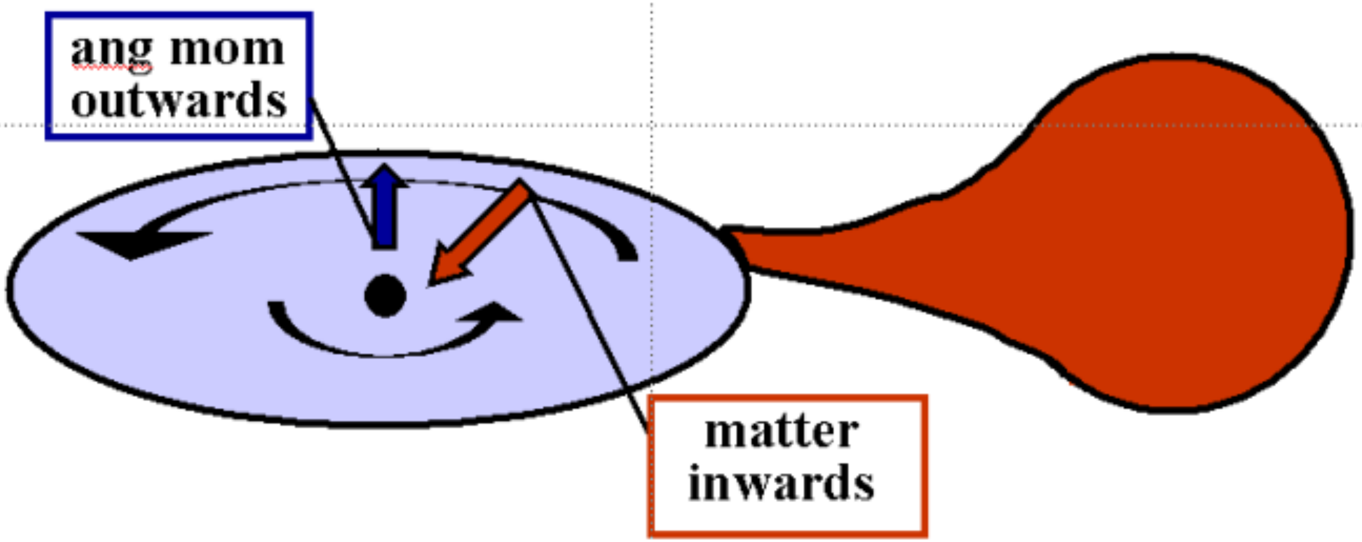

https://mssl.ucl.ac.uk/www_astro/lecturenotes/hea/hea.html

Galactic Sources

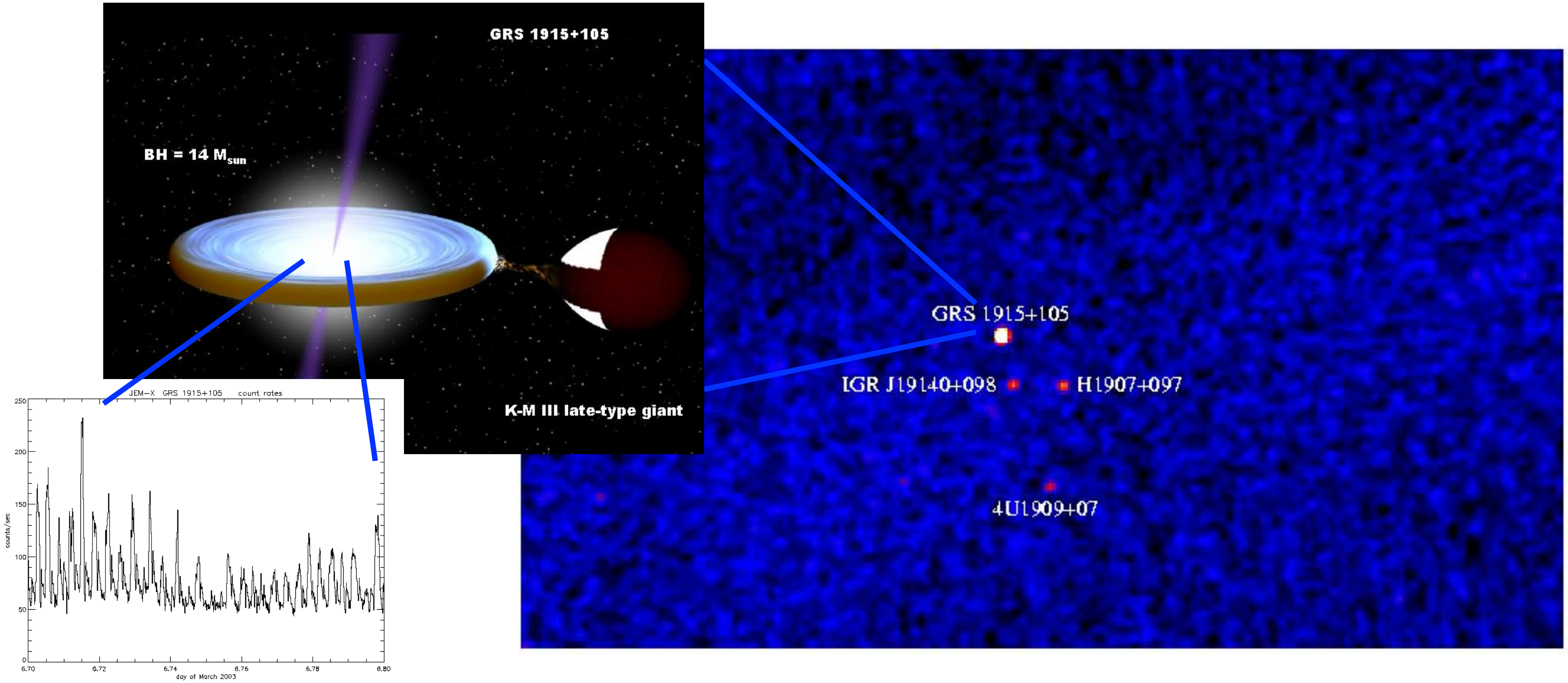

Galactic Sources

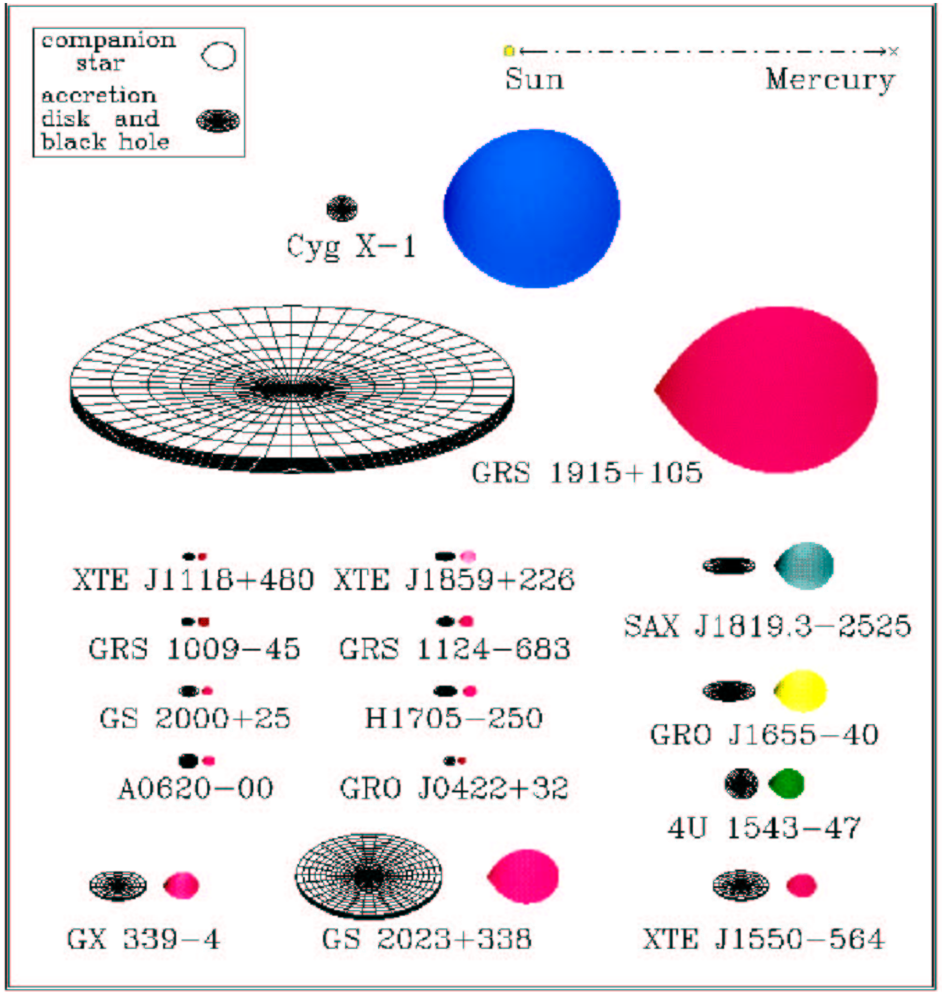

Credit: Jerome A. Orosz

Accretion Power

Accretion onto a compact object

- Principal mechanism for producing high-energy radiation
- Most efficient of energy production known in the Universe.

$$\boxed{E_{acc} = G\frac{Mm}{R}}$$

Gravitational potential energy released for body mass M and radius R when mass m accreted

Accretion Power

Example - neutron star

Accreting mass m=1kg onto a neutron star:

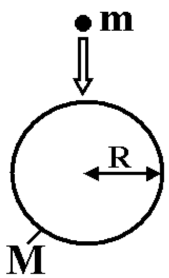

neutron star mass = 1 solar mass

R = 10 km

=> $\sim 10^{16}$ m Joules,

ie approx 10^{16} Joules per kg of accreted matter - as electromagnetic radiation

Efficiency of accretion

- Compare this to nuclear fusion
  H => He releases $\sim 0.007\ mc^2$
  $\sim 6 \times 10^{14}$ m Joules - **<u>20x smaller</u>** (for ns)

$$E_{acc} = G\frac{Mm}{R}$$

So energy released proportional to M/R ie the more compact a body is, the more efficient accretion will be.

Accretion Power

Origin of accreted matter

- Given M/R, luminosity produced depends on accretion rate, $\dot{m}$.

$$L_{acc} = \frac{dE_{acc}}{dt} = \frac{GM}{R}\frac{dm}{dt} = \frac{GM\dot{m}}{R}$$

- Where does accreted matter come from? ISM? No - too small. Companion? Yes.

Accretion

Types of X-ray Binaries

Group I	**Group II**
Luminous (early, massive opt countpart)	Optically faint (blue) opt counterpart
(high-mass systems)	*(low-mass systems)*
hard X-ray spectra	soft X-ray spectra
(T>100 million K)	*(T~30-80 million K)*
often pulsating	non-pulsating
X-ray eclipses	*no X-ray eclipses*
Galactic plane	Gal. Centre + bulge
Population I	*older, population II*

Accretion Power

The Eddington Luminosity

- There is a limit to which luminosity can be produced by a given object, known as the Eddington luminosity.
- Effectively this is when the inward gravitational force on matter is balanced by the outward transfer of momentum by radiation.